Michigan Technological University

Digital Commons @ Michigan Tech

Dissertations, Master's Theses and Master's Reports

2015

MECHANISTIC MODELS ON ENZYMATIC HYDROLYSIS AND ANAEROBIC DIGESTION

Yang Zhang
Michigan Technological University, yzhang15@mtu.edu

Copyright 2015 Yang Zhang

Recommended Citation

Zhang, Yang, "MECHANISTIC MODELS ON ENZYMATIC HYDROLYSIS AND ANAEROBIC DIGESTION", Open Access Dissertation, Michigan Technological University, 2015.
https://doi.org/10.37099/mtu.dc.etdr/63

Follow this and additional works at: https://digitalcommons.mtu.edu/etdr

Part of the Biochemical and Biomolecular Engineering Commons

MECHANISTIC MODELS ON ENZYMATIC HYDROLYSIS AND ANAEROBIC DIGESTION

By

Yang Zhang

A DISSERTATION

Submitted in partial fulfillment of the requirements for the degree of

DOCTOR OF PHILOSOPHY

In Chemical Engineering

MICHIGAN TECHNOLOGICAL UNIVERSITY

2015

© 2015 Yang Zhang

This dissertation has been approved in partial fulfillment of the requirements for the Degree of DOCTOR OF PHILOSOPHY in Chemical Engineering

Department of Chemical Engineering

Dissertation Advisor: *Wen Zhou*

Committee Member: *Susan T. Bagley*

Committee Member: *Tony N. Rogers*

Committee Member: *David R. Shonnard*

Department Chair: *S. Komar Kawatra*

Table of Contents

List of Tables ix
List of Figures xi
Acknowledgements xv
Preface xvii
List of Publications xix
Abstract xxi
Chapter 1 Introduction and Research Objectives 1
Chapter 2 On Improved Mechanistic Modeling for Enzymatic Hydrolysis of Cellulose 5
Abstract 6
2.1 Introduction 7
2.2 Materials and Methods 10
2.2.1 Oligomer reactions with beta-glucanases 10
2.2.2 Inhibition effects 13
2.2.3 Enzymatic thermal deactivation and inactive adsorption 15
2.2.4 Model parameters 17
2.3 Results and Discussion 17
2.3.1 Testing cellulosic substrate accessibility 17
2.3.2 Oligomer reactions 20
2.3.3 Inhibition effects 20
2.3.4 Enzyme decay and the slow-down of enzymatic hydrolysis kinetics 21
2.4 Conclusions 23
Nomenclature 24
Tables 27
Figures 29
References 33
Chapter 3 On a Novel Mechanistic Model for Simultaneous Enzymatic Hydrolysis of Cellulose and Hemicellulose Considering Morphology 35
Abstract 36
3.1 Introduction 37
3.2 Methodology 39
3.2.1 Morphology of substrate containing hemicellulose and cellulose 39

3.2.2 Advanced site concentration formalism 43
3.2.3 Ablation and oligomer rate equations 46
3.3 Numerical Simulation Results and Discussion 48
3.3.1 Comparison with experiments in Qing and Wyman (2011b) and investigation of effects of substrate morphology 50
3.3.2 Comparison with experiments in Banerjee et al. (2010a) 51
3.3.3 Comparison with Experiments in Kumar and Wyman (2009) 52
3.4 Conclusions 53
Nomenclature 55
Acknowledgments 60
Tables 61
Figures 64
References 71
Supporting Information (SI) 73
Appendix 107
Chapter 4 A Mechanistic Design Framework for Optimal Enzyme Usage in Hydrolysis of Hemicellulose-cellulosic Substrates 109
Abstract 110
4.1 Introduction 111
4.2 Methods 113
4.2.1 Morphology of lignocellulosic substrates 113
4.2.2 Reactions of enzyme mixture 113
4.2.3 Model parameters and optimization procedure 115
4.3 Results and Discussion 118
4.3.1 Enzyme optimization and adding time effects for Avicel hydrolysis 118
4.3.2 Enzyme optimization and adding time effects for AFEX-pretreated corn stover hydrolysis 120
4.4 Conclusions 123
Acknowledgments 124
Tables 125
Figures 127
References 132
Supporting Information (SI) 135

Chapter 5 Improved ADM1 Model for Anaerobic Digestion Process Considering Physico-chemical Reactions 147
Abstract 148
5.1 Introduction 149
5.2 Methodology 152
5.2.1 Bio-chemical framework 152
5.2.2 Physico-chemical framework 153
5.3 Results and Discussion 157
5.3.1 Model validation 157
5.3.2 Effects of inorganic components on anaerobic digestion 157
5.4 Conclusions 161
Nomenclature 161
Acknowledgments 163
Tables 165
Figures 169
References 175
Supporting Information (SI) 177
Appendix 183

List of Tables

Table 2.1 Parameters used in the model.....27

Table 3.1 Main components of hemicellulose-cellulosic substrates and their specific enzymes 61

Table 3.2 Simulation results compared with experimental data from Banerjee et al. (2010a) 62

Table 4.1 Optimal enzyme mass fractions for 72 hours hydrolysis of Avicel 125

Table 4.2 Optimal enzyme mass fractions for 72 hours hydrolysis of AFEX pretreated corn stover.....126

Table 5.1 Matrix representation of the rate coefficients and equations for ADM1 bio-chemical framework part 1: soluble components 165

Table 5.2 Matrix representation of the rate coefficients and equations for ADM1 bio-chemical framework part 2: particulate components 166

Table 5.3 Matrix representation of the rate coefficients and equations for ADM1 physico-chemical framework part 1: liquid-gas processes 167

Table 5.4 Matrix representation of the rate coefficients and equations for ADM1 physico-chemical framework part 2: liquid-liquid processes 167

Table 5.5 Matrix representation of the rate coefficients and equations for ADM1 physico-chemical framework part 3: liquid-solid processes.....168

Table 5.6 Acid-base and precipitation reactions considered in anaerobic digestion 168

List of Figures

Figure 2.1 Simulation results using different initial values of FA compared with experimental data. The substrate and enzyme have initial properties of (**a**) 20 g/L Avicel and 4.1 g/L Spezyme CP and (**b**) 10 g/L Avicel and 0.51 g/L Spezyme CP together with 30 IU beta-glucanase/g Avicel (57.69 mg/L beta-glucanase) 29

Figure 2.2 Simulation results of finial conversion level with and without consideration of oligomer reactions in solution. The substrate and enzyme have initial properties of 10 g/L Avicel and 0.51 g/L Spezyme CP together with 30 IU beta-glucanase/g Avicel (57.69 mg/L beta-glucanase).....29

Figure 2.3 Simulation results of glucose concentration with and without consideration of oligomer reactions in solution. The substrate and enzyme have initial properties of 10 g/L Avicel and 0.51 g/L Spezyme CP together with 30 IU beta-glucanase/g Avicel (57.69 mg/L beta-glucanase).....30

Figure 2.4 Simulation results of oligomer concentrations (**a**) without and (**b**) with consideration of oligomer reactions in solution. The substrate and enzyme have initial properties of 10 g/L Avicel and 0.51 g/L Spezyme CP together with 30 IU beta-glucanase/g Avicel (57.69 mg/L beta-glucanase) 30

Figure 2.5 Simulation results considering oligomer reactions and inhibitions compared with experimental data. The substrate and enzyme have initial properties of (**a**) 20 g/L Avicel and 4.1 g/L Spezyme CP and (**b**) 10 g/L Avicel and 0.51 g/L Spezyme CP together with 30 IU beta-glucanase/g Avicel (57.69 mg/L beta-glucanase) 31

Figure 2.6 Simulation results considering different enzyme decay factors compared with experimental data. The substrate and enzyme have initial properties of (**a**) 20 g/L Avicel and 4.1 g/L Spezyme CP and (**b**) 10 g/L Avicel and 0.51 g/L Spezyme CP together with 30 IU beta-glucanase/g Avicel (57.69 mg/L beta-glucanase) 31

Figure 2.7 Simulation results considering all rate-limiting factors compared with experimental data. The substrate and enzyme have initial properties of (**a**) 20 g/L Avicel and 4.1 g/L Spezyme CP and (**b**) 10 g/L Avicel and 0.51 g/L Spezyme CP together with 30 IU beta-glucanase/g Avicel (57.69 mg/L beta-glucanase) 32

Figure 3.1 Structural illustration of cellulose and hemicelluloses in substrates. The core is crystalline cellulose elementary fibril (CEF). The size (i.e. the number of cellulose chains contained) and shape of the CEF are still in debate. The

stricture model of CEF shown here is the 36-chain square shape model. Other models of CEF are not listed here. There is no close relationship between the structure of SAC and CEF 64

Figure 3.2 Structural illustration of cellulose and hemicelluloses in substrates. The core is crystalline cellulose elementary fibril (CEF). The size (i.e. the number of cellulose chains contained) and shape of the CEF are still in debate. The stricture model of CEF shown here is the 36-chain square shape model. Other models of CEF are not listed here. There is no close relationship between the structure of SAC and CEF 65

Figure 3.3 Schematic illustration of the partitioning of an SAC into elementary layers. Each layer is represent by a λ-value such that the layer with the highest λ-value is the first (i.e. outermost) to be removed due to solubilization by attacking enzymes during hydrolysis. The SACs of same geometric class have a same highest λ-value 66

Figure 3.4(a) Example of using Ui and Si to represent the chains of cellulose, arabinoglucuronoxylan and galactoglucomannan in hemicellulose-cellulosic substrate. The chain length is 11 for each component. U1, U2 and U3 represent the D-glucose units, D-xylose units and D-mannose units respectively. S1, S2 and S3 represent three types of side groups: D-galactose, D-glucuronic acid and L-arabinose.....67

Figure 3.4(b) Example of using U_{ij} to represent the bonds and the distribution of the site types along all the backbones shown in Figure 3.4(a). The maximum number of bond types could be 3^2=9, but only 5 types actually exist. The average probability for certain type of bonds appearing on the backbones of certain type of chain depends on the monomer composition of the chain....68

Figure 3.5 Simulation results compared with experimental data from Qing and Wyman (2011b). Solid lines represent simulations results of cellulose conversion. Dash lines represent simulations results of xylan conversion. Filled circles represent experimental data of cellulose conversion. Blank circles represent experimental data of xylan conversion 69

Figure 3.6 Model results testing the impact of initial substrate composition on hydrolysis. The total substrate loading is 0.2g in 10 mL reaction volume with CP (16.1 mg protein/g glucan) and BG (3.16 mg protein/g glucan) for all three cases. The initial percentages of cellulose and xylan are shown in figures 70

Figure 3.7 Model results using two different groups of values of accessibility. The total substrate loading is 0.2g in 10 mL reaction volume with CP (16.1 mg protein/g glucan) and BG (3.16 mg protein/g glucan) for both two cases.

The initial percentages of substrate components for two cases are 5.7% for xylan and 57.6% for cellulose. The #1 accessibility set is: 0.0530 (cellulose); 0.5337 (xylan) and 0.1051 (total). The #2 accessibility set is: 0.2270 (cellulose); 0.0381 (xylan) and 0.2066 (total) 70

Figure 4.1 Ternary plot predictions of glucan conversion (A, B, C) and glucose yield (D, E, F) at 72 hours with 7.5 (A, D), 15 (B, E) and 30 (C, F) mg enzyme/g glucan. Mass fractions of EG1, CBH1 and CBH2 are given for glucan conversions. Mass fractions of EG1, CBH2 and BG are given for glucose yields. Cross mark shows the optimization point 127

Figure 4.2 Simulation results of adding BG at 0, 24 and 48 hours during the hydrolysis of Avicel. Total enzyme loading is 15 mg enzyme/g glucan and enzyme fractions are optimal for glucose yield at 72 hours hydrolysis 128

Figure 4.3 Ternary plot predictions of "glucan+xylan" conversion (A, B, C) and "glucose+xylose" yield (D, E, F) at 72 hours with 7.5 (A, D), 15 (B, E), and 30 (C, F) mg enzyme/g glucan. Mass fractions of CBH1, CBH2, and EX are given for "glucan+xylan" conversion. Mass fractions of CBH2, EX, and BG are given for "glucose+xylose" yield. Cross mark shows the optimization point 129

Figure 4.4 Simulation results of adding BG (A) and BX (B) at 0, 24 and 48 hours for the hydrolysis of AFEX pretreated corn stover. Total enzyme loading is 15 mg enzyme/g glucan and enzyme fractions are optimal for "glucose+xylose" yield at 72 hours hydrolysis 130

Figure 4.5 Simulation results of adding BG, EX and BG+EX after 8 hours hydrolysis of AFEX pretreated corn stover to investigate the yields of glucose (A) and xylose (B). Total enzyme loading and fractions are the same as in Figure 4.4 131

Figure 5.1 Comparison between the predicted (pred.) and measured (meas.) data for calcium and magnesium ions, total carbonate, phosphate, ammonia/ammonium, pH in liquid phase and model prediction of precipitate generation rates in solid phase 169

Figure 5.2 Comparison between the simulation results and experimental data of finial concentrations of precipitates 170

Figure 5.3 Effects of metal ions on biogas production and precipitates generation 171

Figure 5.4 Effects of inorganic phosphorus on biogas in gas phase, substrate in liquid phase and precipitates in solid phase 172

Figure 5.5 Effects of inorganic nitrogen on biogas in gas phase, substrate in liquid phase and precipitates in solid phase 173

Figure 5.6 Effects of different initial inorganic phosphorus to nitrogen ratios on the production of CH4 in gas phase.....174

Acknowledgements

First of all, I would like to express my greatest appreciation to my advisor, Dr. Wen Zhou for his support, guidance and encouragement throughout my entire Ph.D. research career. Without the opportunities and research resources offered by Dr. Wen Zhou, I would not accomplish and publish so many research papers and complete this dissertation. He has provided to me the best of his knowledge and experience which I will never forget in my future life. Besides my advisor, I would like to appreciate Dr. Susan Bagley, Dr. David Shonnard and Dr. Tony Rogers for their serving on my dissertation committee. Their comments and suggestions have broaden my view and helped me improve the quality of the dissertation.

I am grateful to the Chemical Engineering Department of Michigan Technological University for providing me the opportunity to pursue my Ph.D. degree in Chemical Engineering and offering me the position of graduate teaching assistant for three semesters. Thanks to the graduate school of Michigan Technological University for offering me the Doctoral Finishing Fellowship this semester, which provides a great support for me to finish my Ph.D. degree. I would also like to thank Adam S. Marlowe and Sarah Piccard who used to work with me together in our research group. I will never forget the days with them and the assistance and support from them when we did the research together. I would not accomplish and publish so many research papers without their contributions.

Finally, I would like to express my gratitude to my parents Xiaoping Zhang and Ming Jiao for their love and support, which always motivate me to put forth my greatest effort

on study, and special thanks to Beibei Yang for her encouragement. Thanks to all the friends of mine here and in China that helped me and my family.

Preface

This dissertation includes five chapters.

Chapter 2 "On Improved Mechanistic Modeling for Enzymatic Hydrolysis of Cellulose" was published in the Journal of *Chemical Engineering & Process Technology*. In this study, Wen Zhou designed the model and Yang Zhang made the improvements for the model. The manuscript was written by Yang Zhang.

Chapter 3 "On a Novel Mechanistic Model for Simultaneous Enzymatic Hydrolysis of Cellulose and Hemicellulose Considering Morphology" was published in the journal of *Biotechnology and Bioengineering*. In this study, Wen Zhou and Yang Zhang designed the model and Bingqian Xu provided the experimental evidence. The manuscript was written by Yang Zhang.

Chapter 4 "A Mechanistic Design Framework for Optimal Enzyme Usage in Hydrolysis of Hemicellulose-cellulosic Substrates" was submit to the journal of *Bioresource Technology*. In this study, Wen Zhou and Yang Zhang designed the model and Adam S. Marlowe made the improvements for the model. The manuscript was written by Yang Zhang and Adam S. Marlowe.

Chapter 5 "Improved ADM1 Model for Anaerobic Digestion Process Considering Physico-chemical Reactions" was published in the journal of *Bioresource Technology*. In this study, Wen Zhou and Yang Zhang improved the model and Sarah Piccard collected the data. The manuscript was written by Yang Zhang.

List of Publications

Zhang Y, Xu B, Zhou W. 2014 "On a novel mechanistic model for simultaneous enzymatic hydrolysis of cellulose and hemicellulose considering morphology." Biotechnology and Bioengineering, 111, 1767-1781

Zhang Y, Zhou W. 2014 "On improved mechanistic modeling for enzymatic hydrolysis of cellulose." Journal of Chemical Engineering & Process Technology, 5, 190

Zhang Y, Piccard S, Zhou W. 2015 "Improved ADM1 model for anaerobic digestion process considering physico-chemical reactions." Bioresource Technology, 196, 279-289

Zhang Y, Zhou W. 2015 "Mechanistic models for enzymatic hydrolysis of lignocellulosic substrates." Biotechnology and Bioengineering (in review)

Zhang Y, Marlowe A S, Zhou W. 2015 "A Mechanistic Design Framework for Optimal Enzyme Usage in Hydrolysis of Hemicellulose-cellulosic Substrates." Bioresource Technology (in review)

Abstract

For enzymatic hydrolysis, a mechanistic model on enzymatic hydrolysis of pure cellulosic substrates was improved to consider oligomer reactions with beta-glucanases, inhibition of oligomers to cellulases and enzyme decay. Then a novel and general modeling framework was developed for enzymatic hydrolysis of hemicellulose-cellulosic substrates. This mechanistic model, for the first time, took into consideration explicitly the time evolution of morphologies of intertwining cellulose and hemicelluloses. This novel mechanistic model was applied to optimize the composition of enzyme mixtures for substrate conversion and monosaccharides yield during simultaneous enzymatic hydrolysis of different lignocellulosic substrates. For anaerobic digestion, the original "Anaerobic Digestion Model No.1" (ADM1) developed by the International Water Association (IWA) task group was modified by improving the bio-chemical framework and integrating a more detailed physico-chemical framework. The modified ADM1 was used to investigate the effects of metal ions and other inorganic components on anaerobic digestion in batch reactor.

Chapter 1 Introduction and Research Objectives

Biofuel is the fuel derived from biological materials. It is renewable and sustainable and can reduce our high reliance on fossil fuels and thus the greenhouse gas emission. Biofuels includes a wide range of types such as biogas, bioethanol and biodiesel, which can be produced through thermochemical and biochemical conversion processes. Biomass materials have been considered as the major sources for biofuel production. The basic categories of biomass materials include lignocellulosic biomass, food and industrial wastes. Lignocellulosic biomass refers to the plant materials such as wood, grass, agriculture residues and energy crops, which are abundant and sustainable feedstocks for biofuel production. The main components of lignocellulosic biomass include cellulose, hemicelluloses and lignin.

The biochemical conversion process of lignocellulosic biomass mainly contains three steps, which are pretreatment, hydrolysis and fermentation. The goal of the pretreatment step is to break down lignin and increase the enzyme accessibility of cellulose and hemicelluloses. In the hydrolysis step, pretreated substrates are catalyzed by enzymes and converted into soluble sugars, which is also the critical step of converting lignocellulosic biomass into biofuels. In the fermentation step, microorganisms finally convert soluble sugars into biofuels such as bioethanol. Besides lignocellulosic biomass, food and industrial wastes are other important sources for biofuel production. They can be used to produce biogas through anaerobic digestion by microbes. There are five major biochemical processes involved in anaerobic digestion, which are disintegration, hydrolysis, acidogenesis, acetogenesis and methanogenesis. In the disintegration process, solid wastes are disintegrated into carbohydrates, proteins, fats and inerts. In the hydrolysis process, carbohydrates, proteins and fats are hydrolyzed into monosaccharides, amino acids and

long chain fatty acids. These two processes occur outside the microbes and are catalyzed by extracellular enzymes. In the next acidogenesis and acetogenesis processes, the chemicals from the hydrolysis process are converted into acetates, hydrogen and carbon dioxides, which are finally converted into biogas in the final methanogenesis process. These processes occur inside the microbes and are catalyzed by intracellular enzymes. In addition, many other physico-chemical processes simultaneously occur with biochemical processes. These process are not directly mediated by microbes, such as liquid-gas transfer, ion association and dissociation and precipitation, but can affect the bio-chemical processes of anaerobic digestion.

Both enzymatic hydrolysis and anaerobic digestion are important biochemical processes for biofuel production. The main research objective of the dissertation is to better understand and optimize these two processes based on mechanistic models. In chapter two, an improved mechanistic model for enzymatic hydrolysis of pure cellulosic substrates is developed which considers oligomer reactions with beta-glucanases, inhibition of oligomers to cellulases and enzyme decay. In chapter three, a novel and general modeling framework is developed for enzymatic hydrolysis of cellulose and hemicellulose simultaneously. This mechanistic model, for the first time, takes into consideration explicitly the time evolution of morphologies of intertwining cellulose. In chapter four, the novel mechanistic model is applied to optimize the composition of enzyme mixtures for substrate conversion and monosaccharides yield during simultaneous enzymatic hydrolysis of different lignocellulosic substrates. In chapter five, the original "Anaerobic Digestion Model No.1" (ADM1) developed by the International Water Association (IWA) task group is improved by improving the bio-chemical framework and integrating a more detailed

physico-chemical framework. The modified ADM1 is then used to investigate the effects of metal ions and other inorganic components on anaerobic digestion in batch reactor.

Chapter 2 On Improved Mechanistic Modeling for Enzymatic Hydrolysis of Cellulose[1]

[1] Published in the Journal of *Chemical Engineering & Process Technology*

This is an open-access article distributed under the terms of the Creative Commons Attribution License, which permits unrestricted use, distribution, and reproduction in any medium, provided the original author and source are credited. © 2014 Zhang Y, et al.

Abstract

An improved model for enzymatic hydrolysis of cellulose was developed which considered oligomer reactions with beta-glucanases, inhibition of oligomers to cellulases and enzyme decay processes during hydrolysis. The oligomer reactions with beta-glucanases were modeled based on the enzymatic glucan chain fragmentation kinetics which described the further fragmentation of oligomers in solution after being solubilized from the insoluble glucan chains. The inhibition effects on all cellulases by different types of cello-oligomers were taken into account based on competitive adsorption of cello-oligomers to the active site of cellulases, which is a critical factor contributing to the decrease in the rate of enzymatic hydrolysis of cellulose. As another factor affecting the kinetics of cellulose hydrolysis process, enzyme decay factor was incorporated into the model as the typical first order decay process. We considered two different processes for cellulases losing activity during hydrolysis in order to better understand the impact of enzyme decay on hydrolysis. Numerical simulation results were presented to investigate the phenomenon of hydrolysis rate slow-down commonly observed in experiments. Improvement of the predictive capability of the new model over previous one was demonstrated by comparing the simulations with experimental data. After considering all the possible hydrolysis rate slow-down factors, the simulation results could agree with the experimental data very well, showing that the model is capable to fully capture the rate decrease of cellulose hydrolysis.

2.1 Introduction

The enzymatic hydrolysis of cellulose into soluble and fermentable oligomers (e.g., glucose and cellobiose) has been under intensive investigation due to the potential utilization of lignocellulosic biomass to produce sustainable biofuel and replace the non-renewable fossil transportation fuel. In order to optimize the design of reactors and the biofuel production process, it is critical to have a mechanistic model describing the hydrolysis kinetics of solid cellulosic substrates being solubilized by all kinds of cellulases in detail. Unlike non-mechanistic and semi-mechanistic models which usually include less than two substrate and/or enzyme variables and are used to fit experimental data (Zhang and Lynd, 2004), mechanistic models involve multiple substrate and enzyme variables and can provide insights on the complex chemical and physical properties of both enzyme and substrate and all the enzymatic and material transformations occurring during hydrolysis.

Over the past 10 years, many advanced mechanistic models have been developed in full generality to describe the enzymatic hydrolysis process of cellulose based on more realistic representations of cellulosic substrate (Griggs et al., 2012a, b; Hosseini and Shah, 2011a, b; Levine et al., 2010; Levine et al., 2011; Zhang and Lynd, 2006; Zhou et al., 2009b). For example, Zhou et al. (2009b) developed a detailed mechanistic model for enzymatic hydrolysis of cellulose considering the substrate morphologies and their coupling with morphology-depended substrate hydrolysis kinetics. As described in the model, the whole process of cellulose hydrolysis could be viewed as the process of fragmentation and solubilization of glucan chains and lead to the evolution of cellulosic substrate morphology, that is, the organization of glucan chains, which, in turn, significantly influenced the

cellulose hydrolysis kinetics. The concept of smallest accessible compartment (SAC) was first proposed, defined as a minimal volume by external and internal surfaces exposed to enzyme-accessible hydrated interior voids of the solid cellulosic substrate material, and used as minimal time-evolving structural unit to keep track of the cellulosic substrate morphology. In addition, a site representation formalism of enzyme hydrolytic fragmentation coupled with morphology evolution was also introduced in the model. The formalism considered all the β-(1, 4)-glycosidic bonds on glucan chains as six types of bond sites based on their locations and reactions with different kinds of cellulases that mainly act on the solid substrate. Basically, these cellulases can be categorized into two broad classes, which are endo-glucanases and exo-glucanases. Endo-glucanases usually adsorb onto the glucan chains of insoluble part of substrate and randomly cut the internal β-(1,4)-glycosidic bonds. Unlike endo-glucanases, exo-glucanases only cut the terminal β-(1, 4)-glycosidic bonds at the ends of each glucan chain. Since the two ends of each glucan chain are chemically distinct from each other, exo-glucanase can be divided into two groups, which are cellobiohydrolase I (CBH I) and cellobiohydrolase II (CBH II). CBH IIs usually cut the terminal bonds from the non-reducing end of each glucan chain, while CBH Is cut the terminal bonds from the reducing end of each glucan chain. These cellulases can be produced in nature by many different cellulolytic fungi species. The most commonly used species in industry is *Trichoderma* species, especially *Trichoderma reesei* (*T. reesei*). Thus *T. reesei* EG1 (Cel7B), *T. reesei* CBH II (Cel6B) and *T. reesei* CBH I (Cel7A) are the three major cellulases that often used in model simulation work to analyze the process of enzymatic hydrolysis of cellulosic substrate. The site representation formalism was proposed to not only take into account all kinds of solid-substrate-acting cellulases but also

change the view of solid cellulosic substrate from a bundle of glucan chains with different lengths into a composite of six types of bond sites, so that the total number of ordinary differential equations (ODEs) can be reduced at magnitude of two orders and solved much more efficiently.

Almost all of the mechanistic models have recognized that the enzyme accessibility of substrate, or the enzyme-accessible substrate surface area, is a critical rate-limiting factor during the process of enzymatic hydrolysis (Levine et al., 2010; Zhang and Lynd, 2006; Zhou et al., 2009b). In order to increase the kinetics of hydrolysis and obtain more soluble oligomers, it will be helpful to increase the amount of accessible glucose units (β-(1,4)-glycosidic bonds) exposed on substrate surface by pretreatments before hydrolysis proceeding. However, most of the simulation results from the mechanistic models still could not agree with the experimental data completely, especially not be capable to capture the full extent of the hydrolysis rate slow-down, probably due to the reason that these models did not consider the complex inhibition relationships between substrate and oligomers except glucose and cellobiose, and possible enzyme decay and inactive absorption. Some of the models also did not consider the oligomer reactions which happen in liquid phase with the beta-glucanases. Unlike endo- and exo-glucanases, beta-glucanases mainly act on soluble cello-oligomers in solution which often contains no more than 7 glucose units. The most commonly used cellulolytic fungi species to created beta-glucanases in industry is *Aspergillus* species, especially *Aspergillus niger* (*A. niger*) because *Trichoderma* species do not produce significant amount of beta-glucanases compared to other cellulases. *A. niger* beta-glucosidase (BG) is the major beta-glucanase and often used with other cellulases to increase their efficiency during enzymatic

hydrolysis of cellulose, because dissolved oligomers could cause strong inhibition effects by adsorbing the free cellulase molecules. BGs can hydrolyze soluble oligomers into smaller ones mainly by releasing glucose from them and avoid the strong inhibitions between cellulases and long-chain oligomers. It is clear that the oligomer reactions with beta-glucanase will affect hydrolysis kinetics and change inhibition equilibrium. Ignoring the kinetics slow-down factors will also hinder the precise prediction of final conversion level of cellulosic substrate after a long time-scale of enzymatic hydrolysis process.

In this study, we improve the model described by (Zhou et al., 2009b) by incorporating (1) the reactions involving beta-glucanases digesting soluble oligomer sugars in solution, (2) the comprehensive competitive inhibition effects of oligomers from glucose (G1) to cellohexaose (G6) on enzymatic hydrolysis, and (3) the enzymatic thermal deactivation and inactive adsorption. Here, we consider enzymatic thermal deactivation as the process that the hydrolytic enzymes lose the ability of binding to substrates, and consider enzymatic inactive adsorption as the process that the hydrolytic enzymes lose the ability to continue the subsequent catalytic reactions although they are able to bind to substrate. We carry out numerical analysis to investigate the impacts of aforementioned factors on the kinetics of enzymatic hydrolysis of cellulose.

2.2 Materials and Methods

2.2.1 Oligomer reactions with beta-glucanases

The basic part of the model we used in this study was from the mechanistic model of enzymatic hydrolysis of cellulose presented by Zhou et al. (2009b). In their work, the

concept of smallest accessible compartment (SAC) was first proposed to describe the geometrical construction of pretreated pure cellulosic substrate material. An SAC unit was defined as a minimal volume that is delimited by external surfaces and by internal surfaces at the internal surfaces of the voids exposed to all kinds of cellulases. SACs initially had a random distribution of sizes, and to represent the distribution, the parameter of SAC geometry class was used and labeled by "σ" with σ=1, 2... M_{MD} where M_{MD} was the population size of SAC geometry classes. During the process of enzymatic hydrolysis, the size of each SAC would shrink due to the enzymatic ablation of glucose units from the SAC surfaces. And glucose units which were originally blocked would gradually become exposed on the SAC surfaces. In addition, Zhou et al. (2009b) proposed in their work an innovative surface site concentration formalism which treated each SAC as a composite of six different types of β-(1,4)-glycosidic bond sites. These site types were labeled by index "μ" and referred to as N-, O-, X-, Y-, L-, and R-sites. N-site bonds could only adsorb, and only be cut by endo-glucanases. O-site bonds could not adsorb any enzyme molecule due to the obstruction. X-site bonds could adsorb and be cut by either endo-glucanases or cellobiohydrolase IIs, which were located a distance of k_X glucose units from the non-reducing ends of glucan chains. Y-site bonds could adsorb and be cut by either endo-glucanases or cellobiohydrolase Is, which were located a distance of k_Y glucose units from the reducing ends of glucan chains. L- and R-site bonds represented the non-reducing and reducing ends of glucan chains respectively. They were both broken bonds and could not adsorb any enzyme molecule. Then the production rate of glucose units dissolved from glucan chains of class-σ SACs was given by

$$\dot{x}_{S,\sigma} = \sum_{l=1}^{l_S-1} l \cdot R_{S,\sigma}(l) \quad (1)$$

where $R_{S,\sigma}(l)$ is the production rate of oligomers containing l glucose units ($1 \leq l < l_S = 7$) dissolved from insoluble glucan chains exposed on class-σ SAC surface caused by the enzymatic cuts on β-(1,4)-glycosidic bonds. l_S is the minimal length of insoluble glucan chains, which could be varied into any length if needed. In the mode, we considered cellohexaose (G6) as the longest cello-oligomer in solution based on the typical industrial applications.

We improved the mechanistic model to not only consider the processes that endo- or exo-glucanases cut the β-(1,4)-glycosidic bonds of insoluble glucan chains to produce oligomers, but also consider explicitly the reactions of oligomers after being released from solid substrates that involve beta-glucanases in solution. The production rates of soluble oligomers in solution are given by

$$\dot{x}_S(l) = \sum_{\sigma} R_{S,\sigma}(l) + R_S(l) \quad (2)$$

where $R_S(l)$ is the production rate of the oligomers containing l monomer units after being dissolved from glucan chains, which describes the reactions between oligomers and beta-glucanases. $R_S(l)$ did not exist in the model of Zhou et al. (2009b) where all the oligomers kept increasing in solution by being hydrolyzed from solid substrate.

Based on the study of sub-site structure of *A. niger* beta-glucosidase (Yazaki et al., 1997), the reaction mechanism between oligomers and beta-glucanases in solution can be considered as: an oligomer which contains $l-1$ glucose units can adsorb and be

hydrolyzed by an beta-glucanase molecule into a glucose unit and an oligomer containing $l-1$ glucose unit(s). So the expression of $R_S(l)$ can be written as

$$R_S(l) = \begin{cases} \gamma_\kappa(2) \cdot z_\kappa(2) + \sum_2^{l_S-1} \gamma_\kappa(l) \cdot z_\kappa(l), & l = 1 \\ -\gamma_\kappa(l) \cdot z_\kappa(l) + \gamma_\kappa(l+1) \cdot z_\kappa(l+1), & 2 \le l \le l_S - 2 \\ -\gamma_\kappa(l) \cdot z_\kappa(l), & l = l_S - 1 \end{cases} \tag{3}$$

where $\gamma_\kappa(l)$ is the oligomer cutting rate coefficient, $z_\kappa(l)$ is the concentration of (κ, l) enzyme-oligomer (EO) complexes where the oligomers contain l glucose units adsorb the type-κ beta-glucosidase enzyme molecules. The expression of EO complexes $z_\kappa(l)$ can be written, based on the enzyme adsorption equilibrium, as

$$z_\kappa(l) = I_\kappa(l) \cdot v_\kappa \cdot y_S(l) \tag{4}$$

with $1 \le l < l_S = 7$. Here, $I_\kappa(l)$ is the oligomer adsorption coefficient; $y_S(l)$ is the concentration of free oligomers containing l glucose units dissolved from glucan chains, and v_κ is the concentrations of type-κ free enzyme molecules in solution which could be any type of cellulases.

2.2.2 Inhibition effects

Cellulase inhibition describes the process that inhibitors limit the activity of cellulase molecules. Based on the impacts on cellulase, cellulase inhibitors can be classified into reversible and irreversible inhibitors in which the oligomer products of cellulose hydrolysis (e.g. glucose and cellobiose) are reversible inhibitors (Sharma, 2012). Reversible inhibitors can be classified into three types, which are competitive, uncompetitive and mix (or non-

competitive) inhibitors. Most of the inhibition processes between the cello-oligomer inhibitors and cellulases are competitive inhibitions (Sharma, 2012) where inhibitors can only bind free cellulase molecules in solution, which can also be described by adsorption Equation (4), where v_κ is now the concentration of type-κ cellulase (both endo- and exo-glucanases) free enzyme molecules in solution, and $I_\kappa(l)$ is the oligomer adsorption coefficient specifically for different cellulases.

If the EO complexes are formed by oligomers and endo- (or exo-) glucanases by oligomers binding onto active sites of binding domain of cellulases, and since we assume that catalytic domain cannot act on soluble oligomers, their corresponding values of $\gamma_\kappa(l)$, oligomer cutting rate coefficient, will be 0. Similarly, we could consider the inhibition of glucose (G1) to the beta-glucanases hydrolysis, where glucose binds onto the active site of beta-glucanase and no further catalytic action can be taken. Thus for beta-glucanases, if they are adsorbed by glucose units, $\gamma_\kappa(l)$ will also be 0 in that glucose units are the finial products of oligomer reactions and cannot be further dissolved. In Equation (4), v_κ and $y_S(l)$ are related to their corresponding total concentrations u_κ and $x_S(l)$. The relationships are written as

$$u_\kappa = v_\kappa + \sum_{\mu,\sigma} z_{\kappa,\mu,\sigma} + \sum_l z_\kappa(l) \tag{5}$$

$$x_S(l) = y_S(l) + \sum_\kappa z_\kappa(l) \tag{6}$$

$z_{\kappa,\mu,\sigma}$ is the concentration of enzyme-substrate complexes formed by type-μ bond sites and type-κ enzyme molecules on class-σ SAC surfaces. Equations (5) and (6) can be used to

find the expressions of v_κ and $y_S(l)$ as functions of u_κ and $x_S(l)$ respectively, which are written as

$$v_\kappa = \frac{u_\kappa}{1+\sum_{\mu,\sigma} L_{\kappa,\mu} \cdot y_{\mu,\sigma} + \sum_l I_\kappa(l) \cdot y_S(l)} \tag{7}$$

$$y_S(l) = \frac{x_S(l)}{1+\sum_\kappa I_\kappa(l) \cdot v_\kappa} \tag{8}$$

where $y_{\mu,\sigma}$ is the concentration of free type-μ sites on glucan chains exposed on class-σ SAC surfaces, $L_{\kappa,\mu}$ is the adsorption coefficient between type-κ cellulase molecules and type-μ sites on glucan chains. Then the more detailed expressions of $R_S(l)$ can be obtained by combining Equations (3), (4), (7) and (8).

2.2.3 Enzymatic thermal deactivation and inactive adsorption

Many experiments illustrated that even after alleviating the inhibition effects mostly, the rate of enzymatic hydrolysis of cellulose still decreases during hydrolysis, meaning that inhibition effect is not the only rate-limiting factor (Bansal et al., 2009; Levine et al., 2010). Many studies considered the process of cellulases losing activities as a contributing factor to the hydrolysis rate slow-down, which was called enzyme decay process and often modeled as a first order process (Bansal et al., 2009; Levine et al., 2010). Enzyme decay process naturally happen to all hydrolytic enzymes based on experimental observations (Hong et al., 2007; Yang et al., 2006). In principle, the enzyme decay will make the enzymes lose their hydrolytic capability through two possible meanings according to the specific structure of enzymes. Most of the hydrolytic enzymes contain a carbohydrate binding domain and a catalytic domain. Typically, these two domains are away from each

other and connected by a long segment of linker sequence. Some enzymes, however, only contain a catalytic core domain, such as *T. reesei* EG III (Cel12A), which bind to substrate through the substrate-binding sites in the catalytic core domain. So if the carbohydrate binding domains or the substrate-binding sites are deactivated, hydrolytic enzymes will lose the capability of binding to the cellulosic substrate chain sites. On the other hand, if the catalytic domain is deactivated, hydrolytic enzymes are still able to bind to substrate chain sites, but will not carry out the subsequent catalytic reactions.

We incorporated into the model these two different mechanisms, which are referred to as the model the enzymatic thermal deactivation and the enzymatic inactive adsorption, respectively. We defined the enzymatic thermal deactivation in the model as the process that the binding domains or sites of cellulase molecules kept losing the ability to adsorb on glucan chains during hydrolysis. By contrast, we defined enzymatic inactive adsorption in the model as the process that the catalytic domains of all cellulases kept losing the reactivity to cut glucan chains after adsorbing on the substrate. For a single cellulase molecule, the binding and catalyzing abilities could keep losing simultaneously. The decay processes of cellulase may be caused by the affection of temperature during hydrolysis, since each type of enzymes has its own optimal temperature to work efficiently for certain period of time.

The enzyme decay factor D_κ is set to $D_\kappa = (0.5)^{t/T_{1/2,K}}$ in the model for type-κ enzyme molecules where $T_{1/2,K}$ is the half-life for type-κ enzyme molecules, which represent the time for an enzyme lost half of its enzymatic activity. We apply the decay factor D_κ to parameters u_κ and $z_{\kappa,\mu,\sigma}$ to represent the processes of enzymatic thermal deactivation and

enzymatic inactive adsorption respectively and test the impact range of enzyme decay on the cellulose hydrolysis kinetics.

2.2.4 Model parameters

The specific activity and adsorption equilibrium coefficients of Endo-glucanase (EG1) and Exo-glucanases including Cellobiohydrolase I and II (CBH I and II) are from the work by (Zhang and Lynd, 2006). For beta-glucanase (BG), the values of adsorption and kinetics parameters describing the reactions with oligomers are from the literature (Chauve et al., 2010; Yazaki et al., 1997). In the model, the values κ=1, 2, 3 and 4 represent EG1, CBH II, CBH I and BG. The mass ratio of EG1:CBHI:CBHII in the commercial enzyme Spezyme CP was 0.17:0.24:0.13 (Nagendran et al., 2009). The values of inhibition parameters are from various literature sources (Levine et al., 2010; Lo Leggio and Pickersgill, 1999; Tolan and Foody, 1999) due to the fact that we considered several different inhibition effects involving 4 different types of cellulases (EG1, CBHI, CBHII and BG) and 6 types of oligomers from glucose (G1) to cellohexaose (G6). The half-life of all kinds of cellulases was set to 42.5h as reported in the work of Drissen et al. (2007). The substrate and enzyme loadings were set based on the experimental data (Hong et al., 2007; Yang et al., 2006).

2.3 Results and Discussion

2.3.1 Testing cellulosic substrate accessibility

In this section, we investigate the effect of enzymatic accessibility of cellulosic substrates. In the work of Zhou et al. (2009a), the initial value of F_A for Avicel, that is, the

ratio of enzyme-accessible glucose units to the total number of glucose units in Avicel was set to 0.00620, which was originally described in the work of Zhang and Lynd (2004). Not until recently, Hong et al. (2007) determined that the value of F_A for Avicel should be 0.00232 from the experiments testing the adsorption of fluorescent cellulase-like molecules on the substrate surface. We test some new values of F_A and compare the new simulation results with the original ones from the work of Zhou et al. (2010). The experimental data (Hong et al., 2007; Yang et al., 2006) was used in the work of Zhou et al. (2010) to compare their simulation results, and will be adopted in this work.

Figure 2.1 clearly shows that increasing the enzymatic accessibility for substrate prior to hydrolysis could allow more enzyme molecules attack the bonds on glucan chains and thus increase the hydrolysis rate and finial conversion level of substrate. Substrate accessibility in hydrolysis is believed to govern the entire hydrolysis process and act as a critical rate-affecting factor during hydrolysis. The previous initial value 0.00620 for F_A was obtained based on the nitrogen BET measurements. In the process of such adsorption-based measurements, nitrogen was usually used to test the initial accessible surface area of substrate. However, since nitrogen molecules are much smaller than enzyme molecules, and the substrate need to be in dry conditions, the value is probably overestimated and thus not accurate. Hong et al. (2007) determined the accessible surface area of cellulosic substrate by testing the adsorption of molecules containing fluorescent proteins and cellulose-binding modules (CBMs), which had similar size as cellulases could be quantitatively tested. However, the value 0.00232 may be underestimated due to the fact that only one type of cellulose-binding module was used to create cellulase-like molecules.

Recently, Levine et al. (2010) pointed out in their work that the initial value of F_A from the work of Hong et al. (2007) might be underestimated. Based on their estimation by using the Random Sequential Adsorption (RSA) simulation process, the initial accessible surface area of Avicel should be at least $3.5 m^2 g^{-1}$, meaning that initial value of F_A should be 0.00341 for Avicel. We believe that the initial value of F_A should be set between 0.00232 and 0.00620 so that 0.00341 is more accurate and will be used in next sections. The parameter of cellulosic substrate accessibility is critical and reflects the cellulase-accessible surface area. However, it was estimated that during the early stage of hydrolysis the substrate accessibility could either decrease or increase if using different substrate morphologies (Zhou et al., 2009a), remaining the impact of substrate accessibility on the hydrolysis rate unclear. Most of the experiments only tested the value of substrate accessibility at the beginning and the end of hydrolysis and did not keep track of its changing through the entire process. So in order to better understand the role of substrate accessibility, it is highly recommended to test substrate accessibility at different time points during hydrolysis. By using smaller initial values for F_A, the new hydrolysis rates are a little slower than the original ones but still could not capture the full extent of the hydrolysis rate decreases shown in the experimental data. The enormous differences between the simulation results and experimental data also indicate that only considering substrate morphology as hydrolysis rate-limiting factor is not enough to reproduce the kinetics slow-down phenomenon during the process of enzymatic hydrolysis of cellulose. More hydrolysis rate-limiting factors, such as oligomer inhibition, should be considered when constructing a model of enzymatic hydrolysis of cellulose.

2.3.2 Oligomer reactions

In this section, we demonstrate the simulation results after considering the oligomer reactions in solution without inhibition effects. In the work of Zhou et al. (2009b), the reactions involving beta-glucanases were not concerned. Although the main rate-limiting steps of the cellulose hydrolysis process is the reactions that endo- and exo-glucanases depolymerize insoluble long glucan chains into soluble oligomers, the changes of oligomers in solution could also affect the hydrolysis kinetics in turn and thus could not be ignored.

Figure 2.2 shows the comparison of final conversion level of cellulosic substrate between simulations considering and not considering oligomer reactions in solution. As we expected, there is no difference of simulation results after incorporating oligomer reactions. Because the conversion level describe the ratio of the total amount of dissolved substrate to the initial amount of substrate. According to the mass balance, although the amount of each type of oligomer will be changed after considering oligomer reaction, the total amount of soluble substrate should be the same as that considers no oligomer reaction. In Figures 2.3 and 2.4, differences are illustrated for cello-oligomers during hydrolysis, indicating that if considering oligomer inhibition effects, simulation results taking into account the oligomer reactions will be more accurate.

2.3.3 Inhibition effects

In this section, we demonstrate the simulation results after considering the oligomer reactions in solution and all kinds of competitive inhibition effects between 4 types of

cellulases and 6 types of cello-oligomers. As shown in Figure 2.5, after incorporating both the oligomer reactions and inhibitions, the simulation results can capture some extent of the decrease in the rate of cellulose hydrolysis often observed in experiments, showing that inhibition is one of the critical factors contributing to the phenomenon of hydrolysis rate slow-down.

However, the process of inhibition still remains to elucidate in more details. Although we considered all kinds of competitive inhibitions that could possibly happen in solution during enzymatic hydrolysis, it still might exist other types of inhibition relationships, such as uncompetitive inhibitions of cellobiose which can not only bind free cellulase molecules but also EO or ES complexes. Deeper understanding of the inhibitions during cellulose hydrolysis is needed to improve the kinetic models.

2.3.4 Enzyme decay and the slow-down of enzymatic hydrolysis kinetics

In order to reproduce the phenomenon of hydrolysis rate slow-down, we first test the enzymatic decay factor in the model. It is clear that only considering the inhibition effect during hydrolysis is not enough to investigate the rate decrease of enzymatic hydrolysis of cellulose. Similar view was given in the work of Levine et al. (2010) where they tried to fit the data by using much shorter estimated half-life values for cellulases. Here, we use the experimentally-determined half-life values for all the 4 types of cellulases in the model, and test the impact range between enzymatic thermal deactivation and enzymatic inactive adsorption on the hydrolysis kinetics. As shown in Figure 2.6 the impacts of enzymatic thermal deactivation and enzymatic inactive adsorption on the hydrolysis rate are very close to each other, probably because they are both reflecting the affection of temperature

on the rate of hydrolysis. Also, both the impacts of enzymatic thermal deactivation and enzymatic inactive adsorption are weaker than the impact of the inhibition effects if comparing the results in Figures 2.5 and 2.6, indicating that inhibition is the prime factor contributing to the decrease in the rate of hydrolysis. After combining all the possible factor that cause the hydrolysis rate slow-down, the simulation results can agree with the experimental data very well in Figure 2.7, which indicate that considering inhibition and enzyme decay together in the model of enzymatic hydrolysis of cellulose can capture the full extent of the rate decrease phenomenon during the hydrolysis process. In order to enhance the hydrolysis rate and the conversion level of cellulosic substrate, a route is to increase the loading or improve the specific activities of cellulases. However, increasing the amount of cellulases will causes a huge waste of cellulase since only a small part of free cellulase molecules could adsorb onto the substrate and as hydrolysis proceeds all the cellulase molecules will decay and gradually lose the abilities of binding and catalyzing. Besides, since the oligomer inhibition effects impact the hydrolysis rate more than other rate-limiting factors as discussed before, highly efficient cellulases may increase the rate in the early stage of hydrolysis but will unavoidably end up with binding oligomers and could not enhance the conversion level too much. So a better approach would be to add cellulases of small loading at different time points during hydrolysis with substrate filtered from the original solution into another reactor. This approach can theoretically reduce the impact of inhibition and keep the high efficiency of cellulases which need to be further tested by experiments.

Mechanistic modeling the entire process of enzymatic hydrolysis of cellulose is a challenging work. The big differences probably come from two sources: (1) the parameters

used may not be accurate or may not be considered constants along the entire hydrolysis process (i.e. could be functions of time and operational conditions); and (2) there are some other factors that have not been taken into account, for example, lignin effect. Nevertheless, our work in the paper shows that when more affecting factors are considered reasonably, the mechanistic modeling results can be improved, and the simulated trends agree very well with the experimental data which imply that the modeling has captured the intrinsic characteristics of the hydrolysis.

2.4 Conclusions

We have developed a detailed modeling framework for enzymatic hydrolysis of cellulose. The model for the first time not only consider the main hydrolysis step where long insoluble glucan chains are hydrolyzed by endo- and exo-glucanases on the surface of solid substrate, but also the reactions in solution which involve beta-glucanases and oligomers released from the conversion process of insoluble glucan chains. To investigate the phenomenon of hydrolysis rate slow-down often reported in the literature, the model considers the competitive inhibition effects of all possible cello-oligomers on cellulases and two theoretical enzyme decay processes, which are enzymatic thermal deactivation and the enzymatic inactive adsorption.

By using the model, we have presented analyses for the role of enzymatic accessibility of cellulosic substrate. As the enzyme-accessible surface area increases, both the hydrolysis rate and the finial conversion level of substrate could increase, showing that the enzymatic accessibility is a critical rate-limiting factor during the entire process of hydrolysis. After incorporating the reactions involving beta-glucanases and oligomers in solution and

inhibition effects by oligomers, the simulation results can capture some extent of the decrease in the rate of cellulose hydrolysis often observed in experiments. We have tested the impacts of enzymatic thermal deactivation and the enzymatic inactive adsorption on the rate of hydrolysis and found the impacts of the two enzyme decay processes are very close to each other. We have presented detailed investigation of the phenomenon of hydrolysis rate slow-down. From the simulation results, we have found that inhibition effect of oligomer and enzyme decay are both critical factors contributing to the kinetics slow-down phenomenon during the process of enzymatic hydrolysis of cellulose.

Nomenclature

D_κ: decay factor of type-κ enzymes

F_A: enzymatic accessibility of cellulosic substrates

$I_\kappa(l)$: oligomer adsorption coefficient for (κ, l) EO complexes (1/mM)

k, k': number of glucose units contained in a glucan chain

l : chain length, equal to the number of glucose units contained in a glucan chain

l_S: minimum insoluble chain length for glucan chains, =7

$L_{\kappa,\mu}$: substrate adsorption coefficient for (κ, μ) ES complexes (1/mM)

$R_S(l)$: changing rate of soluble oligomers in solution contained l glucose units

$R_{S,\sigma}(l)$: production rate of soluble oligomers contained l glucose units dissolved from glucan chains exposed on class-σ SAC surfaces (mM/min)

$T_{1/2,K}$: half-life of type-κ enzymes (min)

u_κ: total concentration of type-κ enzymes (mM)

v_κ: concentration of free type-κ enzymes in solution (mM)

$x_{S,\sigma}$: total concentration of glucose units dissolved from glucan chains exposed on class-σ SAC surfaces (mM)

$x_S(l)$: concentration of oligomers dissolved from glucan chains containing l glucose units

$y_{\mu,\sigma}$: concentration of free type-μ sites on glucan chains exposed on class-σ SAC surfaces (mM)

$y_S(l)$: concentration of free oligomers dissolved from glucan chains containing l glucose units

$z_{\kappa,\mu,\sigma}$: concentration of (κ, μ) ES complexes exposed on class-σ SAC surfaces (mM)

$z_\kappa(l)$: concentration of (κ, l) EO complexes formed by type-κ enzymes and oligomers containing l glucose units (mM)

κ: index of enzyme types

$\gamma_\kappa(l)$: cutting rate coefficient for (κ, l) EO complexes (1/min)

μ, μ': index of site types

σ: index of SAC classes

Tables

Table 2.1 Parameters used in the model

Parameter	Value	Units	Source
$L_{1,N}$ $L_{1,X}$ $L_{1,Y}$	3	1/mM	(Zhang and Lynd, 2006; Zhou et al., 2009)
$L_{2,X}$ $L_{2,Y}$	4	1/mM	(Zhang and Lynd, 2006; Zhou et al., 2009)
$L_{3,N}$ $L_{3,X}$ $L_{2,N}$ $L_{2,Y}$	0	1/mM	(Zhang and Lynd, 2006; Zhou et al., 2009)
$\gamma_{1,N}$ $\gamma_{1,X}$ $\gamma_{1,Y}$	23.5	1/min	(Zhang and Lynd, 2006; Zhou et al., 2009)
$\gamma_{2,X}$	10.6	1/min	(Zhang and Lynd, 2006; Zhou et al., 2009)
$\gamma_{3,Y}$	6.2	1/min	(Zhang and Lynd, 2006; Zhou et al., 2009)
$\gamma_{3,N}$ $\gamma_{3,X}$ $\gamma_{2,N}$ $\gamma_{2,Y}$	0	1/min	(Zhang and Lynd, 2006; Zhou et al., 2009)
$I_1(1)$	0.06	1/mM	(Levine et al., 2010)
$I_2(1)$ $I_3(1)$	0.032	1/mM	(Levine et al., 2010)
$I_1(2)$ $I_2(2)$ $I_3(2)$	0.13	1/mM	(Tolan and Foody, 1999)
$I_1(3)$ $I_2(3)$ $I_3(3)$	0.3	1/mM	(Lo Leggio and Pickersgill, 1999; Tolan and Foody, 1999)
$I_1(4)$ $I_2(4)$ $I_3(4)$	0.37	1/mM	(Lo Leggio and Pickersgill, 1999; Tolan and Foody, 1999)
$I_1(5)$ $I_2(5)$ $I_3(5)$	0.44	1/mM	(Lo Leggio and Pickersgill, 1999; Tolan and Foody, 1999)
$I_1(6)$ $I_2(6)$ $I_3(6)$	0.51	1/mM	(Lo Leggio and Pickersgill, 1999; Tolan and Foody, 1999)
$I_4(1)$	0.294	1/mM	(Yazaki et al., 1997)

$\boldsymbol{I_4(2)}$	1.136	1/mM	(Chauve et al., 2010; Yazaki et al., 1997)
$\boldsymbol{I_4(3)}$	3.846	1/mM	(Chauve et al., 2010; Yazaki et al., 1997)
$\boldsymbol{I_4(4)}$	4.000	1/mM	(Chauve et al., 2010; Yazaki et al., 1997)
$\boldsymbol{I_4(5)}$	2.174	1/mM	(Chauve et al., 2010; Yazaki et al., 1997)
$\boldsymbol{I_4(6)}$	1.449	1/mM	(Chauve et al., 2010; Yazaki et al., 1997)
$\boldsymbol{\gamma_4(1)}$	0	1/min	This work
$\boldsymbol{\gamma_4(2)}$	1897	1/min	(Yazaki et al., 1997)
$\boldsymbol{\gamma_4(3)}$	1738.9	1/min	(Chauve et al., 2010; Yazaki et al., 1997)
$\boldsymbol{\gamma_4(4)}$	1422.8	1/min	(Chauve et al., 2010; Yazaki et al., 1997)
$\boldsymbol{\gamma_4(5)}$	895.8	1/min	(Chauve et al., 2010; Yazaki et al., 1997)
$\boldsymbol{\gamma_4(6)}$	843.1	1/min	(Chauve et al., 2010; Yazaki et al., 1997)

Figures

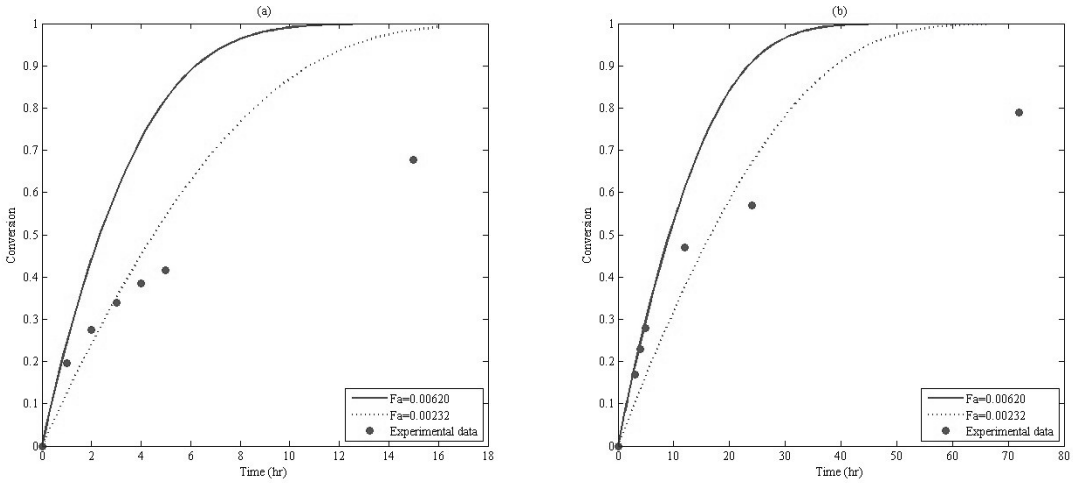

Figure 2.1 Simulation results using different initial values of F_A compared with experimental data. The substrate and enzyme have initial properties of (**a**) 20 g/L Avicel and 4.1 g/L Spezyme CP and (**b**) 10 g/L Avicel and 0.51 g/L Spezyme CP together with 30 IU beta-glucanase/g Avicel (57.69 mg/L beta-glucanase)

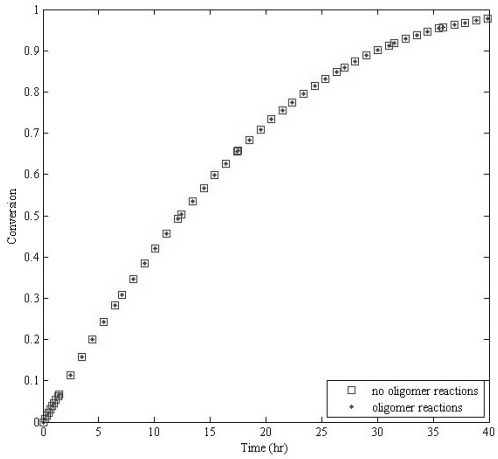

Figure 2.2 Simulation results of finial conversion level with and without consideration of oligomer reactions in solution. The substrate and enzyme have initial properties of 10 g/L Avicel and 0.51 g/L Spezyme CP together with 30 IU beta-glucanase/g Avicel (57.69 mg/L beta-glucanase)

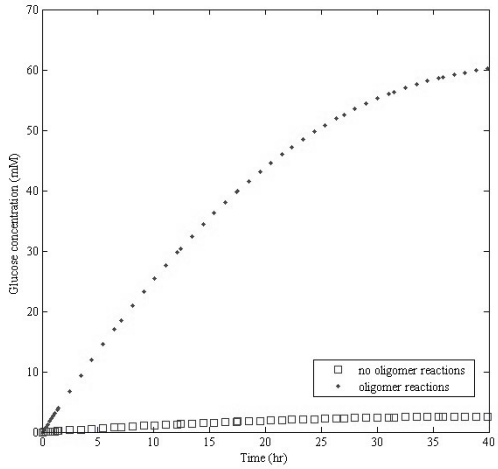

Figure 2.3 Simulation results of glucose concentration with and without consideration of oligomer reactions in solution. The substrate and enzyme have initial properties of 10 g/L Avicel and 0.51 g/L Spezyme CP together with 30 IU beta-glucanase/g Avicel (57.69 mg/L beta-glucanase)

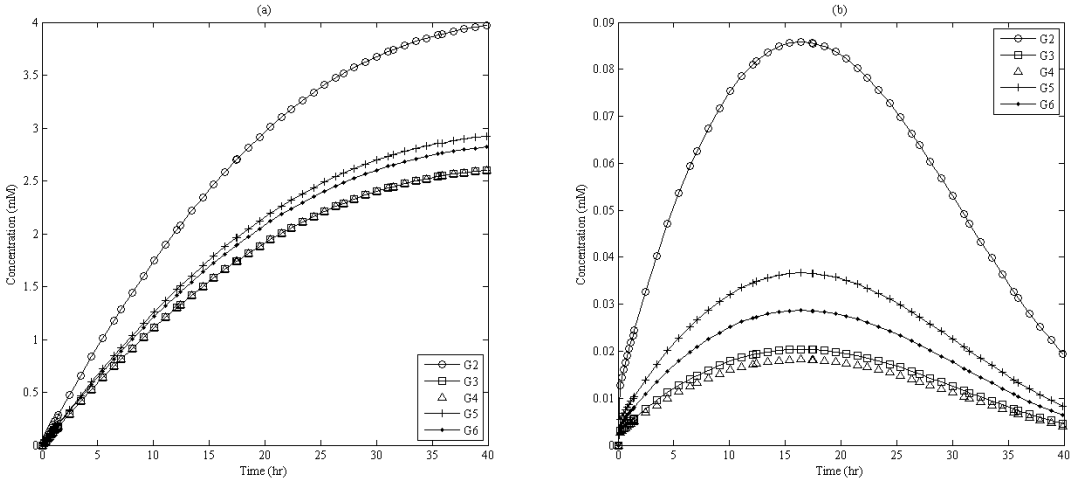

Figure 2.4 Simulation results of oligomer concentrations (**a**) without and (**b**) with consideration of oligomer reactions in solution. The substrate and enzyme have initial properties of 10 g/L Avicel and 0.51 g/L Spezyme CP together with 30 IU beta-glucanase/g Avicel (57.69 mg/L beta-glucanase)

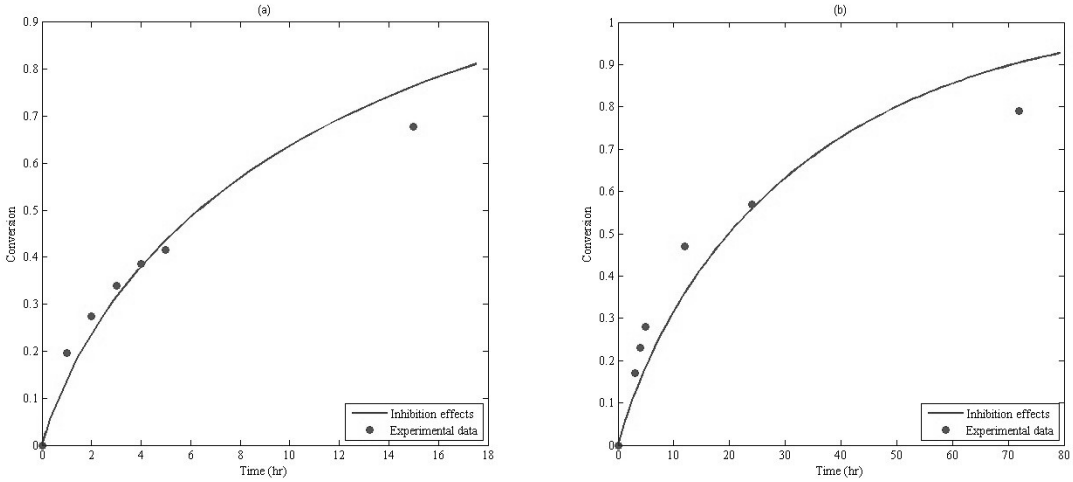

Figure 2.5 Simulation results considering oligomer reactions and inhibitions compared with experimental data. The substrate and enzyme have initial properties of (**a**) 20 g/L Avicel and 4.1 g/L Spezyme CP and (**b**) 10 g/L Avicel and 0.51 g/L Spezyme CP together with 30 IU beta-glucanase/g Avicel (57.69 mg/L beta-glucanase)

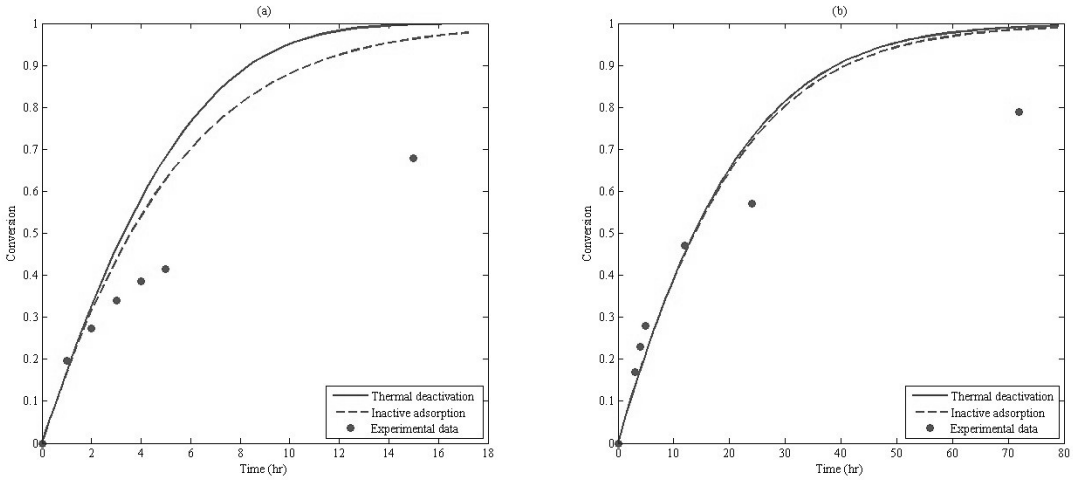

Figure 2.6 Simulation results considering different enzyme decay factors compared with experimental data. The substrate and enzyme have initial properties of (**a**) 20 g/L Avicel and 4.1 g/L Spezyme CP and (**b**) 10 g/L Avicel and 0.51 g/L Spezyme CP together with 30 IU beta-glucanase/g Avicel (57.69 mg/L beta-glucanase)

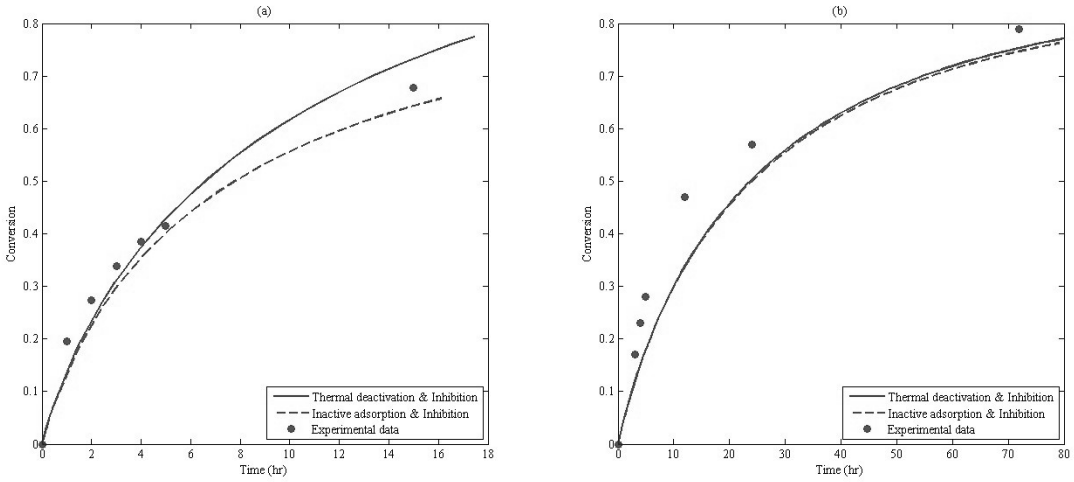

Figure 2.7 Simulation results considering all rate-limiting factors compared with experimental data. The substrate and enzyme have initial properties of (**a**) 20 g/L Avicel and 4.1 g/L Spezyme CP and (**b**) 10 g/L Avicel and 0.51 g/L Spezyme CP together with 30 IU beta-glucanase/g Avicel (57.69 mg/L beta-glucanase)

References

Bansal, P., Hall, M., Realff, M. J., Lee, J. H. and Bommarius, A. S. 2009. "Modeling cellulase kinetics on lignocellulosic substrates." Biotechnology advances 27(6): 833-848.

Chauve, M., Mathis, H., Huc, D., Casanave, D., Monot, F. and Lopes Ferreira, N. 2010. "Comparative kinetic analysis of two fungal beta-glucosidases." Biotechnology for biofuels 3(1): 3.

Drissen, R. E. T., Maas, R. H. W., Van Der Maarel, M. J. E. C., Kabel, M. A., Schols, H. A., Tramper, J. and Beeftink, H. H. 2007. "A generic model for glucose production from various cellulose sources by a commercial cellulase complex." Biocatalysis and Biotransformation 25(6): 419-429.

Griggs, A. J., Stickel, J. J. and Lischeske, J. J. 2012a. "A mechanistic model for enzymatic saccharification of cellulose using continuous distribution kinetics I: depolymerization by EGI and CBHI." Biotechnol Bioeng 109(3): 665-675.

Griggs, A. J., Stickel, J. J. and Lischeske, J. J. 2012b. "A mechanistic model for enzymatic saccharification of cellulose using continuous distribution kinetics II: cooperative enzyme action, solution kinetics, and product inhibition." Biotechnol Bioeng 109(3): 676-685.

Hong, J., Ye, X. and Zhang, Y. H. 2007. "Quantitative determination of cellulose accessibility to cellulase based on adsorption of a nonhydrolytic fusion protein containing CBM and GFP with its applications." Langmuir 23(25): 12535-12540.

Hosseini, S. A. and Shah, N. 2011a. "Enzymatic hydrolysis of cellulose part II: Population balance modelling of hydrolysis by exoglucanase and universal kinetic model." Biomass and Bioenergy 35(9): 3830-3840.

Hosseini, S. A. and Shah, N. 2011b. "Modelling enzymatic hydrolysis of cellulose part I: Population balance modelling of hydrolysis by endoglucanase." Biomass and Bioenergy 35(9): 3841-3848.

Levine, S. E., Fox, J. M., Blanch, H. W. and Clark, D. S. 2010. "A mechanistic model of the enzymatic hydrolysis of cellulose." Biotechnol Bioeng 107(1): 37-51.

Levine, S. E., Fox, J. M., Clark, D. S. and Blanch, H. W. 2011. "A mechanistic model for rational design of optimal cellulase mixtures." Biotechnol Bioeng 108(11): 2561-2570.

Lo Leggio, L. and Pickersgill, R. W. 1999. "Xylanase-oligosaccharide interactions studied by a competitive enzyme assay." Enzyme and Microbial Technology 25(8-9): 701-709.

Nagendran, S., Hallen-Adams, H. E., Paper, J. M., Aslam, N. and Walton, J. D. 2009. "Reduced genomic potential for secreted plant cell-wall-degrading enzymes in the ectomycorrhizal fungus Amanita bisporigera, based on the secretome of Trichoderma reesei." Fungal Genetics and Biology 46(5): 427-435.

Sharma, R. 2012. "Enzyme Inhibition: Mechanisms and Scope, Enzyme Inhibition and Bioapplications." Prof. Rakesh Sharma (Ed.).

Tolan, J. S. and Foody, B. 1999. "Cellulase from submerged fermentation." Advances in Biochemical Engineering/Biotechnology 65: 41-67.

Yang, B., Willies, D. M. and Wyman, C. E. 2006. "Changes in the enzymatic hydrolysis rate of Avicel cellulose with conversion." Biotechnol Bioeng 94(6): 1122-1128.

Yazaki, T., Ohnishi, M., Rokushika, S. and Okada, G. 1997. "Subsite structure of the beta-glucosidase from Aspergillus niger, evaluated by steady-state kinetics with cello-oligosaccharides as substrates." Carbohydrate Research 298(1-2): 51-57.

Zhang, Y. H. and Lynd, L. R. 2004. "Toward an aggregated understanding of enzymatic hydrolysis of cellulose: noncomplexed cellulase systems." Biotechnol Bioeng 88(7): 797-824.

Zhang, Y. H. and Lynd, L. R. 2006. "A functionally based model for hydrolysis of cellulose by fungal cellulase." Biotechnol Bioeng 94(5): 888-898.

Zhou, W., Hao, Z., Xu, Y. and Schuttler, H. B. 2009a. "Cellulose hydrolysis in evolving substrate morphologies II: Numerical results and analysis." Biotechnol Bioeng 104(2): 275-289.

Zhou, W., Schuttler, H. B., Hao, Z. and Xu, Y. 2009b. "Cellulose hydrolysis in evolving substrate morphologies I: A general modeling formalism." Biotechnol Bioeng 104(2): 261-274.

Zhou, W., Xu, Y. and Schuttler, H. B. 2010. "Cellulose hydrolysis in evolving substrate morphologies III: time-scale analysis." Biotechnol Bioeng 107(2): 224-234.

Chapter 3 On a Novel Mechanistic Model for Simultaneous Enzymatic Hydrolysis of Cellulose and Hemicellulose Considering Morphology[2]

[2] Published in *Biotechnology and Bioengineering*

Reprinted with permission from (Zhang Y, Xu B, Zhou W. 2014 "On a novel mechanistic model for simultaneous enzymatic hydrolysis of cellulose and hemicellulose considering morphology." Biotechnology and Bioengineering, 111, 1767-1781). © 2014 Wiley Periodicals, Inc.

See Appendix for documentation of permission to republish this material

Abstract

We develop a novel and general modeling framework for enzymatic hydrolysis of cellulose and hemicellulose simultaneously. Our mechanistic model, for the first time, takes into consideration explicitly the time evolution of morphologies of intertwining cellulose and hemicelluloses within substrate during enzymatic hydrolysis. This morphology evolution is driven by hydrolytic chain fragmentation and solubilization, which is, in turn, profoundly affected by the substrate morphology. We represent the substrate morphology as a randomly distributed Smallest Accessible compartments (SACs) which are described by geometric functions to track total volume and exposed surface substrate materials, including both cellulose and hemicelluloses. Our morphology-plus-kinetics approach then couple the time-dependent morphology with chain fragmentation and solubilization resulting from enzymatic reactions between various bonds in cellulose and hemicelluloses and a mixture (i.e. endo-, exo- and oligomer- acting) of cellulases and hemicellulases. In addition, we propose an advanced and generalized site concentration formalism that considers different polysaccharide chain types and different monomer unit types on chains. The resulting ODE system has a substantially reduced size compared to conventional chain concentration formalism. We present numerical simulation results under real enzymatic hydrolysis experimental conditions from literature. The comparisons between the simulation results and the experiment measurements demonstrate effectiveness and wide applicability of the proposed mechanistic model.

3.1 Introduction

Cellulose and hemicelluloses are the major polysaccharides existing in the cell wall of woods, straws, grasses and other natural plants on the earth. The amount of cellulose and hemicelluloses are, respectively, about 33%-51% and 25%-39% of the dry weight of plants (Sjöström, 1993; Sun et al., 2004). Both Cellulose and hemicelluloses have been recognized as important renewable energy sources due to their abundance and potential to produce biofuels.

The mechanism of enzymatic hydrolysis of cellulose and hemicelluloses is not well understood due to the complexity of the enzyme system and structural and morphological heterogeneity of the substrate. During the last 40 years, a great number of kinetic models have been developed in order to better understand the mechanism and to facilitate the experimental studies of enzymatic hydrolysis of cellulose (see Zhang and Lynd, 2004 for detailed review). A majority of these models are either non-mechanistic or semi-mechanistic models which are mainly used in data fitting (Zhang and Lynd, 2004). More recently, studies have been focused on the development of detailed mechanistic models for enzymatic hydrolysis of cellulose (Griggs et al., 2012a, b; Levine et al., 2010; Zhou et al., 2009a; Zhou et al., 2009b; Zhou et al., 2010). These models involved more than one substrate and/or enzyme variable and described the mechanisms of hydrolysis in detail. Most importantly, they avoided the unrealistic simplification in the past that viewed cellulose as an assembly of isolated glucan chains without obstructive interactions, so that most of the glucan chains are initially inaccessible to enzymes and gradually become accessible by hydrolytic removal of overlaying glucan chains. These mechanistic models

not only provide tools for studying the reaction mechanisms involved in enzymatic hydrolysis process, but also have potential utilities for industrial process design and enzymatic system optimization.

On the other hand, the development of detailed mechanistic model considering enzymatic hydrolysis of hemicelluloses is much less advanced, regardless of the equal importance of hemicellulose to biofuel production. By now, only a few models of enzymatic hydrolysis of hemicelluloses have been developed (Belkacemi and Hamoudi, 2003; Feng et al., 2003; Harjunpaa et al., 1995; Liu et al., 2012). Most of the models were only considering one certain group of hemicelluloses and obviously cannot be used to predict the conversion of plant materials that usually contain several groups of hemicelluloses with different structural characteristics of backbones and side-groups. Furthermore, to our best knowledge, there exists no mechanistic model that takes consideration of both cellulose and hemicelluloses simultaneously during enzymatic hydrolysis. While for hydrolysis of substrate where a large percentage of the hemicelluloses could have already been removed by pretreatment techniques, the need for such comprehensive model is less obviously urgent, the major reason of absence of the model is probably due to much higher mathematic complexity caused by the large variation of hemicelluloses and their complicated structural interactions with cellulose.

In this work, we develop a detailed mechanistic model for simultaneous enzymatic hydrolysis of cellulose and hemicelluloses, considering the substrate morphologies and their coupling with morphology-depended substrate hydrolysis kinetics. The cellulose and hemicellulose hydrolysis, i.e. chain fragmentation and solubilization, also significantly

influence the concurrent hydrolysis-driven evolution of the substrate morphology. We extend the concept of smallest accessible compartment (SAC) as a minimal volume by external and internal surfaces exposed to enzyme-accessible hydrated interior voids of the solid substrate material with consideration of intertwining between hemicellulose and cellulose chains. In addition, an advanced site representation formalism of enzyme hydrolytic fragmentation coupled with morphology evolution is introduced. The new formalism considers all bond sites, which can be attacked by a variety of hydrolytic enzymes, between monomer units of both cellulose chains and various hemicellulose chains. This model is developed in full generality to present a replication of real-world hydrolysis and allows us to predict the enzymatic accessibility and conversion level for both hemicellulose and cellulose within substrates.

3.2 Methodology

3.2.1 Morphology of substrate containing hemicellulose and cellulose

Cellulose is known as a composite of linear glucan chains whose backbone is only composed of D-glucose units linked to each other by β-(1, 4)-glycosidic bonds. Cellulose exists in most of the plant species on the earth and differs in degree of polymerization (Zhang and Lynd, 2004). Unlike cellulose, hemicelluloses are a group of polysaccharides varying in the composition and the degree of polymerization. Based on the characteristics of backbones hemicelluloses can be categorized into several groups in which the most predominant ones are mannans and xylans (Tenkanen, 2004). The backbone of mannans is a linear or slightly branched chain composed of β-(1, 4)-linked D-mannose units and D-glucose units. Other monomer units, mainly D-galactose units, usually attach on the

backbones as side groups. The backbones of xylan is composed of β-(1, 4)-linked D-xylose units and also have some monomer units attached as side groups such as L-arabinose units (Sun et al., 2004; Tenkanen, 2004). Some pretreatment of lignocellulosic biomass, such as ammonia fiber expansion, could retain majority of cellulose and hemicellulose, and dissolve and re-distribute lignin (Chundawat et al., 2011). Hereafter, we refer to the substrates, which mainly contain cellulose and hemicellulose with lignin being ignored during hydrolysis, as hemicellulose-cellulosic substrate, as compared to pure cellulosic and ligno-cellulosic substrate.

Within the hemicellulose-cellulosic substrate, all the chains tend to be a dense and spatially correlated organization. Such substrate morphology will unavoidably limit the rate of hydrolysis because a large fraction of chains are initially inaccessible to enzyme molecules and cannot be hydrolyzed. In addition, hemicellulose-cellulosic substrates, like cellulosic substrates, often have larger internal enzyme accessible area than external enzyme accessible area due to the large and sufficiently-distributed pores and cracks within the substrate particles (Weimer et al., 1990). In the work of Zhou et al. (2009b), two concepts, smallest accessible void (SAV) and smallest accessible compartment (SAC), were first proposed and used to describe the morphology of cellulosic substrates. These two concepts can be extended and used here in a way that morphology of substrate containing both cellulose and hemicellulose can be depicted. For hemicellulose-cellulosic substrates, the smallest void that can be invaded by enzyme molecules is called SAV, which could have different sizes for different enzyme species. SAC is defined as a minimal volume of the substrate delimited by enzyme-accessible surfaces which not only contain external surfaces but also internal surfaces from the voids in the interior of the substrate.

Figures 3.1 and 3.2 illustrate a cellulose elementary fibril and hemicelluloses, and respectively the subdivision of a single contiguous hemicellulose-cellulosic substrate particle into SACs by SAVs. Note here we use the 36-chain square shape model only as an example to represent crystalline cellulose elementary fibril and its positional relation with hemicelluloses. While there may have different structural shapes and sizes of elementary fibril, there is no close relationship between the structure and distribution of SAC and shape and size of elementary fibril. As illustrated in Figure 3.2, substrate is composed of a great variety of SACs that represent a random distribution of shapes and sizes including any extremes, that is then modeled with a large but finite number of SAC geometry classes. Our general SAC concept can consider different possible directions of enzyme attack during hydrolysis that is due to the severity of orientational and directional disorder of the cellulose and hemicellulose chains, including but not limited to (1) chains within the SAC exhibit orientational order with all chain ribbon faces oriented approximately parallel to the SAC surface, (2) chains within the SAC are orientationally disordered, but remain directional ordered, with all chain directions aligned approximately parallel, i.e. substrate comprises highly aligned fibers of random chain facial orientations, and (3) chains within the SAC are highly both orientationally and directionally disordered, i.e. substrate is highly amorphous (Zhou et al., 2009b).

As hydrolysis happens, the chains on the surface of SAC is solubilized into solution and the previously buried chains will be exposed to enzyme access, which leads to the shrinkage of SACs. To quantify the substrate morphology evolution, each SAC is further defined in terms of elementary layers, where each layer is a fraction of the given SAC which can be removed from the surface if all the monomer units in the outer layers are

hydrolyzed. Figure 3.3 illustrates the partitioning of an SAC, selected from Figure 3.2, into elementary layers. Each elementary layer is represented by a different value of layer number λ in the way that the highest value represents the outermost one. Notice that the concept of elementary layer is not a real reflection of the layered structure of SAC but only a convenient counting tool to keep track of the amount of monomers either exposed on each SAC surface or contained in its volume at any time during hydrolysis.

To represent the variety of the linear chains and side groups presented in hemicellulose-cellulosic substrate, a finite number of SAC "chain types", such as glucan chain and xylan chain, labeled by ρ is introduced so that x_V, the total concentration of monomer units contained in substrate, and x_M, the total concentration of exposed monomer units on the surfaces of substrate, have such expressions

$$x_V = \sum_\sigma x_{V,\sigma}(\lambda_\sigma) = \sum_\rho x_{V,\rho} = \sum_{\rho,\sigma} x_{V,\rho,\sigma}(\lambda_\sigma) \tag{1a}$$

$$x_M = \sum_\sigma x_{M,\sigma}(\lambda_\sigma) = \sum_\rho x_{M,\rho} = \sum_{\rho,\sigma} x_{M,\rho,\sigma}(\lambda_\sigma) \tag{1b}$$

where $x_{V,\rho,\sigma}$ is the total concentration of monomer units of type-ρ chains contained in the class-σ SACs, and $x_{M,\rho,\sigma}$ is the concentration of monomer units of type-ρ chains exposed on the class-σ SACs. λ is treated as a continuous variable used to keep track of the elementary layers of each SAC, and the indexes σ and ρ describe the sizes of SACs and the chain types contained in SACs respectively. By way of terms shown in Equations (1a) and (1b), four parameters $\Phi_{V,\rho,\sigma}(\lambda_\sigma)$, $\Phi_{M,\rho,\sigma}(\lambda_\sigma)$, $\bar{\Phi}_{V,\rho}$ and $\bar{\Phi}_{M,\rho}$ can be created and expressed as $\Phi_{V,\rho,\sigma}(\lambda_\sigma) = x_{V,\rho,\sigma}(\lambda_\sigma)/x_{V,\sigma}(\lambda_\sigma)$, $\Phi_{M,\rho,\sigma}(\lambda_\sigma) = x_{M,\rho,\sigma}(\lambda_\sigma)/x_{M,\sigma}(\lambda_\sigma)$, $\bar{\Phi}_{V,\rho} = x_{V,\rho}/x_V$ and $\bar{\Phi}_{M,\rho} = x_{M,\rho}/x_M$. Here, $\Phi_{V,\rho,\sigma}(\lambda_\sigma)$ is defined as the native ratio of the total

concentration of monomer units contained in type-ρ chains to those contained in all types of chains of class-σ SACs, and $\Phi_{M,\rho,\sigma}(\lambda_\sigma)$ is defined as the native ratio of the concentration of exposed monomer units contained in the type-ρ chains to those contained in all types of chains of class-σ SACs. $\bar{\Phi}_{V,\rho}$ is defined as the overall fraction of total monomer units contained in type-ρ chains, and $\bar{\Phi}_{M,\rho}$ is defined as the overall fraction of exposed monomer units of type-ρ chains. The SAC geometric functions of hemicellulose-cellulosic substrate are developed in Supporting Information section A and given as

$$\sum_\rho x_{V,\rho,\sigma}(\lambda_\sigma) = B_{V,\sigma}\lambda_\sigma^{d_{A,\sigma}} \tag{2a}$$

$$\sum_\rho x_{M,\rho,\sigma}(\lambda_\sigma) = \sum_\rho x_{V,\rho,\sigma}(\lambda_\sigma) - \sum_\rho x_{V,\rho,\sigma}(\lambda_\sigma - 1)\Theta(\lambda_\sigma - 1) \tag{2b}$$

where $B_{V,\sigma}$ is the molar volume prefactor for class-σ SACs, and $d_{A,\sigma}$ is the ablation dimension factor for class-σ SACs. For all the SAC classes, we set $d_{A,\sigma} = 2$ because all chains within an SAC are believed to exhibit "directional" order directions, as shown in Figure 3.1.

3.2.2 Advanced site concentration formalism

To greatly reduce the large amount of ordinary differential equation variables generated from chain formalism, the site formalism was first proposed and developed for cellulosic substrate hydrolysis in which all glucan chains were treated as a composite of only 6 different types of β-(1,4)-glycosidic bond sites, referred to as N-, O-, X-, Y-, L-, R-sites (Zhou et al., 2009b). The classification of these 6 site types was based on the interactions between β-(1, 4)-glycosidic bonds on pure cellulose chains and 3 cellulase species:

endoglucanase, cellobiohydrolase I and cellobiohydrolase II. For hemicellulose-cellulosic substrate hydrolysis, however, there will be different types of chains possessing different types of monomer units and side groups. Besides, more enzyme species may also be involved during hydrolysis, as show in Table 3.1, making it necessary to develop advanced and generalized site formalism for hemicellulose-cellulosic substrate hydrolysis, as illustrated in Figures 3.4a-b.

First, two parameters are created and labeled by U_i and U_{ij} respectively. U_i denotes the type-i monomer unit and the broken bonds (i.e. left or right ends) belonging to the type-i monomer units, whereas U_{ij} denotes the intact bonds formed by the left ends of type-i monomer units and the right ends of type-j monomer units in which the subscripts "i" and "j" could be the same. Both U_i and U_{ij} are used to describe the diversities of monomer units and bonds contained in the backbones. After incorporating them into the previous six-type bond site formalism for cellulose, the type of sites are expanded and could be categorized into six site groups, referred to as $N_{U_{ij}}$, $X_{U_{ij}}$, $Y_{U_{ij}}$, L_{U_i}, R_{U_i} and O.

Second, considering the side groups, another two parameters are created and labeled by S_i and J_i respectively. S_i denotes the type-i side groups, whereas J_i denotes the type-i side bonds linking the backbones and side groups. So now there are seven groups of site types: $N_{U_{ij}}$, $X_{U_{ij}}$, $Y_{U_{ij}}$, L_{U_i}, R_{U_i}, J_i and O in the new bond site formalism, which can be used to represent any type of chains in hemicellulose-cellulosic substrate, as illustrated by Figures 3.4a-b. The concentration relationship between bond sites and monomer units on the substrate surface is $\sum_{\mu,\rho} \omega_\mu x_{\mu,\rho,\sigma}(t) = x_{M,\sigma}(\lambda_\sigma(t))$, where μ represents any site type, the

weight factor ω_μ represents the fraction of a monomer unit associated to certain site type in backbones, that is, $\omega_\mu = 1$ for intact bond site types $N_{U_{ij}}$, $X_{U_{ij}}$, $Y_{U_{ij}}$ and O; $\omega_\mu = 1/2$ for broken bond site types L_{U_i} and R_{U_i}. For the side bond site types J_i, $\omega_\mu = 1$ is also set to count the side groups.

As hydrolysis proceeds, all types of chains exposed on each SAC surface can be cut by enzymes. The chain length l is defined as the number of monomer units contained in the backbone of a chain. If the length of a type-ρ chain fragment resulting from a cut is less than a certain minimum insoluble length, denoted by $l_{S,\rho}$, then the fragment will immediately be dissolved, which results in the SAC surface layer ablation. So the SAC surfaces changing rate during hydrolytic ablation can be described by a system of coupled rate equations containing two dynamic variables $\lambda_\sigma(t)$ and $x_{\mu,\rho,\sigma}(t)$. The surface layer ablation rate equations are derived in Supporting Information section B and given by

$$\dot{x}_{\mu,\rho,\sigma} = R_{\mu,\rho,\sigma} - \bar{R}_\sigma \eta_\sigma(\lambda_\sigma) \Phi_{M,\rho,\sigma}(\lambda_\sigma - 1) g_{\mu,\rho,\sigma} \tag{3a}$$

$$\dot{\lambda}_\sigma = \bar{R}_\sigma / (B_{V,\sigma} d_{A,\sigma} \lambda_\sigma^{d_{A,\sigma}-1}) \tag{3b}$$

$$\eta_\sigma(\lambda_\sigma) = 1 - \partial_{\lambda_\sigma} x_{M,\sigma}(\lambda_\sigma) / \partial_{\lambda_\sigma} x_{V,\sigma}(\lambda_\sigma) \tag{3c}$$

$$\bar{R}_\sigma = \sum_{\mu,\rho} \omega_\mu R_{\mu,\rho,\sigma} \tag{3d}$$

In Equation (3a), the first term $R_{\mu,\rho,\sigma}$ is the net production rate of type-μ sites due to site fragmentation and the second term $-\bar{R}_\sigma \eta_\sigma(\lambda_\sigma) \Phi_{M,\rho,\sigma}(\lambda_\sigma - 1) g_{\mu,\rho,\sigma}$ is due to native site

exposure from underlying layer as a result of hydrolytic removal of all types of overlaying sites in the surface layer.

The production rate of monomer units dissolved from type-ρ chains of class-σ SACs and the production rate of soluble oligomers originally belonging to type-ρ chains are given by

$$\dot{x}_{S,\rho,\sigma} = \sum_{l=1}^{l_{S,\rho}-1} l R_{S,\rho,\sigma}(l) \tag{4a}$$

$$\dot{x}_{S,\rho}(l) = \sum_{\sigma} R_{S,\rho,\sigma}(l) + R_{S,\rho}(l) \tag{4b}$$

where $R_{S,\rho,\sigma}(l)$ is the production rate of oligomers containing l monomer units ($1 \leq l < l_{S,\rho}$) and dissolved from type-ρ chains exposed on class-σ SAC surfaces. $R_{S,\rho}(l)$ is the changing rate of the oligomers containing l monomer units and dissolved from type-ρ chains, which describes the reactions between oligomers and beta-enzymes in solution. The constructions of $R_{\mu,\rho,\sigma}$ and $R_{S,\rho,\sigma}(l)$ both require (i) the concomitant solutions of the enzyme adsorption and inhibition equilibriums, (ii) the chain fragmentation probabilities and (iii) the enzymatic bond cutting reaction rate coefficients, whereas the construction of $R_{S,\rho}(l)$ only need to consider the enzyme adsorption and inhibition equilibriums as described in Supporting Information section C.

3.2.3 Ablation and oligomer rate equations

In general, cutting a type-μ site belonging to type-ρ chains will change the number of all types of sites belonging to type-ρ chains at SAC surfaces. To describe the sites change, $\Delta\overline{N}_{\mu',\mu,\rho,\sigma}$ is denoted as the mean increment of type-μ' sites per type-μ site being

cut on type-ρ chains exposed on class-σ SAC surfaces. So $R_{\mu',\rho,\sigma}$, that is, the production rate of type-μ' sites resulting from cuts of all site types belonging to type-ρ chains, subject to all enzyme types κ, per class-σ SAC, can be expressed as

$$R_{\mu',\rho,\sigma} = \sum_{\kappa,\mu} \gamma_{\kappa,\mu,\rho} z_{\kappa,\mu,\rho,\sigma} \Delta\bar{N}_{\mu',\mu,\rho,\sigma} \tag{5a}$$

$$\Delta\bar{N}_{\mu',\mu,\rho,\sigma} = \sum_{k=1}^{\infty} \sum_{k'=1}^{\infty} P_{\rho,\sigma}(k,k'|\mu,+1) \Delta N_{\mu',\rho,\sigma}(k,k') \tag{5b}$$

where $\Delta N_{\mu',\rho,\sigma}(k,k')$ is the increment of type-μ' sites that is produced by a bond cut generating a (k,k') type-ρ chain fragment pair, and $P_{\rho,\sigma}(k,k'|\mu,+1)$ is the probability for a randomly selected intact bond of given site type μ to be located k monomer units from the L-end and k' monomer units from the R-end of a type-ρ chain exposed on surface of a class-σ SAC. The detailed expression of $\Delta\bar{N}_{\mu',\mu,\rho,\sigma}$ shown in Supporting Information section F is obtained based on the expressions of $\Delta N_{\mu',\rho,\sigma}(k,k')$ and $P_{\rho,\sigma}(k,k'|\mu,+1)$ from Supporting Information sections D and E.

By definition, the production rate of soluble oligomers $R_{S,\rho,\sigma}(k)$ can be expressed as

$$R_{S,\rho,\sigma}(k) = \sum_{\kappa,\mu} \gamma_{\kappa,\mu,\rho} z_{\kappa,\mu,\rho,\sigma} \sum_{k'=l_{S,\rho}-k}^{\infty} \left[P_{\rho,\sigma}(k,k'|\mu,+1) + P_{\rho,\sigma}(k',k|\mu,+1)\right] \tag{6}$$

which can be simplified into

$$R_{S,\rho,\sigma}(k) = \sum_{\kappa,\mu} \gamma_{\kappa,\mu,\rho} z_{\kappa,\mu,\rho,\sigma} \Delta\bar{N}_{S,\mu,\rho,\sigma}(k) \tag{7}$$

$\Delta\bar{N}_{S,\mu,\rho,\sigma}(k)$ is defined as the production factor of oligomers. The detailed expression of $\Delta\bar{N}_{S,\mu,\rho,\sigma}(k)$ is given in Supporting Information section E which, like the expression of

$\Delta\bar{N}_{\mu',\mu,\rho,\sigma}$ contains the type-ρ chain number probability variable $P_{\rho,\sigma}(l)$ with a few "short" chain lengths up to the cut-off length $l_{C,\rho}$ defined by $l_{C,\rho} \equiv l_{S,\rho} + \max(l_{L,\rho}, l_{R,\rho}) - 2$. The expression of $P_{\rho,\sigma}(l)$ is given by Equation (H.9) as described in Supporting Information section H.

The closed ordinary differential equation (ODE) system for the site concentration formalism now is completed, including Equations (3a-d), (4a-b), (5a-b), (7) and (C.3), (E.10), (F.1), (H.1), (H.6), (H.8) in SI. The independent dynamical variables of this ODE system are $x_{\mu,\rho,\sigma}$, λ_σ and $H_{\rho,\sigma}(l)$ with $l_{S,\rho} \leq l < l_{C,\rho}$. Intermediate variables $z_{\kappa,\mu,\rho,\sigma}$ are evaluated from enzyme adsorption and inhibition equations. In addition, we can obtain the concentrations of dissolved monomer units $x_{S,\rho}(l)$ by solving enzyme adsorption and inhibition equations and oligomer production rate equations together.

3.3 Numerical Simulation Results and Discussion

In this section, numerical simulations are carried out using real experimental conditions, and simulation results are compared with the experimental data from literature. The substrates used in the experiments were either poplar solids or corn stover, where the major type of hemicellulose is xylan. All the experiments used ammonia fiber expansion (AFEX) to pretreat substrate. It has been shown in recent studies that AFEX pretreatment could cut the linkages between lignin and side-groups of hemicelluloses, create pores within the substrate and relocate extractable lignin to the substrate surfaces (Chundawat et al., 2011). In this work, to focus on the interactions between cellulose and hemicelluloses, we assume that after the AFEX pretreatment the blocking effect of lignin can be neglected.

All SACs could be categorized into three groups based on the components contained. The first and the second group of SACs are composed of pure cellulose and pure xylan respectively, while SACs belonging to the third group contain both cellulose and xylan. Xylan, like other hemicelluloses, is believed to have intimate interconnection with cellulose by twisting together the cellulosic microfibrils. However, the detailed structural characteristics about how cellulose and hemicelluloses are spatially organized have still remained unclear. We assume that for each SAC containing both cellulose and xylan, the fraction of monomer units belonging to xylan linearly decreases as follows:

$$\Phi_{M,Xyl,\sigma}(\lambda_\sigma) = \max\left[\frac{\lambda_\sigma - \Lambda_{CO,\sigma}}{\Lambda_\sigma - \Lambda_{CO,\sigma}}\left[\Phi_{M,Xyl,\sigma}(\Lambda_\sigma) - \Phi_{M,Xyl,\sigma}\left(\Lambda_{CO,\sigma}\right)\right] + \Phi_{M,Xyl,\sigma}\left(\Lambda_{CO,\sigma}\right), 0\right] \tag{8}$$

with $1 \leq \Lambda_{CO,\sigma} \leq \Lambda_\sigma$. $\Lambda_{CO,\sigma}$ represents the largest layer of class-σ SACs containing the smallest amount of hemicelluloses. The model requires a variety of kinetic, adsorption and inhibition parameters for enzymes, which are determined from the literature. We assume the initial values for $\bar{\Phi}_{M,Xyl}$ and $\bar{F}_A$ which are the key parameters describing the enzyme accessibilities of cellulose and xylan. The value of $\bar{F}_A$ is decided by adjusting two Gaussian distribution parameters Λ_{Avg} and Λ_{Wid} as shown in Supporting Information section A. Although currently we do not know the experimentally-decided values for these two key parameters, we believe that they could be studied and measured by appropriate methods in the future. All the parameters and their values are shown in Supporting Information section I.

3.3.1 Comparison with experiments in Qing and Wyman (2011b) and investigation of effects of substrate morphology

The total substrate loading was 0.2g of AFEX-treated corn stover in 10 mL reaction volume. The amount of cellulose, and xylan were about 39.6% and 24.5% by weight respectively. Spezyme CP cellulase (CP) (16.1 mg protein/g glucan), Novozyme 188 beta-glucosidase (BG) (3.16 mg protein/g glucan), Multifect xylanase (MX) (16.1 mg protein/g glucan) and a non-commercial beta-xylosidase (BX) (32.2 mg protein/g glucan) were used in the experiments. The commercial enzyme Spezyme CP mainly contained endo-glucanase (EG), cellobiohydrolase II (CBH2), cellobiohydrolase I (CBH1) and endo-xylanase (EX) in mass ratio 0.17:0.13:0.24:0.17 (EG:CBH2:CBH1:EX) (Nagendran et al., 2009). Due to the current lack of the exact compositions of the other three commercial or non-commercial enzymes, simplified compositions are used in the model: (i) MX contains 50% EX (about the same percentage of cellulases in Spezyme CP) and 50% other unknown enzymatic species which are neglected, (ii) BG contains 100% beta-glucosidase, and (iii) BX contains 100% beta-xylosidase. The total amount of debranching enzymes in the commercial enzyme mixture are unknown and are believed to be, if there is any, very small amount, thus the side chain reactions can be neglected in the substrate.

As shown in Figures 3.5A-D, simulation results for conversion times of both cellulose and xylan agree with the experimental data very well. However, discrepancies are shown in Figures 3.5E-F. Notice that in these two experimental conditions only BX (beta-xylosidase) is applied, while in other conditions (A-D) either MX (contain endo-xylanases) or MX-BX mixture is used. So the reason could be that beta-xylosidase itself may also

have ability to hydrolyze xylan chains on solid substrate. This possible "Endo-acting" ability of beta-xylosidase can also be found from other experiments (Banerjee et al., 2010a; Banerjee et al., 2010b; Banerjee et al., 2010c) and need to be further studied.

We further investigate the effect of substrate composition on hydrolysis by testing different initial percentages of cellulose and xylan with the same values of overall substrate accessibility and the initial amount of exposed D-xylose units. The results shown in Figures 3.6A-B illustrate that decreasing the content of xylan in substrate could increase the hydrolysis rates and the finial conversion levels of both cellulose and xylan. It seems that the initial amount of xylan is the key factor affecting the final conversion level of substrate. However, the most critical factor is, to be more precisely, the initial accessibility of xylan. As shown in Figure 3.7, we test two substrates with the same amount of each component but different conditions of accessibility and find that the substrate with higher value of xylan accessibility can be hydrolyzed faster and reach higher level of conversion. So in order to obtain higher conversion level of the substrate, we can either decrease the total amount of xylan or increase the amount of accessible xylan before hydrolysis.

3.3.2 Comparison with experiments in Banerjee et al. (2010a)

The total substrate loading was 2.9 mg of AFEX-treated corn stover in 500 μL reaction volume. The amount of glucan and xylan were 34.4% and 22.4% by weight respectively. Hydrolysis conversion experimental data are extracted from the Table 1 and the Supplementary Table S2 of the article. As shown in Table 3.2, the discrepancies between the simulation results and experimental data are within 10% if considering all kinds of inhibitions. Also, considering more inhibition effects in the simulation could decrease the

results of conversion level. Notice that in this study only commercial enzyme CP, no beta-glucosidase or beta-xylosidase, was used during hydrolysis, indicating that there would be a large amount of different types of oligomers in solution. Such discrepancies may be caused by the complex inhibition effects of oligomers on enzymes. Our model considers common competitive inhibition effects (gluco-oligomers on cellulases and xylo-oligomers on hemicellulases) and "crossover" inhibition effects (xylo-oligomers on cellulases and gluco-oligomers on hemicellulases). The discrepancies may indicate that some of the assumed values of the inhibition parameters are not accurate, especially those crossover inhibition parameters. Although recently some studies (Qing and Wyman, 2011a, b) have been focusing on the crossover inhibition effect of different xylo-oligomers on cellulases due to the structural similarity between D-glucose and D-xylose units. The crossover inhibition effects still need to be further investigated, especially the unclear inhibition effects of gluco-oligomers on hemicellulases.

3.3.3 Comparison with Experiments in Kumar and Wyman (2009)

The glucan loading was 0.1g of AFEX-treated poplar solids in 10 mL reaction volume. The amount of glucan and xylan were about 46.6% and 15% by weight respectively. Spezyme CP cellulase (CP) (28.1 mg protein/g glucan) and Novozyme 188 beta-glucosidase (BG) (5.5 mg protein/g glucan) were used in the experiments. In the study, the accessibility of cellulose during hydrolysis was measured by the amount of adsorbed CBH1. The mass loading of purified CBH1 was 75 mg per g glucan initially contained in the poplar solids. As described in the article, there were four stages during the process of hydrolyzing AFEX-pretreated poplar. When the conversion level of glucan (cellulose)

reached 35.2%, 45%, 65%, 85%, the conversion level of xylan respectively reached 55%, 70%, 80%, 85%.

Simulation results as shown in Table 3.3, are in great agreement with the experimental data. It was concluded in the study that the cellulose accessibility would not change much before late stage, which is confirmed by the simulation results. The reason for this constant cellulose accessibility for a long period of hydrolysis time could be partially due to the time evolution of substrate morphology. Before hydrolysis, the initial percentage of xylan is higher in the outer layers than inner layers. As hydrolysis proceeds, surface layers will be ablated by enzymes and underlying layers become exposed and accessible. Although the total amount of accessible substrate will keep decreasing due to the shrinkage of the surface area, the amount of accessible cellulose could remain stable for a long time period as the percentage of cellulose keeps increasing.

3.4 Conclusions

A novel mechanistic model has been developed for the enzymatic hydrolysis of hemicellulose-cellulosic substrates for the first time. This model couples the enzymatic fragmentation kinetics of surface-exposed and enzyme-accessible chains of both cellulose and hemicellulose within the substrate to rate equations describing the time evolution of substrate morphology, resulting from the hydrolytic ablation of solid substrate surface externally and internally. To describe the morphology of hemicellulose-cellulosic substrate, the concepts of smallest accessible compartment (SAC) and smallest accessible void (SAV) are adopted and further developed. Geometric functions based on SAC elementary layer variables are developed to keep track of the volume and surface substrate

materials for both cellulose and hemicelluloses. We then use a randomly distributed population of SAC geometry classes to represent the random distribution of accessible surface geometries commonly seen in real substrates. The intertwining feature of the cellulose and hemicelluloses with substrates is depicted by distribution functions of hemicellulose along SAC elementary layer variables.

The forgoing morphological concepts are then integrated with enzymatic chain fragmentation and solubilization. The hydrolytic time evolution of the SAC structures is modeled by a surface layer ablation formalism which couples the hydrolytic shrinkage of SAC units to the enzymatic ablation of surface-exposed, both cellulosic and hemicellulosic, chains. A general site concentration formalism is developed considering the fact that hemicellulose chains consist of different types of monomer units and side groups connected to backbone chains. The reactions involving beta-enzymes in solution and the inhibition effects caused by soluble oligomers are also incorporated into the model. Three case studies are carried out for the numerical simulation of enzymatic hydrolysis process. These cases are carefully selected from literature experiments to use enzyme mixture of both cellulases and hemicellulases to hydrolyze wood biomass pretreated by AFEX, which is believed to retain majority of the cellulose and hemicellulose content in the biomass. The simulation results show that this general modeling framework has the capability to simulate the hydrolysis process, up to total completion, of hemicellulose-cellulosic substrates. The effectiveness of the detailed mechanistic model is clearly illustrated by the good agreement between the simulation results and experimental data. Further numerical analysis with changed substrate morphology and inhibition gains some insights on how the distribution

and intertwining of cellulose and hemicellulose would affect the enzymatic hydrolysis performance.

Nomenclature

B_V: molar volume prefactor for substrate

$B_{V,\sigma}$: molar volume prefactor for class-σ SACs

d_A: ablation dimension for substrate

$d_{A,\sigma}$: ablation dimension for class-σ SACs

$f_{\mu,\rho,\sigma}$: fraction of type-μ sites on type-ρ chains exposed on class-σ SAC surfaces, $\equiv x_{\mu,\rho,\sigma}/x_{M,\rho,\sigma}$

$f_{E,\rho,\sigma}$: fraction of L-end broken sites on type-ρ chains exposed on class-σ SAC surfaces, $\equiv \sum_i f_{L_{U_i},\rho,\sigma}$

$\bar{F}_A$: overall fraction of exposed monomer units of substrate

$F_{A,\sigma}$: fraction of exposed monomer units of class-σ SACs

$g_{\mu,\rho,\sigma}$: native fraction of type-μ sites on type-ρ chains contained in class-σ SACs

$g_{E,\rho,\sigma}$: native fraction of L-end broken sites on type-ρ chains contained in class-σ SACs, $\equiv \sum_i g_{L_{U_i},\rho,\sigma}$

$H_{\rho,\sigma}(l)$: concentration of type-ρ chains with length-l exposed on class-σ SAC surfaces (mM)

$I_{\kappa,\rho}(l)$: oligomer adsorption coefficient for (κ,ρ,l) EO complexes (1/mM)

k, k': number of monomer units contained in a chain

$k_{X,\rho}$ ($k_{Y,\rho}$): site position from L-end (R-end) which can be cut by exo-L (exo-R) enzymes, =2 (=2)

l: chain length, equal to the number of monomer units contained in a chain

$\langle l \rangle_{\rho,\sigma}$: average chain length for type-ρ chains exposed on class-σ SAC surfaces

$l_{S,\rho}$: minimum insoluble chain length for type-ρ chains, =7

$l_{L,\rho}$ ($l_{R,\rho}$): length of L- (R-) terminal segment for type-ρ chains, $\equiv k_{X,\rho} + 1$ ($\equiv k_{Y,\rho} + 1$)

$l_{LR,\rho}$: $\equiv l_{L,\rho} + l_{R,\rho} - 1$

$l_{C,\rho}$: cut-off length for type-ρ chains, $\equiv l_{S,\rho} + \max(l_{L,\rho}, l_{R,\rho}) - 2$

$l_{E,\rho}$: $= \max(l_{L,\rho}, l_{R,\rho}) - 1$

$L_{\kappa,\mu,\rho}$: substrate adsorption coefficient for (κ, μ, ρ) ES complexes (1/mM)

M_{MD}: population size of SAC geometric class

$N_{\mu,\rho,\sigma}(k)$: average number of type-μ sites per type-ρ chain of class-σ SACs

$\Delta N_{\mu',\rho,\sigma}(k, k')$: increment of type-μ' sites of type-ρ main chains produced by a cut on a type-ρ chain generating a (k, k') type-ρ chain fragment pair

$\Delta \bar{N}_{\mu',\mu,\rho,\sigma}$: mean increment of type-μ' sites per type-μ site being cut on type-ρ chains exposed on class-σ SAC surfaces

$\Delta \bar{N}_{S,\mu,\rho,\sigma}(k)$: production factor of soluble oligomers

$\Delta \bar{N}_{H,\mu,\rho,\sigma}(k)$: production factor of chain lengths

$P^{(I)}_{\mu,\rho,\sigma}$, $P^{(L)}_{\mu,\rho,\sigma}$, $P^{(R)}_{\mu,\rho,\sigma}$: contributions to $P_{\rho,\sigma}(\mu|k, k', +1)$ for finding type-μ sites on class-σ SAC surfaces from the Interior, L-terminal and R-terminal segments

$P_{\rho,\sigma}(l)$: probability of a randomly selected insoluble type-ρ chain, exposed on a class-σ SAC surface, to contain l monomer units

$P_{\rho,\sigma}(k, k', \zeta)$: probability that a bond randomly selected from the "super type-ρ chain" is a ζ-bond, and that this bond is located k and k' monomer units from its nearest L-end and R-end, respectively

$P_{\rho,\sigma}(\mu|k, k', \zeta)$: probability for a randomly selected bond from the "super type-ρ chain" to be of type-μ site, given that the bond is a ζ-bond; and given that it is located k and k' monomer units from its nearest L-end and R-end, respectively

$P_{\rho,\sigma}(k, k'|\mu, +1)$: probability for a randomly selected intact bond of given type-μ site to be located k monomer units from the L-end and k' monomer units from the R-end of a type-ρ chain exposed on a class-σ SAC

$Q_{\rho,\sigma}$: native length distribution of type-ρ chains contained in class-σ SACs

$\bar{R}_{\sigma}$: negative rate of monomer units loss from class-σ SACs into solution (mM/min)

$R_{\mu,\rho,\sigma}$: production rate of type-μ sites on type-ρ chains exposed on class-σ SAC surfaces (mM/min)

$R_{S,\rho,\sigma}(l)$: production rate of soluble oligomers contained l monomer units dissolved from type-ρ chains exposed on class-σ SAC surfaces (mM/min)

$R_{H,\rho,\sigma}(l)$: production rate of surface-exposed type-ρ chains of length l on class-σ SAC surfaces (mM/min)

$R_{\rho,\sigma}(l \rightarrow k, k')$: rate at which surface-exposed type-ρ chains of length l exposed on class-σ SAC surfaces are being cut into two type-ρ chain fragments of length k and k', from the L-ends and R-ends of the original type-ρ chains respectively. (mM/min)

S_i: type-i side groups

u_{κ}: total concentration of type-κ enzymes (mM)

U_i: index of broken site types L and R

U_{ij}: index of intact site types N, X and Y

v_κ: concentration of free type-κ enzymes in solution (mM)

$x_{\mu,\rho,\sigma}$: concentration of type-μ sites on type-ρ chains exposed on class-σ SAC surfaces (mM)

$x_{E,\rho,\sigma}$: concentration of insoluble type-ρ chains exposed on class-σ SAC surfaces (mM)

$x_{S,\rho,\sigma}$: total concentration of monomer units dissolved from the type-ρ chains exposed on class-σ SAC surfaces (mM)

$x_{S,\rho}(l)$: concentration of oligomers dissolved from the type-ρ chains and contained l monomer units

x_M: total concentration of monomer units exposed on the substrate surface (mM)

$x_{M,\sigma}$: concentration of monomer units exposed on class-σ SAC surfaces (mM)

$x_{M,\rho,\sigma}$: concentration of monomer units belonging to type-ρ chains exposed on class-σ SAC surfaces (mM)

x_V: total concentration of monomer units contained in the substrate (mM)

$x_{V,\sigma}$: concentration of monomer units contained in class-σ SACs (mM)

$x_{V,\rho,\sigma}$: concentration of monomer units belonging to type-ρ chains contained in class-σ SACs (mM)

$y_{\mu,\rho,\sigma}$: concentration of free type-μ sites on type-ρ chains exposed on class-σ SAC surfaces (mM)

$y_{S,\rho}(l)$: concentration of free oligomers dissolved from type-ρ chains and containing l monomer units

$z_{\kappa,\mu,\rho,\sigma}$: concentration of (κ, μ, ρ) ES complexes exposed on class-σ SAC surfaces (mM)

$z_{\kappa,\rho}(l)$: concentration of (κ, ρ, l) EO complexes in which oligomers containing l monomer units (mM)

β_{κ}: footprint of type-κ enzymes

η_{σ}: geometrical factor accounting for surface curvature effect

κ: index of enzyme types

ρ: index of chain types

$\gamma_{\kappa,\mu,\rho}$: cutting rate coefficient for (κ, μ, ρ) ES complexes (cuts per (κ, μ, ρ) ES complex per time)

λ_{σ}: layer number variable of class-σ SACs

$\Lambda_{CO,\sigma}$: cut-off layer of class-σ SACs (the largest layer of class-σ SACs containing the smallest amount of hemicelluloses)

μ, μ': index of site types (N-, O-, X-, Y-, L-, R-, J-)

σ: index of SAC classes

$\varphi_{O,\rho,\sigma}$: fraction of O-sites on type-ρ chains of class-σ SACs

$\varphi_{U_i,\rho}$: average fraction of type-i monomer units contained in type-ρ chains

$\varphi_{J_i,\rho}$: average ratio of side groups to the total number of monomer units contained in the backbones of type-ρ chains

$\Phi_{M,\rho,\sigma}$: fraction of exposed monomer units contained in type-ρ chains of class-σ SACs

$\bar{\Phi}_{M,\rho}$: overall fraction of exposed monomer units belonging to type-ρ chains of substrate

$\Phi_{V,\rho,\sigma}$: fraction of monomer units belonging to type-ρ chains contained in class-σ SACs

$\bar{\Phi}_{V,\rho}$: overall fraction of monomer units belonging to type-ρ chains contained in substrate

$\Theta(\Delta l)$: heavy-side step function, =1 if $\Delta l > 0$, =0 if $\Delta l < 0$

ξ_σ: molar fraction of monomer units contained in class-σ SACs, $\equiv x_{V,\sigma}/x_V$

ζ: integrity variable with $\zeta = +1(-1)$ indicating intact (broken) bond, in the "super type-ρ chain" construction of fragmentation probability

ω_μ: weight factor for type-μ bond site: =1 for intact bond sites, =1/2 for broken bond sites, =0 for side bond sites

Acknowledgments

We acknowledge the National Science Foundation (CBET 1138734, CHE 1230803) for financial support.

Tables

Table 3.1 Main components of hemicellulose-cellulosic substrates and their specific enzymes

Main Component	Main units	Linkage	Enzymes	Linkage hydrolyzed
Cellulose				
Backbone	D-glucose	β-1,4	Endoglucanase	Internal β-1,4
			Cellobiohydrolase I	terminal β-1,4 from reducing end
			Cellobiohydrolase II	terminal β-1,4 from non-reducing end
Oligomers			β-glucosidase	Terminal β-1,4
Xylans				
Backbone	D-xylose	β-1,4	Endoxylanase	Internal β-1,4
			Exoxylanase	Terminal β-1,4 (not classified)
Side groups	L-arabinose	α-1,3	α-arabinosidase	Terminal α-1,3
	D-glucuronic acid	α-1,2	α-glucuronidase	Terminal α-1,2
Oligomers			β-xylosidase	Terminal β-1,4
Mannans				
Backbone	D-glucose	β-1,4	Endomannannase	Internal β-1,4 after D-mannose
	D-mannose		Endoglucanase	Internal β-1,4 after D-glucose
Side groups	D-galactose	α-1,6	α-galactosidase	Terminal α-1,6
Oligomers			β-mannosidase	Terminal β-1,4 after D-mannose
			β-glucosidase	Terminal β-1,4 after D-glucose

Table 3.2 Simulation results compared with experimental data from Banerjee et al. (2010a)

CP Loading (mg/g glucan)	% Glucan conversion (24h)				% Xylan conversion (24h)				% Glucan conversion (48h)				% Xylan conversion (48h)			
	E	**S (a)**	**S (b)**	**S (c)**	**E**	**S (a)**	**S (b)**	**S (c)**	**E**	**S (a)**	**S (b)**	**S (c)**	**E**	**S (a)**	**S (b)**	**S (c)**
7.5	22.4 ± 0.7	33.03	35.42	38.49	22.9 ± 0.4	14.44	15.58	20.00	35.5 ± 0.8	37.16	38.85	44.30	26.4 ± 0.1	18.13	19.65	26.23
15	32.5 ± 2.9	41.80	45.70	55.68	26.3 ± 1.3	25.86	28.31	39.61	48.8 ± 0.1	47.36	50.88	67.54	28.8 ± 0.4	30.90	33.37	49.39
30	45.6 ± 1.2	54.88	60.59	85.06	32.4 ± 2.4	40.54	43.40	64.57	56.5 ± 0.9	62.07	67.76	95.75	34.6 ± 0.8	45.91	49.17	73.53

E: Experimental data
S (a): Simulation results considering all inhibitions
S (b): Simulation results not considering "crossover" inhibitions
S (c): Simulation results considering no inhibitions

Table 3.3 Simulation results compared with experimental data from Kumar and Wyman (2009)

Stage	Cellulose conversion (simulation& experiment)	Hemicellulose conversion (experiment)	Hemicellulose conversion (simulation)	CBH I adsorption [mg/g solids] (experiment)	CBH I adsorption [mg/g solids] (simulation)
1	35.2%	55%	53.58%	18.7	17.2
2	45%	70%	63.55%	19.3	17.5
3	65%	80%	79.07%	14.7	16.1
4	85%	85%	89.16%	15.5	9.6

Figures

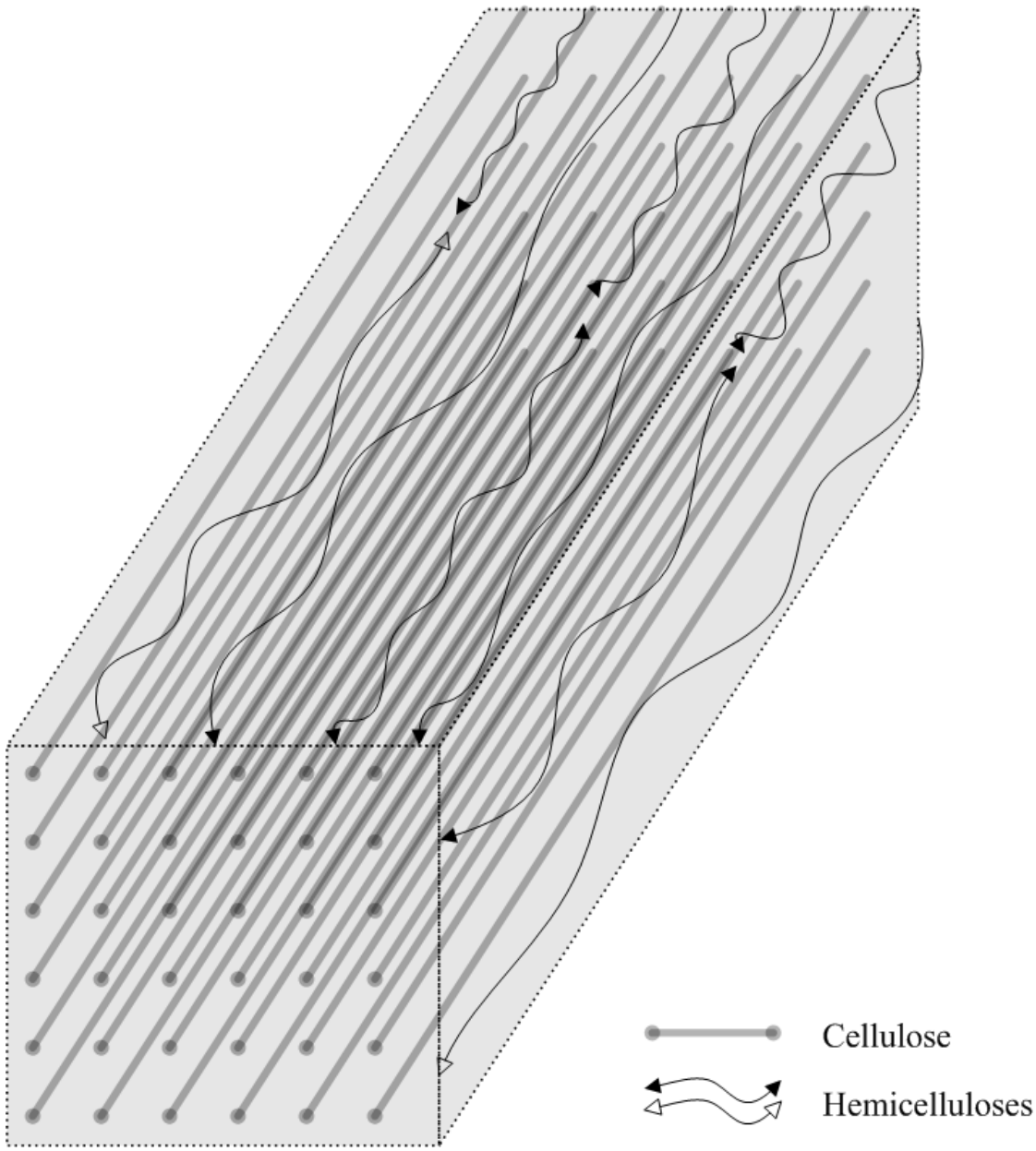

Figure 3.1 Structural illustration of cellulose and hemicelluloses in substrates. The core is crystalline cellulose elementary fibril (CEF). The size (i.e. the number of cellulose chains contained) and shape of the CEF are still in debate. The stricture model of CEF shown here is the 36-chain square shape model. Other models of CEF are not listed here. There is no close relationship between the structure of SAC and CEF

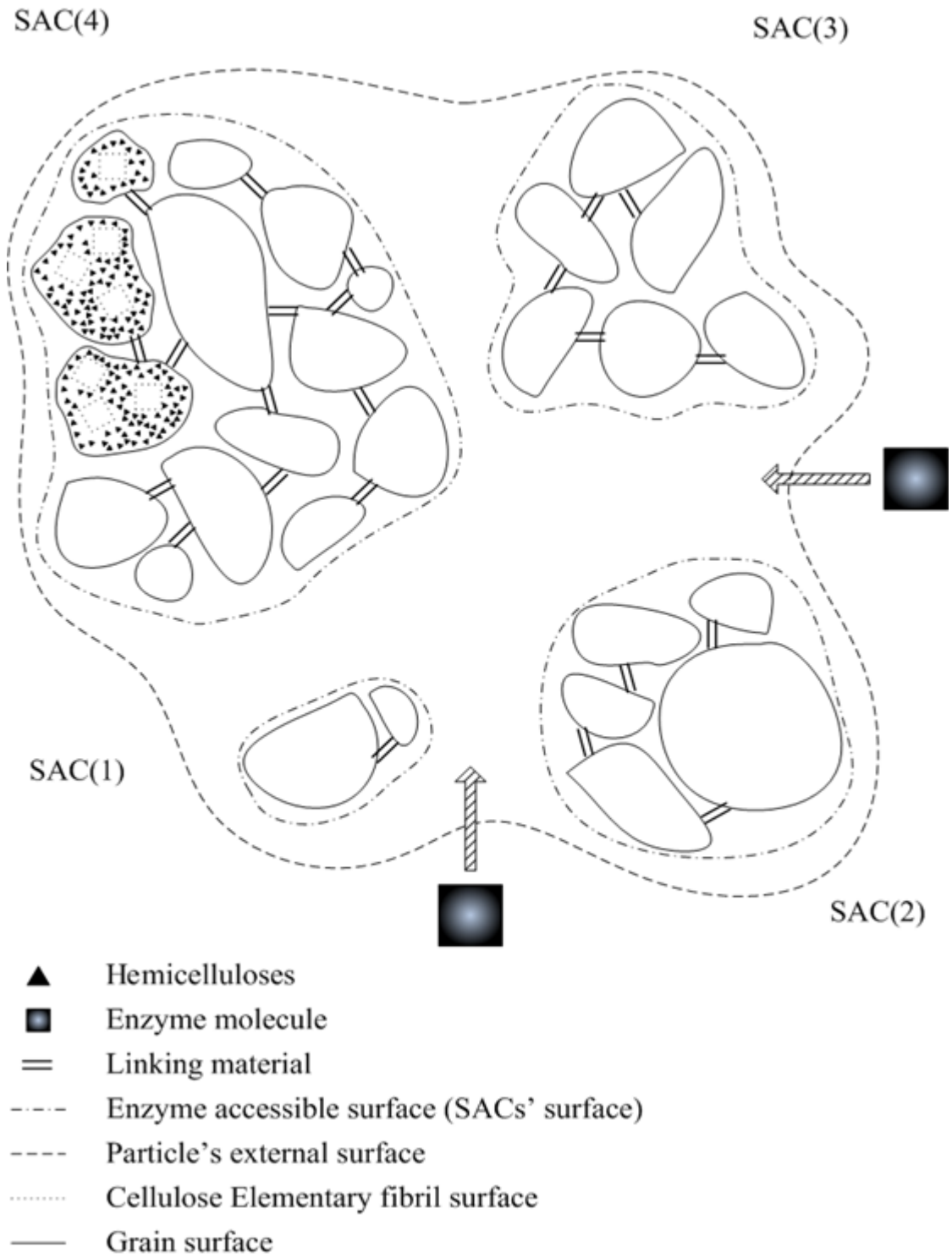

Figure 3.2 Structural illustration of cellulose and hemicelluloses in substrates. The core is crystalline cellulose elementary fibril (CEF). The size (i.e. the number of cellulose chains contained) and shape of the CEF are still in debate. The stricture model of CEF shown here is the 36-chain square shape model. Other models of CEF are not listed here. There is no close relationship between the structure of SAC and CEF

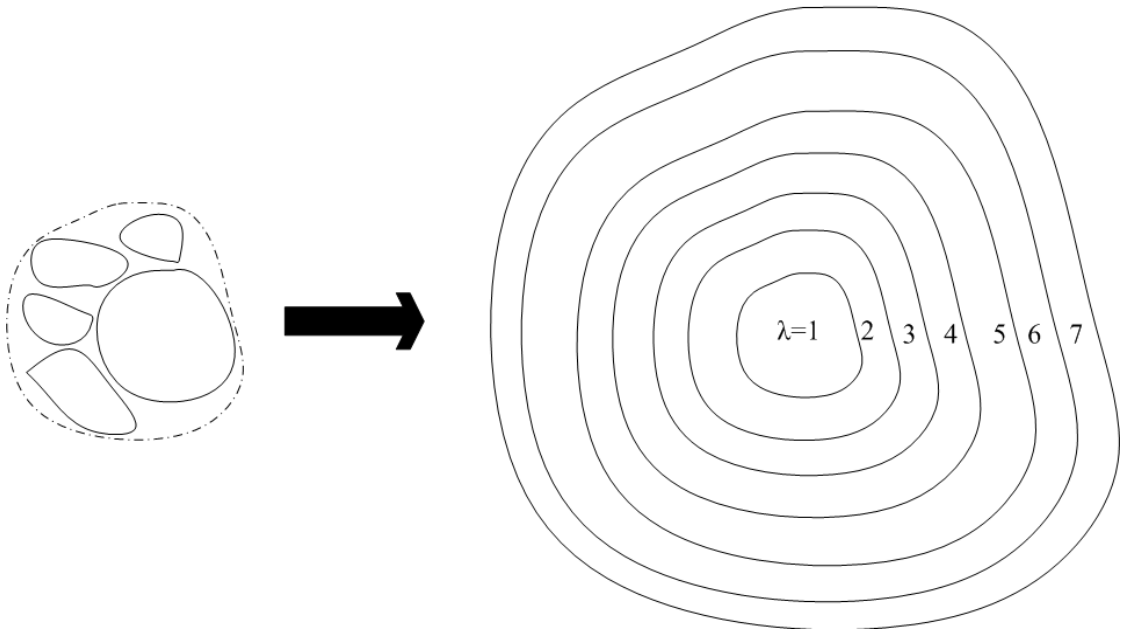

Figure 3.3 Schematic illustration of the partitioning of an SAC into elementary layers. Each layer is represent by a λ-value such that the layer with the highest λ-value is the first (i.e. outermost) to be removed due to solubilization by attacking enzymes during hydrolysis. The SACs of same geometric class have a same highest λ-value

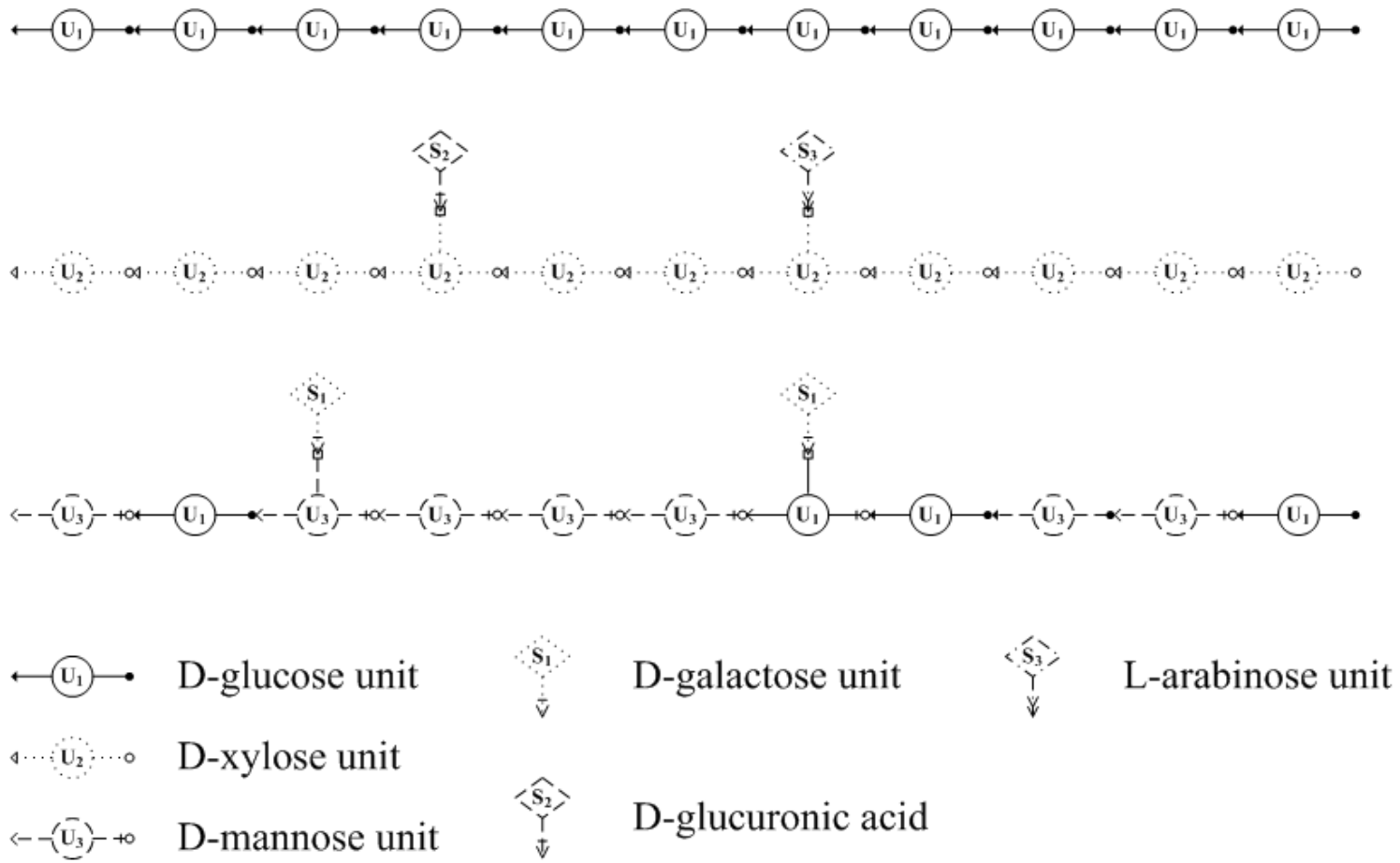

Figure 3.4(a) Example of using Ui and Si to represent the chains of cellulose, arabinoglucuronoxylan and galactoglucomannan in hemicellulose-cellulosic substrate. The chain length is 11 for each component. U1, U2 and U3 represent the D-glucose units, D-xylose units and D-mannose units respectively. S1, S2 and S3 represent three types of side groups: D-galactose, D-glucuronic acid and L-arabinose

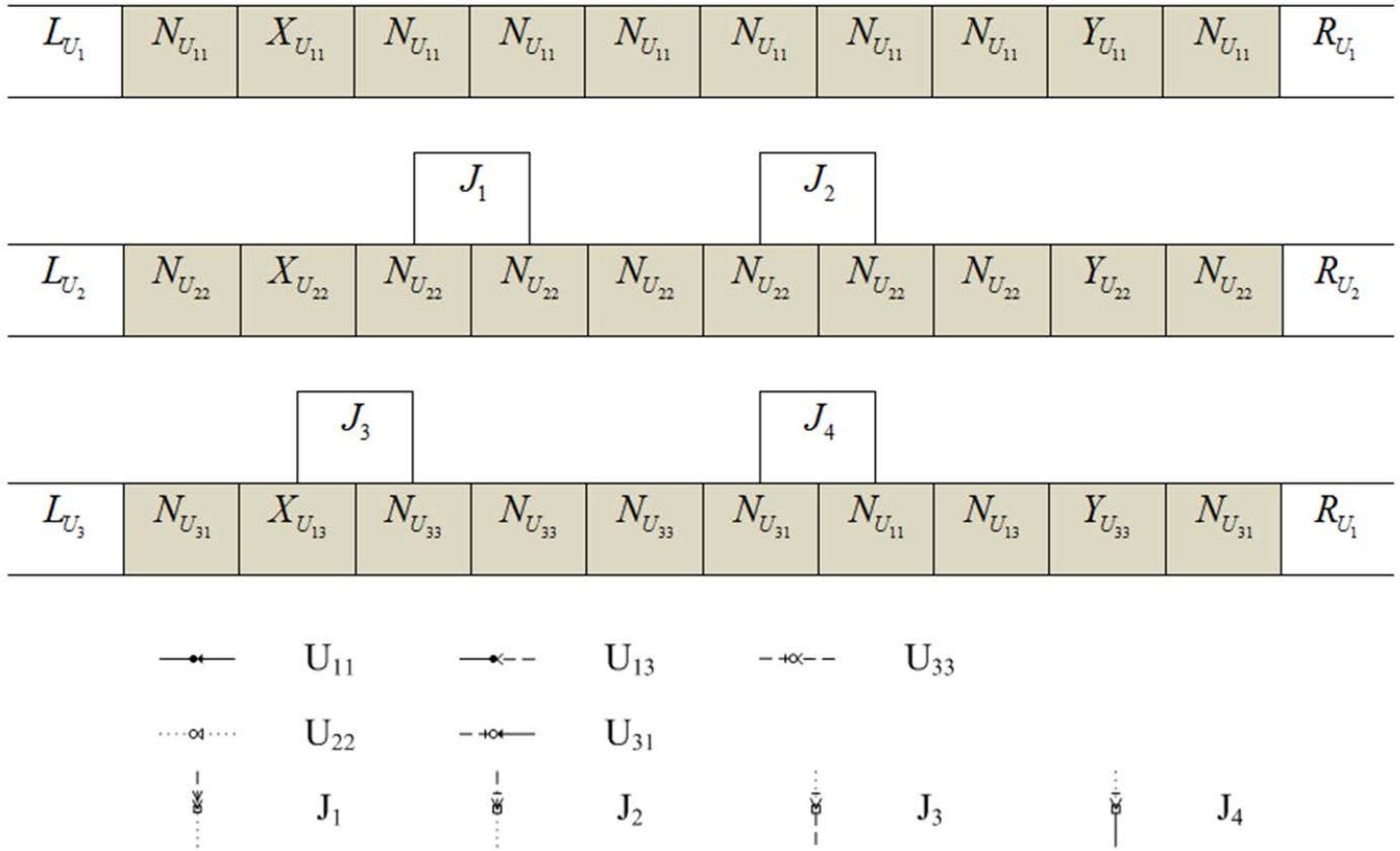

Figure 3.4(b) Example of using U_{ij} to represent the bonds and the distribution of the site types along all the backbones shown in Figure 3.4(a). The maximum number of bond types could be 3^2=9, but only 5 types actually exist. The average probability for certain type of bonds appearing on the backbones of certain type of chain depends on the monomer composition of the chain

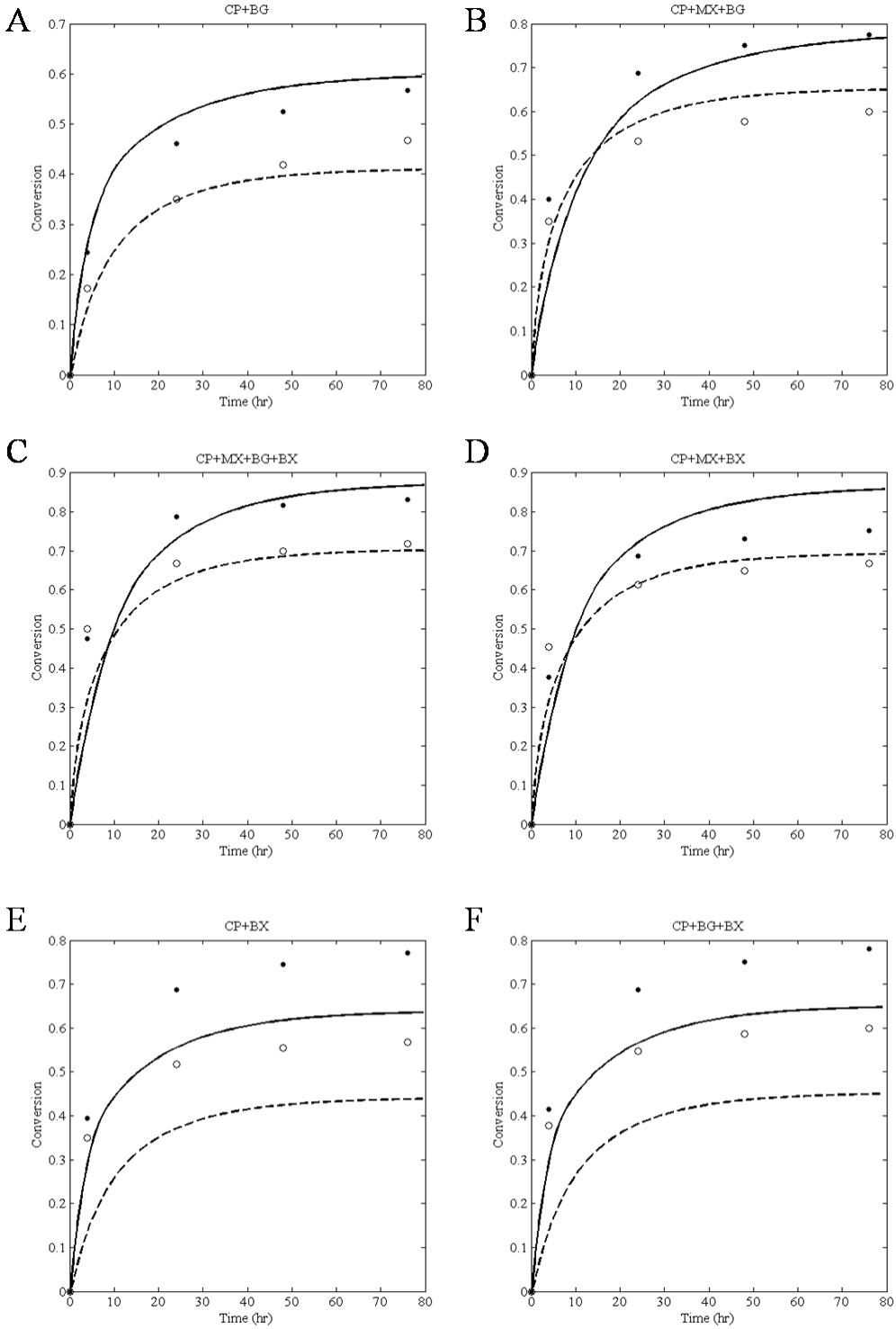

Figure 3.5 Simulation results compared with experimental data from Qing and Wyman (2011b). Solid lines represent simulations results of cellulose conversion. Dash lines represent simulations results of xylan conversion. Filled circles represent experimental data of cellulose conversion. Blank circles represent experimental data of xylan conversion

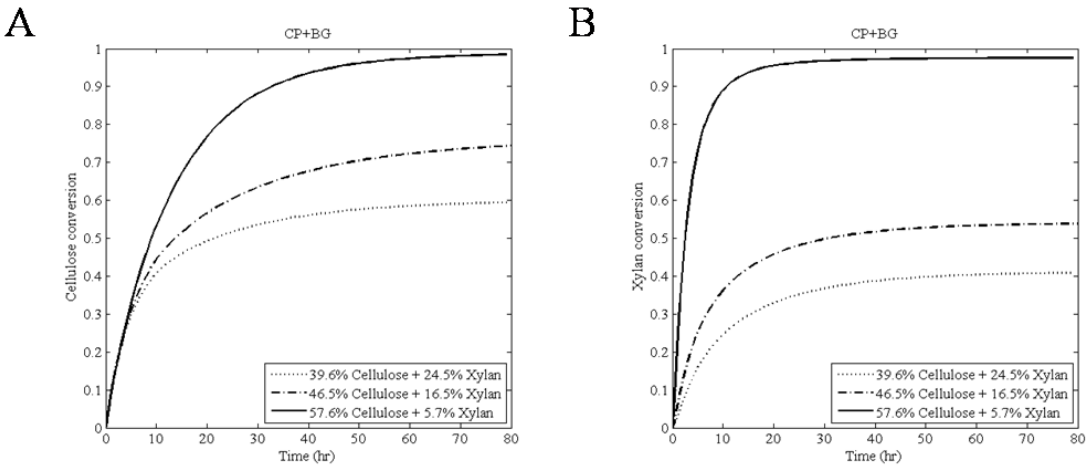

Figure 3.6 Model results testing the impact of initial substrate composition on hydrolysis. The total substrate loading is 0.2g in 10 mL reaction volume with CP (16.1 mg protein/g glucan) and BG (3.16 mg protein/g glucan) for all three cases. The initial percentages of cellulose and xylan are shown in figures

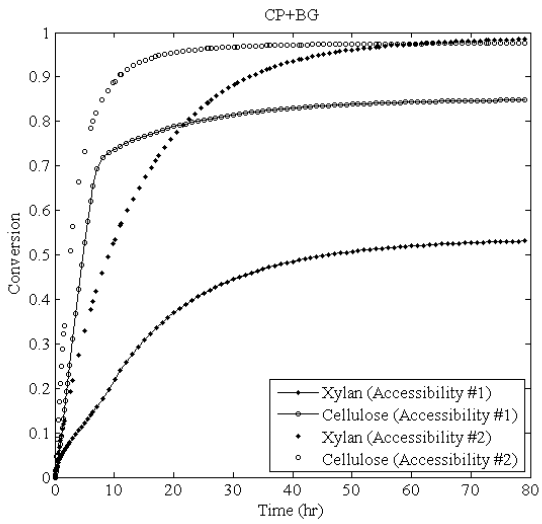

Figure 3.7 Model results using two different groups of values of accessibility. The total substrate loading is 0.2g in 10 mL reaction volume with CP (16.1 mg protein/g glucan) and BG (3.16 mg protein/g glucan) for both two cases. The initial percentages of substrate components for two cases are 5.7% for xylan and 57.6% for cellulose. The #1 accessibility set is: 0.0530 (cellulose); 0.5337 (xylan) and 0.1051 (total). The #2 accessibility set is: 0.2270 (cellulose); 0.0381 (xylan) and 0.2066 (total)

References

Banerjee, G., Car, S., Scott-Craig, J. S., Borrusch, M. S., Bongers, M. and Walton, J. D. 2010b. "Synthetic multi-component enzyme mixtures for deconstruction of lignocellulosic biomass." Bioresource technology 101(23): 9097-9105.

Banerjee, G., Car, S., Scott-Craig, J. S., Borrusch, M. S. and Walton, J. D. 2010c. "Rapid optimization of enzyme mixtures for deconstruction of diverse pretreatment/biomass feedstock combinations." Biotechnology for biofuels 3: 22.

Belkacemi, K. and Hamoudi, S. 2003. "Enzymatic hydrolysis of dissolved corn stalk hemicelluloses: reaction kinetics and modeling." Journal of Chemical Technology & Biotechnology 78(7): 802-808.

Chundawat, S. P. S., Donohoe, B. S., da Costa Sousa, L., Elder, T., Agarwal, U. P., Lu, F., Ralph, J., Himmel, M. E., Balan, V. and Dale, B. E. 2011. "Multi-scale visualization and characterization of lignocellulosic plant cell wall deconstruction during thermochemical pretreatment." Energy & Environmental Science 4(3): 973.

Feng, Y. Y., He, Z. M., Song, L. F., Ong, S. L., Hu, J. Y., Zhang, Z. G. and Ng, W. J. 2003. "Kinetics of beta-mannanase fermentation by Bacillus licheniformis." Biotechnology letters 25(14): 1143-1146.

Griggs, A. J., Stickel, J. J. and Lischeske, J. J. 2012a. "A mechanistic model for enzymatic saccharification of cellulose using continuous distribution kinetics I: depolymerization by EGI and CBHI." Biotechnology and bioengineering 109(3): 665-675.

Griggs, A. J., Stickel, J. J. and Lischeske, J. J. 2012b. "A mechanistic model for enzymatic saccharification of cellulose using continuous distribution kinetics II: cooperative enzyme action, solution kinetics, and product inhibition." Biotechnology and bioengineering 109(3): 676-685.

Harjunpaa, V., Teleman, A., Siika-Aho, M. and Drakenberg, T. 1995. "Kinetic and stereochemical studies of manno-oligosaccharide hydrolysis catalysed by beta-mannanases from Trichoderma reesei." European journal of biochemistry / FEBS 234(1): 278-283.

Kumar, R. and Wyman, C. E. 2009. "Does change in accessibility with conversion depend on both the substrate and pretreatment technology?" Bioresource Technology 100(18): 4193-4202.

Levine, S. E., Fox, J. M., Blanch, H. W. and Clark, D. S. 2010. "A mechanistic model of the enzymatic hydrolysis of cellulose." Biotechnology and bioengineering 107(1): 37-51.

Liu, X. J., Lu, M. Z., Ai, N., Yu, F. W. and Ji, J. B. 2012. "Kinetic model analysis of dilute sulfuric acid-catalyzed hemicellulose hydrolysis in sweet sorghum bagasse for xylose production." Industrial Crops and Products 38: 81-86.

Nagendran, S., Hallen-Adams, H. E., Paper, J. M., Aslam, N. and Walton, J. D. 2009. "Reduced genomic potential for secreted plant cell-wall-degrading enzymes in the ectomycorrhizal fungus Amanita bisporigera, based on the secretome of Trichoderma reesei." Fungal Genetics and Biology 46(5): 427-435.

Qing, Q. and Wyman, C. E. 2011a. "Hydrolysis of different chain length xylooliogmers by cellulase and hemicellulase." Bioresource technology 102(2): 1359-1366.

Qing, Q. and Wyman, C. E. 2011b. "Supplementation with xylanase and beta-xylosidase to reduce xylo-oligomer and xylan inhibition of enzymatic hydrolysis of cellulose and pretreated corn stover." Biotechnology for biofuels 4(1): 18.

Sjöström, E. 1993. Wood chemistry : fundamentals and applications. San Diego, Academic Press.

Sun, R. C., Sun, X. F. and Tomkinson, I. 2004. "Hemicelluloses and their derivatives." Hemicelluloses: Science and Technology 864: 2-22.

Tenkanen, M. 2004. "Enzymatic tailoring of hemicelluloses." Hemicelluloses: Science and Technology 864: 292-311.

Weimer, P. J., Lopez-Guisa, J. M. and French, A. D. 1990. "Effect of cellulose fine structure on kinetics of its digestion by mixed ruminal microorganisms in vitro." Appl Environ Microbiol 56(8): 2421-2429.

Zhang, Y. H. and Lynd, L. R. 2004. "Toward an aggregated understanding of enzymatic hydrolysis of cellulose: noncomplexed cellulase systems." Biotechnology and bioengineering 88(7): 797-824.

Zhou, W., Hao, Z., Xu, Y. and Schuttler, H. B. 2009a. "Cellulose hydrolysis in evolving substrate morphologies II: Numerical results and analysis." Biotechnology and bioengineering 104(2): 275-289.

Zhou, W., Schuttler, H. B., Hao, Z. and Xu, Y. 2009b. "Cellulose hydrolysis in evolving substrate morphologies I: A general modeling formalism." Biotechnology and bioengineering 104(2): 261-274.

Zhou, W., Xu, Y. and Schuttler, H. B. 2010. "Cellulose hydrolysis in evolving substrate morphologies III: time-scale analysis." Biotechnology and bioengineering 107(2): 224-234.

Supporting Information (SI)

Section A: SAC Geometric Functions

The expression of $x_V(\lambda)$ can be written as

$$x_V(\lambda) = B_V \lambda^{d_A} \tag{A.1}$$

where d_A is the ablation dimension and B_V is the molar volume prefactor. x_V is dependent on λ with a simple power law. The assumed power low behavior $x_V(\lambda) \propto \lambda^{d_A}$ shows that the shape of SAC will be preserved during hydrolysis (Zhou et al., 2009). To keep track of monomer units exposed on the SAC surface, we have

$$x_M(\lambda) = x_V(\lambda) - x_V(\lambda - 1)\Theta(\lambda - 1) \tag{A.2a}$$

with

$$\Theta(\lambda - 1) = \begin{cases} 1, & \lambda > 1 \\ 0, & 0 < \lambda \leq 1 \end{cases} \tag{A.2b}$$

To represent the random distribution of SAC sizes, we use the parameter of SAC geometric class, which is labeled by σ with σ=1, 2..., M_{MD} where M_{MD} is the population size of SAC geometric classes. So that $x_{V,\sigma}(\lambda)$, the total concentration of monomer units contained in class-σ SACs, and $x_{M,\sigma}(\lambda)$, the concentration of enzyme-accessible monomer units exposed on the surfaces of class-σ SACs are given by

$$x_{V,\sigma}(\lambda_\sigma) = B_{V,\sigma} \lambda^{d_{A,\sigma}} \tag{A.3}$$

$$x_{M,\sigma}(\lambda_\sigma) = x_{V,\sigma}(\lambda_\sigma) - x_{V,\sigma}(\lambda_\sigma - 1)\Theta(\lambda_\sigma - 1) \tag{A.4a}$$

with

$$\Theta(\lambda_\sigma - 1) = \begin{cases} 1, & \lambda_\sigma > 1 \\ 0, & 0 < \lambda_\sigma \leq 1 \end{cases} \tag{A.4b}$$

where $B_{V,\sigma}$ is the molar volume prefactor for class-σ SACs, and $d_{A,\sigma}$ is the ablation dimension factor for class-σ SACs. $x_{V,\sigma}$ and $x_{M,\sigma}$ must obey the relationships written as

$$x_V = \sum_\sigma x_{V,\sigma}(\lambda_\sigma) \tag{A.5}$$

$$x_M = \sum_\sigma x_{M,\sigma}(\lambda_\sigma) \tag{A.6}$$

We use two parameters to describe the enzyme accessibility, which are $\bar{F}_A$, the overall fraction of enzyme-accessible monomer units, and$F_{A,\sigma}$, the fraction of enzyme-accessible monomer units for the class-σ SACs. Their expressions are given by

$$F_{A,\sigma}(\lambda_\sigma) = \frac{x_{M,\sigma}(\lambda_\sigma)}{x_{V,\sigma}(\lambda_\sigma)} \tag{A.7}$$

$$\bar{F}_A = \frac{x_M}{x_V} = \sum_\sigma \xi_\sigma F_{A,\sigma}(\lambda_\sigma) \tag{A.8}$$

where $\xi_\sigma \equiv x_{V,\sigma}/x_V$. The value of $\bar{F}_A$ can be directly observed before enzymatic hydrolysis and used as an initial input value, that is, $\bar{F}_{\mathrm{A}}^{(0)}$, in the model, and decide the initial value of ξ_σ. We use the assumption of the Gaussian distribution for the total molar concentration of monomer units per geometric class, and then have

$$\xi_{\mathrm{A}}^{(0)} = \exp\left[-\left(\frac{\Lambda_\sigma - \Lambda_{Avg}}{\Lambda_{Wid}}\right)^2/2\right] / \sum_\sigma \exp\left[-\left(\frac{\Lambda_\sigma - \Lambda_{Avg}}{\Lambda_{Wid}}\right)^2/2\right] \tag{A.9}$$

By adjusting the two Gaussian distribution parameters Λ_{Avg} and Λ_{Wid}, a proper initial distribution of the molar monomer concentration per geometry class can be obtained to match the value of $\bar{F}_{\mathrm{A}}^{(0)}$.

Section B: Derivation of Surface Layer Ablation Rate Equations

In order to derive the surface layer ablation rate equations, we first define $-R_{\mu,\rho,\sigma} > 0$ as the loss rate of type-μ sites belonging to type-ρ chains exposed on class-σ SAC surfaces, and $-\bar{R}_{\sigma} > 0$ as the total loss rate of monomer units exposed on class-σ SAC surfaces into solution. So that we can obtain

$$\bar{R}_{\sigma} = \sum_{\mu,\rho} \omega_{\mu} R_{\mu,\rho,\sigma} = \frac{d}{dt} x_{V,\sigma}\big(\lambda_{\sigma}(t)\big) = \partial_{\lambda_{\sigma}} x_{V,\sigma}(\lambda_{\sigma})\dot{\lambda}_{\sigma} \tag{B.1}$$

where $\partial_{\lambda_{\sigma}}$ is shorthand for the derivative $\partial/\partial_{\lambda_{\sigma}}$. The removal of a small fraction of a layer during a short time interval dt will result in a removal of $-dx_{V,\sigma}^{(fra)} = -\partial_{\lambda_{\sigma}} x_{V,\sigma} d\lambda_{\sigma}$ monomer units from the SAC surface by chain fragmentation and then result in a change of SAC exposed surface area by $dx_{M,\sigma}^{(fra)} = \partial_{\lambda_{\sigma}} x_{M,\sigma} d\lambda_{\sigma}$ monomer units. The net concentration of newly exposed monomer units at the surface, resulting from the removal of overlaying monomer units and the change of surface area, is thus

$$\begin{aligned} dx_{M,\sigma}^{(exp)} &= -dx_{V,\sigma}^{(fra)} + dx_{M,\sigma}^{(fra)} = -\big(\partial_{\lambda_{\sigma}} x_{V,\sigma} - \partial_{\lambda_{\sigma}} x_{M,\sigma}\big) d\lambda_{\sigma} \\ &= -\bar{R}_{\sigma}\big(1 - \partial_{\lambda_{\sigma}} x_{M,\sigma}/\partial_{\lambda_{\sigma}} x_{V,\sigma}\big) dt \end{aligned} \tag{B.2}$$

Based on Eq. (B.2), the net concentration of newly exposed sites is given by

$$dx_{\mu,\rho,\sigma}^{(exp)} = dx_{M,\sigma}^{(exp)} \Phi_{M,\rho,\sigma}(\lambda_\sigma - 1) g_{\mu,\rho,\sigma}(\lambda_\sigma) \tag{B.3}$$

where $g_{\mu,\rho,\sigma}(\lambda_\sigma)$ is the native site fraction functions representing the fraction of type-μ sites contained in type-ρ chains in the interior of the class-σ SACs. $g_{\mu,\rho,\sigma}(\lambda_\sigma)$ can be treated as a layer–independent parameter, which means $g_{\mu,\rho,\sigma}(\lambda_\sigma) \equiv g_{\mu,\rho,\sigma}(\Lambda_\sigma) = g_{\mu,\rho,\sigma}$. In addition, we denote $g_{E,\rho,\sigma}$ as the native L-end (or R-end) broken site fraction of type-ρ chains in class-σ SACs, which has such relationship $\sum_i g_{L_{U_i},\rho,\sigma} = \sum_i g_{R_{U_i},\rho,\sigma} = g_{E,\rho,\sigma}$ and can be obtained from the degree of polymerization of type-ρ chains DP_ρ.

Combining the surface exposure contribution $dx_{\mu,\rho,\sigma}^{(fra)}$ with the surface fragmentation contribution $dx_{\mu,\rho,\sigma}^{(fra)}$ given by

$$dx_{\mu,\rho,\sigma}^{(fra)} = R_{\mu,\rho,\sigma} dt \tag{B.4}$$

we can obtain the net increment of type-μ surface sites, that is, $dx_{\mu,\rho,\sigma} = dx_{\mu,\rho,\sigma}^{(fra)} + dx_{\mu,\rho,\sigma}^{(exp)}$, and the rate function Equation (3a). Then from Eq. (B.1) we can immediately obtain the changing rate of λ_σ, which is Equation (3b).

Section C: Enzyme Adsorption and Inhibition Equilibriums

The first step for an enzyme molecule to cut an intact bond is to form an enzyme–substrate (ES) complex, that is, to adsorb a bond site exposed on SAC surfaces. The cutting rate for a intact bond site of type μ in a chain belonging to type ρ, having already adsorbed an enzyme molecule on the surface of an SAC belonging class σ, is thus given by the product of rate coefficient and ES complex concentration, $\gamma_{\kappa,\mu,\rho} z_{\kappa,\mu,\rho,\sigma}$. Here κ represents the type

of enzymes; $z_{\kappa,\mu,\rho,\sigma}$ represents the concentration of (κ, μ, ρ) ES complexes on class-σ SAC surfaces; and $\gamma_{\kappa,\mu,\rho}$ represents the cutting rate coefficient (in the unit of cuts per second per ES complex), which is identical for all the geometric classes. It is assumed that the ES complex formation process is much faster than the bond cutting kinetics. Therefore, the enzyme adsorption quasi-equilibrium is maintained at the SAC surfaces during hydrolysis and given by

$$z_{\kappa,\mu,\rho,\sigma} = L_{\kappa,\mu,\rho} v_\kappa y_{\mu,\rho,\sigma} \tag{C.1}$$

where $y_{\mu,\rho,\sigma}$ is the molar concentration of free type-μ sites contained in type-ρ chains on class-σ SAC surfaces, v_κ is the concentration of free type-κ enzymes and $L_{\kappa,\mu,\rho}$ is the substrate adsorption coefficient which is the inverse of the conventional desorption equilibrium coefficient.

As hydrolysis proceeds, some enzyme molecules may also be inhibited by soluble oligomers to form enzyme-oligomer (EO) complexes in solution. This type of enzyme adsorption equilibrium in solution can be written as

$$z_{\kappa,\rho}(l) = I_{\kappa,\rho}(l) v_\kappa y_{S,\rho}(l) \tag{C.2}$$

with $1 \leq l < l_{S,\rho}$. Here, $z_{\kappa,\rho}(l)$ is the concentration of (κ, ρ, l) EO complexes in which each oligomer contains l monomer units, $I_{\kappa,\rho}(l)$ is the oligomer adsorption coefficient; $y_{S,\rho}(l)$ is the molar concentration of free oligomers contained l monomer units and dissolved from type-ρ chains, and v_κ is the same parameter as in Equation (C.1). As described in Supporting Information section B, $z_{\kappa,\mu,\rho,\sigma}$ and $z_{\kappa,\rho}(l)$ can be calculated and

expressed in terms of $x_{\mu,\rho,\sigma}$ and $x_{S,\rho}(l)$ by solving enzyme adsorption and inhibition equations.

The construction of $R_{S,\rho}(l)$ describes the reactions between oligomers and beta-enzymes and requires the solutions of the enzyme adsorption and inhibition equilibriums. In this model, the reaction mechanism of beta-enzymes in solution is simplified as: a free oligomer which contains l monomer units can adsorb and be hydrolyzed by its corresponding beta-enzymes into a monomer unit and an oligomer containing $l-1$ monomer unit(s). So the expression of $R_{S,\rho}(l)$ can be written as

$$R_{S,\rho}(l) = \begin{cases} \gamma_{\kappa,\rho}(2)\cdot z_{\kappa,\rho}(2) + \sum_{2}^{l_{S,\rho}-1}\gamma_{\kappa,\rho}(l)\cdot z_{\kappa,\rho}(l), & l = 1 \\ -\gamma_{\kappa,\rho}(l)\cdot z_{\kappa,\rho}(l) + \gamma_{\kappa,\rho}(l+1)\cdot z_{\kappa,\rho}(l+1), & 2 \le l \le l_{S,\rho}-2 \\ -\gamma_{\kappa,\rho}(l)\cdot z_{\kappa,\rho}(l), & l = l_{S,\rho}-1 \end{cases} \quad \text{(C.3)}$$

where $\gamma_{\kappa,\rho}(l)$ is the oligomer cutting rate coefficient. Note that in this model, only beta-enzymes could hydrolyze oligomers in solution after forming EO complexes with them in solution. So for endo- and exo- enzymes, their corresponding values of $\gamma_{\kappa,\rho}(l)$ are 0, which means they are inhibited by forming EO complexes with oligomers. And for any monomer unit, $\gamma_{\kappa,\rho}(1)$ is also 0 which means all the enzymes will inevitably be inhibited by monomer units during hydrolysis. Furthermore, both the cutting rate coefficient $\gamma_{\kappa,\rho}(l)$ and the oligomer adsorption coefficient $I_{\kappa,\rho}(l)$ have two dimensions representing the enzyme types and the chain types.

The free enzyme and surface site concentrations v_κ and $y_{\mu,\rho,\sigma}$ are related to their total concentrations u_κ and $x_{\mu,\rho,\sigma}$, respectively, by way of the total enzyme and total site balance relations:

$$u_\kappa = v_\kappa + \sum_{\mu,\rho,\sigma} z_{\kappa,\mu,\rho,\sigma} + \sum_{\rho,l} z_{\kappa,\rho}(l) \tag{C.4}$$

$$x_{S,\rho}(l) = y_{S,\rho}(l) + \sum_\kappa z_{\kappa,\rho}(l) \tag{C.5}$$

$$x_{\mu,\rho,\sigma} = y_{\mu,\rho,\sigma} + \sum_\kappa z_{\kappa,\mu,\rho,\sigma} + \sum_{\kappa,\mu',\rho'} \bar{f}_{\mu,\rho,\sigma} \beta_\kappa z_{\kappa,\mu',\rho',\sigma} \tag{C.6}$$

where $\bar{f}_{\mu,\rho,\sigma}$=$x_{\mu,\rho,\sigma}/x_{M,\sigma}$. The last term in the Equation (C.6) arises from the fact that the footprint area of a surface-adsorbed enzyme molecule is far greater than the average surface area of a bond site. Hence, a type-κ enzyme molecule, bound to a type-μ' surface site, will in effect cover up, and obstruct access to some number (β_κ) of other surface sites that are located in spatial proximity to the type-μ' binding site. Due to the current lack of value of β_κ for each type enzymes discussed in this work, we simply use the value of cellulase, that is, 39, for all the enzymes.

Equations. (C.1), (C.2), (C.4), (C.5) and (C.6) can then be solved simply by iteration in order for v_κ, $y_{\mu,\rho,\sigma}$, $z_{\kappa,\mu,\rho,\sigma}$ and $z_{\kappa,\rho}(l)$. Combining the mass action and balance relations, the general form of enzyme adsorption and inhibition equilibrium can be shown as

$$v_\kappa = \frac{u_\kappa}{1+\sum_{\mu,\rho,\sigma} L_{\kappa,\mu,\rho} y_{\mu,\rho,\sigma} + \sum_{\rho,l} I_{\kappa,\rho}(l) y_{S,\rho}(l)} \tag{C.7}$$

$$y_{S,\rho}(l) = \frac{x_{S,\rho}(l)}{1+\sum_\kappa I_{\kappa,\rho}(l) v_\kappa} \tag{C.8}$$

$$y_{\mu,\rho,\sigma} = \frac{x_{\mu,\rho,\sigma}}{\chi_{\mu,\rho}(1+\sum_{\mu',\rho'} \theta_{\mu',\rho',\sigma}\psi_{\mu',\rho'})} \tag{C.9}$$

$$\chi_{\mu,\rho} = 1 + \sum_{\kappa} L_{\kappa,\mu,\rho} v_{\kappa} \tag{C.10}$$

$$\psi_{\mu,\rho} = \sum_{\kappa} \beta_{\kappa} L_{\kappa,\mu,\rho} v_{\kappa} \tag{C.11}$$

$$\theta_{\mu',\rho',\sigma} = \frac{x_{\mu,\rho,\sigma}}{\chi_{\mu,\rho} x_{M,\sigma}} \tag{C.12}$$

To calculate v_{κ} and $y_{\mu,\rho,\sigma}$, as functions of u_{κ} and $x_{\mu,\rho,\sigma}$ this system of coupled non-linear equations can be solved iteratively, starting from the initial guess

$$\begin{cases} v_{\kappa}^{(0)} = u_{\kappa} \\ y_{S,\rho}^{(0)}(l) = x_{S,\rho}(l) \\ y_{\mu,\rho,\sigma}^{(0)} = x_{\mu,\rho,\sigma} \end{cases} \tag{C.13}$$

Section D: Site Number Increments and Chain Site Distribution Model

$\Delta N_{\mu',\rho,\sigma}(k,k')$ can be expressed as

$$\Delta N_{\mu',\rho,\sigma}(k,k') = N_{\mu,\rho,\sigma}(k) + N_{\mu,\rho,\sigma}(k') - N_{\mu,\rho,\sigma}(k+k') \tag{D.1}$$

where $N_{\mu,\rho,\sigma}(k)$ denotes the average number of type-μ sites per insoluble type-ρ chain of class-σ SACs for $k \geq l_{S,\rho}$, with $N_{\mu,\rho,\sigma}(k) \equiv 0$ for $k < l_{S,\rho}$, and $\Delta N_{\mu',\rho,\sigma}(k,k')$ is thus the difference of the number of type-μ sites belonging to type-ρ chain caused by a cut.

The specific functional form of $N_{\mu,\rho,\sigma}(k)$ depends on the distribution of site types along a type-ρ chain. So we construct the site distribution model based on the assumption that O-sites are randomly distributed with a uniform probability $\varphi_{O,\rho,\sigma}$ over all $(l-1)$ intact

bonds within a type-ρ chain. By straightforward site counting, we thus construct $N_{\mu,\rho,\sigma}(l)$ for any insoluble type-ρ chain with $l \geq l_{S,\rho} = 7$

$$N_{\mu,\rho,\sigma}(l) = \begin{cases} (l-1)\varphi_{O,\rho,\sigma} & ,\mu = O \\ \varphi_{U_i,\rho} & ,\mu = L_{U_i}, R_{U_i} \\ \left(1-\varphi_{O,\rho,\sigma}\right)\varphi_{U_i,\rho}\varphi_{U_j,\rho} & ,\mu = X_{U_{ij}}, Y_{U_{ij}} \\ (l-3)\left(1-\varphi_{O,\rho,\sigma}\right)\varphi_{U_i,\rho}\varphi_{U_j,\rho} & ,\mu = N_{U_{ij}} \\ l\varphi_{J_i,\rho} & ,\mu = J_i \end{cases} \tag{D.2}$$

Here, $\varphi_{U_i,\rho}$ is the average molar ratio of the type-i monomer units to all the monomer units contained in the backbone of a type-ρ chain, and $\varphi_{J_i,\rho}$ is the average molar ratio of the type-J_i side groups to all the monomer units contained in the backbone of a type-ρ chain. Both of them actually characterize the natural composition of the type-ρ chains which can be easily obtained from literature and used in the model. Based on Equations (D.1) and (D.2),we can easily obtain the detailed expression of $\Delta N_{\mu',\rho,\sigma}(k,k')$.

Section E: Derivation of Chain Fragmentation Probabilities

This section shows the derivation of how to express $P_{\rho,\sigma}(k,k'|\mu,+1)$ in terms of $P_{\rho,\sigma}(l)$ and $P_{\rho,\sigma}(\mu|k,k',+1)$. Here, $P_{\rho,\sigma}(l)$ is defined as the probability of a randomly selected insoluble type-ρ chain, exposed on a class-σ SAC surface, to contain l monomer units, and $P_{\rho,\sigma}(\mu|k,k',+1)$ is the probability for a randomly selected intact bond to be of site type μ on a type-ρ chain, provided that the site is located k monomer units from the L-end and k' monomer units from the R-end of the type-ρ chain. $P_{\rho,\sigma}(\mu|k,k',+1)$ describes the distribution of different site types along a type-ρ chain (relative to the chain ends).

In order to express $P_{\rho,\sigma}(k,k'|\mu,+1)$ in terms of $P_{\rho,\sigma}(l)$ and $P_{\rho,\sigma}(\mu|k,k',+1)$, first, let us consider a random sample of type-ρ chains, with random chain lengths and a very large sample size NL →∞. Let these NL type-ρ chains be concatenated, in random order, into a "super type-ρ chain" where the R-end of each individual chain is connected to the L-end of its right neighbor chain by a fictitious bond, referred to as a "−1-bond", and the real internal bonds between monomer units contained in each chain are referred to as "+1-bonds". Hence, we are assigning to each bond site on the "super type-ρ chain" a "bond integrity" variable ζ, with $\zeta = +1$ for intact bond site types $N_{U_{ij}}$, $X_{U_{ij}}$, $Y_{U_{ij}}$ and O, and $\zeta = -1$ for broken bond site types L_{U_i} and R_{U_i} between adjacent chain ends (i.e. for a pair of adjacent L, R-sites).

Then, let us consider the average chain length for type-ρ main chains $\langle l \rangle_{\rho,\sigma}$, that is, the average degree of polymerization (DP), for type-ρ chains exposed on class-σ SAC surfaces. $\langle l \rangle_{\rho,\sigma}$ can be expressed in terms of the L-end broken site fraction of type-ρ chains $f_{E,\rho,\sigma}$, or the concentration of type-ρ chain $x_{E,\rho,\sigma}$, given by

$$\langle l \rangle_{\rho,\sigma} = \sum_{l=1}^{\infty} l P_{\rho,\sigma}(l) = \frac{1}{f_{E,\rho,\sigma}} = x_{M,\rho,\sigma}/x_{E,\rho,\sigma} \tag{E.1}$$

In Equation (E.1), $f_{E,\rho,\sigma}$ comes from the site type fractions $f_{\mu,\rho,\sigma}$, which is, for any site type belonging to type-ρ chains on class-σ SAC surfaces, defined by

$$f_{\mu,\rho,\sigma} = x_{\mu,\rho,\sigma}/x_{M,\rho,\sigma} \tag{E.2}$$

Based on the "uniform segment exposure" assumption (Zhou et al., 2009), the number of left chain ends must equal the number of right chain ends, that is $\sum_i x_{L_{U_i},\rho,\sigma} = \sum_i x_{R_{U_i},\rho,\sigma} =$

$x_{E,\rho,\sigma}$. Also, because of the relationship between L_{U_i} and $X_{U_{ij}}$ site groups, and between R_{U_i} and $Y_{U_{ij}}$ site groups, we can get $\sum_i f_{L_{U_i},\rho,\sigma} = \sum_{i,j} f_{X_{U_{ij}},\rho,\sigma} /(1-\varphi_{O,\rho,\sigma})$ and $\sum_i f_{R_{U_i},\rho,\sigma} = \sum_{i,j} f_{Y_{U_{ij}},\rho,\sigma} /(1-\varphi_{O,\rho,\sigma})$, so that $f_{E,\rho,\sigma}$ can be expressed as

$$f_{E,\rho,\sigma} = \sum_i f_{L_{U_i},\rho,\sigma} = \sum_i f_{R_{U_i},\rho,\sigma} \tag{E.3}$$

Next, we denote $P_{\rho,\sigma}(k,k',\zeta)$ as the probability that a bond randomly selected from the "super type-ρ chain" is a ζ-bond, where ζ is either +1 or −1, and that this randomly selected ζ-bond will be located $k \geq 1$ monomer units from its nearest L-end and be located $k' \geq 1$ monomer units from its nearest R-end. The expression of $P_{\rho,\sigma}(k,k',\zeta)$ is given by:

$$\begin{cases} P_{\rho,\sigma}(k,k',+1) = f_{E,\rho,\sigma} P_{\rho,\sigma}(k+k') \\ P_{\rho,\sigma}(k,k',-1) = f_{E,\rho,\sigma} P_{\rho,\sigma}(k) P_{\rho,\sigma}(k') \end{cases} \tag{E.4}$$

This can be derived from the "super type-ρ chain" construction as follows: for $\zeta = +1$, $P_{\rho,\sigma}(k,k',+1)$ is a joint probability for two conditions meeting at the same time: the first one is that the bond located k monomer units to the left of the randomly selected ζ-bond should be a "−1-bond"; the second one is that the adjacent $k+k'$ monomer units to the right of that "−1-bond" should form a single contiguous chain of length $l = k+k'$. The probabilities for these two conditions are $f_{E,\rho,\sigma}$ and $P_{\rho,\sigma}(k+k')$, respectively, hence the joint probability $P_{\rho,\sigma}(k,k',+1)$ is the product of $f_{E,\rho,\sigma}$ and $P_{\rho,\sigma}(k+k')$. For $\zeta = -1$, $P_{\rho,\sigma}(k,k',-1)$ can be derived by a similar way. And it can be easily verified that $\sum_{k,k',\zeta} P_{\rho,\sigma}(k,k',\zeta) = 1$.

Next, we introduce the conditional site type probability, given the type-ρ chain fragments, denoted by $P_{\rho,\sigma}(\mu|k,k',\zeta)$ which is the probability for a randomly selected "super type-ρ chain" bond to be of site type μ, given that the randomly selected bond is a ζ-bond; and given that it is located k and k' monomer units from its nearest "−1-bond" to the left and to the right, respectively. Just like $N_{\mu,\rho,\sigma}(k)$, the conditional type-ρ chain site probabilities $P_{\rho,\sigma}(\mu|k,k',\zeta)$ depend on the distribution of type-μ sites along the type-ρ chains. In fact, for purposes of the fragmentation kinetics $P_{\rho,\sigma}(\mu|k,k',\zeta)$ comprises the complete mathematical description of the chain site distribution model. The values of $P_{\rho,\sigma}(\mu|k,k',+1)$ and $N_{\mu,\rho,\sigma}(k)$ are not independent of each other: for any type-ρ chain site distribution, $P_{\rho,\sigma}(\mu|k,k',\zeta)$ must be normalized to $\sum_{\mu} P_{\rho,\sigma}(\mu|k,k',\zeta) = 1$, and $P_{\rho,\sigma}(\mu|k,k',+1)$ and $N_{\mu,\rho,\sigma}(k)$ must obey the following general chain site number counting relations for all intact bond site types:

$$N_{\mu,\rho,\sigma}(l) = \Theta\left(l - l_{S,\rho} + 1\right) \sum_{k=1}^{l-1} P_{\rho,\sigma}(\mu|k, l-k, +1) \tag{E.5a}$$

for $\mu = N_{U_{ij}}, X_{U_{ij}}, Y_{U_{ij}}, O$ with

$$\Theta(\Delta l) \equiv \begin{cases} 1, & \Delta l > 0 \\ 0, & \Delta l \leq 0 \end{cases} \tag{E.5b}$$

where $P_{\rho,\sigma}(\mu|k,k',+1)$ completely determines $N_{\mu,\rho,\sigma}(k)$ for site groups $N_{U_{ij}}, X_{U_{ij}}, Y_{U_{ij}}, O$. Based on the chain site model $N_{\mu,\rho,\sigma}(l)$, we thus assign the site groups $N_{U_{ij}}, X_{U_{ij}}, Y_{U_{ij}}, O$ of the intact type-ρ chain bonds to the corresponding "super type-ρ chain +1-bonds", while formally L_{U_i} and R_{U_i} are randomly assigned to each "super type-ρ chain −1-bond" with

probability $\varphi_{U_i,\rho,\sigma}/2$ corresponding to $\omega_\mu = 1/2$ for site groups formally L_{U_i} and R_{U_i}. Then $P_{\rho,\sigma}(\mu|k,k',\zeta)$ can be written as

$$P_{\rho,\sigma}(\mu|k,k',\zeta) =$$

$$\begin{cases} \delta_{\zeta,+1}\varphi_{O,\rho,\sigma} & ,\mu = O \\ \delta_{\zeta,-1}\varphi_{U_i,\rho,\sigma}/2 & ,\mu = L_{U_i}, R_{U_i} \\ \delta_{\zeta,+1}\delta_{k,k_{X,\rho}}\left(1-\varphi_{O,\rho,\sigma}\right)\varphi_{U_i,\rho,\sigma}\varphi_{U_j,\rho,\sigma} & ,\mu = X_{U_{ij}} \\ \delta_{\zeta,+1}\delta_{k',k_{Y,\rho}}\left(1-\varphi_{O,\rho,\sigma}\right)\varphi_{U_i,\rho,\sigma}\varphi_{U_j,\rho,\sigma} & ,\mu = Y_{U_{ij}} \\ \delta_{\zeta,+1}\left(1-\delta_{k,k_{X,\rho}}\right)\left(1-\delta_{k',k_{Y,\rho}}\right)\left(1-\varphi_{O,\rho,\sigma}\right)\varphi_{U_i,\rho,\sigma}\varphi_{U_j,\rho,\sigma} & ,\mu = N_{U_{ij}} \end{cases} \tag{E.6}$$

Finally, we can construct the conditional type-ρ fragmentation probability, given the site type, $P_{\rho,\sigma}(k,k'|\mu,\zeta)$, defined as the probability for a randomly selected bond in "super type-ρ chain" to be located k and k' monomer units from its nearest "−1-bond" to the left and to the right, respectively, given that the bond is a ζ-bond and that it is of site type μ. By Bayes' theorem, we have

$$P_{\rho,\sigma}(k,k'|\mu,\zeta) = \frac{P_{\rho,\sigma}\left(\mu\middle|k,k',\zeta\right)P_{\rho,\sigma}(k,k',\zeta)}{P_{\rho,\sigma}(\mu,\zeta)} \tag{E.7}$$

where the unconditional site type probability $P_{\rho,\sigma}(\mu,\zeta)$ is given by:

$$P_{\rho,\sigma}(\mu,\zeta) = \sum_{k,k'} P_{\rho,\sigma}(k,k',\mu,\zeta) = \begin{cases} \delta_{\zeta,+1}f_{\mu,\rho,\sigma} & ,\mu = N_{U_{ij}}, X_{U_{ij}}, Y_{U_{ij}}, O \\ \delta_{\zeta,-1}f_{\mu,\rho,\sigma}/2 & ,\mu = L_{U_i}, R_{U_i} \end{cases} \tag{E.8}$$

$P_{\rho,\sigma}(k,k'|\mu,\zeta)$is defined only when $P_{\rho,\sigma}(\mu,\zeta) > 0$. The fragmentation probabilities are normalized as $\sum_{k=1}^{\infty}\sum_{k'=1}^{\infty} P_{\rho,\sigma}(k,k'|\mu,\zeta) = 1$. So we obtain the expression of $P_{\rho,\sigma}(k,k'|\mu,+1)$ in terms of $P_{\rho,\sigma}(l)$ and $P_{\rho,\sigma}(\mu|k,k',+1)$, given by

$$P_{\rho,\sigma}(k,k'|\mu,+1) = \frac{f_{E,\rho,\sigma}}{f_{\mu,\rho,\sigma}} P_{\rho,\sigma}(\mu|k,k',+1) P_{\rho,\sigma}(k+k') \tag{E.9}$$

By using Equation (E.9), the expression of $\Delta\overline{N}_{S,\mu,\rho,\sigma}(k)$ can be written as

$$\Delta\overline{N}_{S,\mu,\rho,\sigma}(k) = \begin{cases} \frac{f_{E,\rho,\sigma}}{f_{\mu,\rho,\sigma}} \left[\varphi_{U_i,\rho,\sigma}\varphi_{U_j,\rho,\sigma}(1-\varphi_{O,\rho,\sigma})\right]\left[2-\delta_{k,k_{X,\rho}}-\delta_{k,k_{Y,\rho}}-P_{\rho,\sigma}(k+k_{X,\rho})-P_{\rho,\sigma}(k+k_{Y,\rho})\right] & ,\mu = N_{U_{ij}} \\ \frac{f_{E,\rho,\sigma}}{f_{\mu,\rho,\sigma}} \left[\varphi_{U_i,\rho,\sigma}\varphi_{U_j,\rho,\sigma}(1-\varphi_{O,\rho,\sigma})\right]\left[\delta_{k,k_{X,\rho}}+P_{\rho,\sigma}(k+k_{X,\rho})\right] & ,\mu = X_{U_{ij}} \\ \frac{f_{E,\rho,\sigma}}{f_{\mu,\rho,\sigma}} \left[\varphi_{U_i,\rho,\sigma}\varphi_{U_j,\rho,\sigma}(1-\varphi_{O,\rho,\sigma})\right]\left[\delta_{k,k_{Y,\rho}}+P_{\rho,\sigma}(k+k_{Y,\rho})\right] & ,\mu = Y_{U_{ij}} \end{cases} \tag{E.10}$$

Section F: Detailed Expression of the Surface Sites Increment Factor $\Delta\overline{N}_{\mu',\mu,\rho,\sigma}$

$$
\begin{cases}
\Pi_{NXY}\left[P_{\rho,\sigma}(l_{S,\rho}) + P_{\rho,\sigma}(l_{S,\rho} + k_{X,\rho} - 1)\right], \mu = X_{U_{ij}}, \mu' = X_{U_{i'j'}} \\
\Pi_{NXY}\left[P_{\rho,\sigma}(l_{S,\rho}) + P_{\rho,\sigma}(l_{S,\rho} + k_{X,\rho} - 1)\right], \mu = X_{U_{ij}}, \mu' = Y_{U_{i'j'}} \\
\Pi_{NXY}\left[P_{\rho,\sigma}(l_{S,\rho}) + P_{\rho,\sigma}(l_{S,\rho} + k_{Y,\rho} - 1)\right], \mu = Y_{U_{ij}}, \mu' = X_{U_{i'j'}} \\
\Pi_{NXY}\left[P_{\rho,\sigma}(l_{S,\rho}) + P_{\rho,\sigma}(l_{S,\rho} + k_{Y,\rho} - 1)\right], \mu = Y_{U_{ij}}, \mu' = Y_{U_{i'j'}} \\
\Pi_{NXY}\left[2l_{S,\rho} - 1 - \frac{1}{f_{E,\rho,\sigma}}\right], \mu = N_{U_{ij}}, \mu' = X_{U_{i'j'}} \\
\Pi_{NXY}\left[2l_{S,\rho} - 1 - \frac{1}{f_{E,\rho,\sigma}}\right], \mu = N_{U_{ij}}, \mu' = Y_{U_{i'j'}} \\
\Pi_{NXY}\left[k_{X,\rho} + \sum_{l=l_{S,\rho}}^{l_{S,\rho}+k_{X,\rho}-1}(l - k_{X,\rho} - 3)P_{\rho,\sigma}(l)\right], \mu = X_{U_{ij}}, \mu' = N_{U_{i'j'}} \\
\Pi_{NXY}\left[k_{Y,\rho} + \sum_{l=l_{S,\rho}}^{l_{S,\rho}+k_{Y,\rho}-1}(l - k_{Y,\rho} - 3)P_{\rho,\sigma}(l)\right], \mu = Y_{U_{ij}}, \mu' = N_{U_{i'j'}} \\
\Pi_{NXY}\left[\frac{3}{f_{E,\rho,\sigma}} + {l_{S,\rho}}^2 - 7l_{S,\rho} + 3 - k_{X,\rho} - k_{Y,\rho} + \sum_{l=l_{S,\rho}}^{l_{S,\rho}+k_{X,\rho}-1}(k_{X,\rho} + 3 - l)P_{\rho,\sigma}(l) + \sum_{l=l_{S,\rho}}^{l_{S,\rho}+k_{Y,\rho}-1}(k_{Y,\rho} + 3 - l)P_{\rho,\sigma}(l)\right], \mu = N_{U_{ij}}, \mu' = N_{U_{i'j'}} \\
\Pi_{O}\left[k_{X,\rho} + \sum_{l=l_{S,\rho}}^{l_{S,\rho}+k_{X,\rho}-1}(l - k_{X,\rho} - 1)P_{\rho,\sigma}(l)\right], \mu = X_{U_{ij}}, \mu' = O \\
\Pi_{O}\left[k_{Y,\rho} + \sum_{l=l_{S,\rho}}^{l_{S,\rho}+k_{Y,\rho}-1}(l - k_{Y,\rho} - 1)P_{\rho,\sigma}(l)\right], \mu = Y_{U_{ij}}, \mu' = O \\
\Pi_{O}\left[\frac{1}{f_{E,\rho,\sigma}} + {l_{S,\rho}}^2 - 3l_{S,\rho} + 1 - k_{X,\rho} - k_{Y,\rho} + \sum_{l=l_{S,\rho}}^{l_{S,\rho}+k_{X,\rho}-1}(k_{X,\rho} + 1 - l)P_{\rho,\sigma}(l) + \sum_{l=l_{S,\rho}}^{l_{S,\rho}+k_{Y,\rho}-1}(k_{Y,\rho} + 1 - l)P_{\rho,\sigma}(l)\right], \mu = N_{U_{ij}}, \mu' = O \\
\Pi_{J}\left[k_{X,\rho} + \sum_{l=l_{S,\rho}}^{l_{S,\rho}+k_{X,\rho}-1}(l - k_{X,\rho})P_{\rho,\sigma}(l)\right], \mu = X_{U_{ij}}, \mu' = J_i \\
\Pi_{J}\left[k_{Y,\rho} + \sum_{l=l_{S,\rho}}^{l_{S,\rho}+k_{Y,\rho}-1}(l - k_{Y,\rho})P_{\rho,\sigma}(l)\right], \mu = Y_{U_{ij}}, \mu' = J_i \\
\Pi_{J}\left[{l_{S,\rho}}^2 - l_{S,\rho} - k_{X,\rho} - k_{Y,\rho} + \sum_{l=l_{S,\rho}}^{l_{S,\rho}+k_{X,\rho}-1}(k_{X,\rho} - l)P_{\rho,\sigma}(l) + \sum_{l=l_{S,\rho}}^{l_{S,\rho}+k_{Y,\rho}-1}(k_{Y,\rho} - l)P_{\rho,\sigma}(l)\right], \mu = N_{U_{ij}}, \mu' = J_i
\end{cases}
\tag{F.1}
$$

$$
\begin{cases}
\Pi_{NXY} = -\left(\frac{f_{E,\rho,\sigma}}{f_{\mu,\rho,\sigma}}\right)\left[\varphi_{U_i,\rho,\sigma}\varphi_{U_j,\rho,\sigma}\varphi_{U_{i'},\rho,\sigma}\varphi_{U_{j'},\rho,\sigma}(1 - \varphi_{O,\rho,\sigma})^2\right] \\
\Pi_{O} = -\left(\frac{f_{E,\rho,\sigma}}{f_{\mu,\rho,\sigma}}\right)\left[\varphi_{U_i,\rho,\sigma}\varphi_{U_j,\rho,\sigma}(1 - \varphi_{O,\rho,\sigma})\varphi_{O,\rho,\sigma}\right] \\
\Pi_{J} = -\left(\frac{f_{E,\rho,\sigma}}{f_{\mu,\rho,\sigma}}\right)\left[\varphi_{U_i,\rho,\sigma}\varphi_{U_j,\rho,\sigma}(1 - \varphi_{O,\rho,\sigma})\varphi_{J,\rho,\sigma}\right]
\end{cases}
\tag{F.2}
$$

Section G: Derivation of Production Factor of Oligomer

As $P_{\rho,\sigma}(k,k'|\mu,+1)$ can be expressed in terms of $P_{\rho,\sigma}(l)$ and $P_{\rho,\sigma}(\mu|k,k',+1)$, we can obtain

$$\Delta\bar{N}_{S,\mu,\rho,\sigma}(k) = \frac{f_{E,\rho,\sigma}}{f_{\mu,\rho,\sigma}} \sum_{k'=l_{S,\rho}-k}^{\infty} \left[P_{\rho,\sigma}(\mu|k,k',+1) + P_{\rho,\sigma}(\mu|k',k,+1)\right] P_{\rho,\sigma}(k'+k) \quad \text{(G.1)}$$

By using the "Chain End Decomposition" theory (Zhou et al., 2009) we can separate the effects of the near-chain-end sites, which can be cut by both exo- and endo-enzymes, from the chain interior sites, which can only be cut by endo-enzymes. $P_{\rho,\sigma}(\mu|k,k',+1)$ can then be decomposed into left end (L), right end (R) and interior (I) contributions of the type-ρ main chain, which can be written as

$$P_{\rho,\sigma}(\mu|k,k',+1) = P_{\mu,\rho,\sigma}^{(I)} + \Theta_{L,\rho}(k)P_{\mu,\rho,\sigma}^{(L)}(k) + \Theta_{R,\rho}(k')P_{\mu,\rho,\sigma}^{(R)}(k') \quad \text{(G.2)}$$

where $\Theta_{L,\rho}(k) \equiv \Theta(l_{L,\rho} - k)$ and $\Theta_{R,\rho}(k') \equiv \Theta(l_{R,\rho} - k')$ are the cut-off factors dividing a type-ρ chain into three parts with $l_{L,\rho} \equiv k_{X,\rho} + 1$ and $l_{R,\rho} \equiv k_{Y,\rho} + 1$. Also, $k' + k > l_{LR,\rho} \equiv l_{L,\rho} + l_{R,\rho} - 1$ and $P_{\rho,\sigma}(\mu|k,k',+1) = P_{\mu,\rho,\sigma}^{(I)}$ is independent of k and k' when there are $k > l_{L,\rho}$ and $k' > l_{R,\rho}$. Based on the functional form, we can obtain in detail the values of three contributions for each hydrolysable intact bond site, shown as

$$
\begin{cases}
\begin{cases}
P_{\mu,\rho,\sigma}^{(I)} = \left(1-\varphi_{O,\rho,\sigma}\right)\varphi_{U_i,\rho,\sigma}\varphi_{U_j,\rho,\sigma} \\
P_{\mu,\rho,\sigma}^{(L)}(k) = -\delta_{k,k_{X,\rho}}\left(1-\varphi_{O,\rho,\sigma}\right)\varphi_{U_i,\rho,\sigma}\varphi_{U_j,\rho,\sigma} \\
P_{\mu,\rho,\sigma}^{(R)}(k') = -\delta_{k',k_{Y,\rho}}\left(1-\varphi_{O,\rho,\sigma}\right)\varphi_{U_i,\rho,\sigma}\varphi_{U_j,\rho,\sigma}
\end{cases} & ,\mu = N_{U_{ij}} \\
\begin{cases}
P_{\mu,\rho,\sigma}^{(I)} = 0 \\
P_{\mu,\rho,\sigma}^{(L)}(k) = \delta_{k,k_{X,\rho}}\left(1-\varphi_{O,\rho,\sigma}\right)\varphi_{U_i,\rho,\sigma}\varphi_{U_j,\rho,\sigma} \\
P_{\mu,\rho,\sigma}^{(R)}(k') = 0
\end{cases} & ,\mu = X_{U_{ij}} \\
\begin{cases}
P_{\mu,\rho,\sigma}^{(I)} = 0 \\
P_{\mu,\rho,\sigma}^{(L)}(k) = 0 \\
P_{\mu,\rho,\sigma}^{(R)}(k') = \delta_{k',k_{Y,\rho}}\left(1-\varphi_{O,\rho,\sigma}\right)\varphi_{U_i,\rho,\sigma}\varphi_{U_j,\rho,\sigma}
\end{cases} & ,\mu = Y_{U_{ij}}
\end{cases}
\tag{G.3}
$$

which then can be used to obtain the detailed expressions of $\Delta\bar{N}_{S,\mu,\rho,\sigma}(k)$.

Section H: Derivations of Chain Concentration Rate Equations and Rate Equations Closure

In order to find the solution for $P_{\rho,\sigma}(l)$ with $l \leq l_{C,\rho}$, a new rate equation system is developed for type-ρ chains concentration variables $H_{\rho,\sigma}(l)$ by defining $H_{\rho,\sigma}(l) \equiv P_{\rho,\sigma}(l)x_{E,\rho,\sigma}$, with $H_{\rho,\sigma}(l) \equiv 0$ for $l < l_{S,\rho}$. Here, $x_{E,\rho,\sigma}$ is the concentration of insoluble type-ρ chains, as discussed in Supporting Information section D. All the surface site concentration variables now could be expressed in terms of $H_{\rho,\sigma}(l)$ by using $x_{M,\rho,\sigma} = \sum_{l=l_{S,\rho}}^{\infty} lH_{\rho,\sigma}(l)$ and $x_{\mu,\rho,\sigma} = \sum_{l=l_{S,\rho}}^{\infty} N_{\mu,\rho,\sigma}(l)H_{\rho,\sigma}(l)$. Analogous to the site ablation rate equations, the rate equations of $H_{\rho,\sigma}(l)$ is given by

$$
\dot{H}_{\rho,\sigma}(l) = R_{H,\rho,\sigma}(l) - \bar{R}_\sigma \eta_\sigma(\lambda_\sigma)\Phi_{M,\rho,\sigma}(\lambda_\sigma - 1)Q_{\rho,\sigma}(l,\lambda_\sigma - 1) / \sum_{j=l_{S,\rho}}^{\infty} jQ_{\rho,\sigma}(j,\lambda_\sigma - 1)
\tag{H.1}
$$

where $R_{H,\rho,\sigma}(l)$ is the changing rate of type-ρ chains of length l due to bonds cutting, and the second term of the equation above gives the rate of exposure of new type-ρ chains due to the removal of overlaying material. $Q_{\rho,\sigma}(l,\lambda_\sigma)$ is the type-ρ chain length distribution of the native substrate material in each layer of class-σ SACs, which obeys the delta-function native type-ρ chain length distribution $Q_{\rho,\sigma}(l,\lambda_\sigma) \equiv \delta_{l,DP_\rho}$. $Q_{\rho,\sigma}(l,\lambda_\sigma)$ has a close relationship with the native site fraction $g_{\mu,\rho,\sigma}$, which is given by

$$g_{E,\rho,\sigma} = 1/\left[\sum_{l=l_{S,\rho}}^{\infty} lQ_{\rho,\sigma}(l,\lambda_\sigma)\right] \tag{H.2}$$

$$g_{\mu,\rho,\sigma}(\lambda_\sigma) = g_{E,\rho,\sigma}\sum_{l=l_{S,\rho}}^{\infty} N_{\mu,\rho,\sigma}(l)Q_{\rho,\sigma}(l,\lambda_\sigma) \tag{H.3}$$

As described in Supporting Information section G, $R_{H,\rho,\sigma}(k)$ can be written by

$$R_{H,\rho,\sigma}(l) = -\sum_{k,k'=1}^{\infty} R_{\rho,\sigma}(l \to k,k') + \sum_{k=1}^{\infty}\sum_{j=l+1}^{\infty}\left[R_{\rho,\sigma}(j \to k,l) + R_{\rho,\sigma}(j \to l,k)\right] \tag{H.4}$$

with

$$R_{\rho,\sigma}(l \to k,k') = \sum_{\kappa,\mu}\gamma_{\kappa,\mu,\rho}z_{\kappa,\mu,\rho,\sigma}P_{\rho,\sigma}(k,k'|\mu,+1)\delta_{l,k+k'} \tag{H.5}$$

$R_{\rho,\sigma}(l \to k,k')$ is denoted as the rate at which surface-exposed type-ρ chains of length l on class-σ SACs are being cut into two type-ρ chain fragments of length k and k', from the L-end and R-end of the original type-ρ chains respectively. As $P_{\rho,\sigma}(k,k'|\mu,+1)$ can be expressed in terms of $P_{\rho,\sigma}(l)$ and $P_{\rho,\sigma}(\mu|k,k',+1)$, we can rewrite $R_{H,\rho,\sigma}(l)$ as

$$R_{H,\rho,\sigma}(l) = \sum_{\kappa,\mu} \gamma_{\kappa,\mu,\rho} z_{\kappa,\mu,\rho,\sigma} \Delta\bar{N}_{H,\mu,\rho,\sigma}(l) \tag{H.6}$$

By using the "Chain End Decomposition" (Zhou et al., 2009) theory, we can obtain

$$\Delta\bar{N}_{H,\mu,\rho,\sigma}(l) = \frac{f_{E,\rho,\sigma}}{f_{\mu,\rho,\sigma}} \left[A_{H,\mu,\rho,\sigma}(l) + B_{H,\mu,\rho,\sigma}(l) + D_{H,\mu,\rho,\sigma}(l)\right] \tag{H.7a}$$

where

$$A_{H,\mu,\rho,\sigma}(l) = -N_{\mu,\rho,\sigma}(l) P_{\rho,\sigma}(l) \tag{H.7b}$$

$$B_{H,\mu,\rho,\sigma}(l) = \left[2P^{(I)}_{\mu,\rho,\sigma} + \Theta_{L,\rho}(l) P^{(L)}_{\mu,\rho,\sigma}(l) + \Theta_{R,\rho}(l) P^{(R)}_{\mu,\rho,\sigma}(l)\right]\left[1 - \sum_{j=1}^{l} P_{\rho,\sigma}(j)\right] \tag{H.7c}$$

$$D_{H,\mu,\rho,\sigma}(l) = \sum_{j=l+1}^{l+l_{E,\rho}} P_{\rho,\sigma}(l)\left[\Theta_{L,\rho}(j-l) P^{(L)}_{\mu,\rho,\sigma}(j-l) + \Theta_{R,\rho}(j-l) P^{(R)}_{\mu,\rho,\sigma}(j-l)\right] \tag{H.7d}$$

with $l_{E,\rho} = max\left(l_{L,\rho}, l_{R,\rho}\right) - 1$. The detailed expression of $\Delta\bar{N}_{H,\mu,\rho,\sigma}(l)$ can be obtained by combining Equations (H.7a), (H.7b), (H.7c), (H.7d) and (D.2), written as

$$\Delta\bar{N}_{H,\mu,\rho,\sigma}(l) = \begin{cases} \frac{f_{E,\rho,\sigma}}{f_{\mu,\rho,\sigma}}\left[\varphi_{U_i,\rho,\sigma}\varphi_{U_j,\rho,\sigma}\left(1-\varphi_{O,\rho,\sigma}\right)\right]\left[2 - 2\sum_{k=1}^{l} P_{\rho,\sigma}(k) - (l-3)P_{\rho,\sigma}(l) - P_{\rho,\sigma}\left(l+k_{X,\rho}\right) - P_{\rho,\sigma}\left(l+k_{Y,\rho}\right)\right] & ,\mu = N_{U_{ij}} \\ \frac{f_{E,\rho,\sigma}}{f_{\mu,\rho,\sigma}}\left[\varphi_{U_i,\rho,\sigma}\varphi_{U_j,\rho,\sigma}(1-\varphi_{O,\rho,\sigma})\right]\left[P_{\rho,\sigma}\left(l+k_{X,\rho}\right) - P_{\rho,\sigma}(l)\right] & ,\mu = X_{U_{ij}} \\ \frac{f_{E,\rho,\sigma}}{f_{\mu,\rho,\sigma}}\left[\varphi_{U_i,\rho,\sigma}\varphi_{U_j,\rho,\sigma}(1-\varphi_{O,\rho,\sigma})\right]\left[P_{\rho,\sigma}\left(l+k_{Y,\rho}\right) - P_{\rho,\sigma}(l)\right] & ,\mu = Y_{U_{ij}} \end{cases} \tag{H.8}$$

To solve the chain concentration rate equations for $H_{\rho,\sigma}(l)$ at short chain lengths from l to the cut-off length $l_{C,\rho}$, it is necessary to use the value of $P_{\rho,\sigma}(l)$ at chain lengths from l to $l_{C,\rho} + l_{E,\rho}$. Obviously, the length ranges of l are different for $H_{\rho,\sigma}(l)$ and $P_{\rho,\sigma}(l)$, which

will make the equation system redundant. So in order to solve $H_{\rho,\sigma}(l)$ with the length range of $l_{S,\rho} \leq l \leq l_{C,\rho}$ by using $P_{\rho,\sigma}(l)$ with the same length range, the Local Poisson (LP) approximation scheme (Zhou et al., 2009) is used here for $P_{\rho,\sigma}(l)$, so that we have

$$P_{\rho,\sigma}(l) = P_{\rho,\sigma}(l_{C,\rho})\left[P_{\rho,\sigma}(l_{C,\rho})/P_{\rho,\sigma}(l_{C,\rho}-1)\right]^{(l-l_{C,\rho})} \tag{H.9}$$

for $l_{C,\rho} + 1 \leq l \leq l_{C,\rho} + l_{E,\rho}$. By using Equation (H.9) with the relationship $P_{\rho,\sigma}(l) \equiv H_{\rho,\sigma}(l)/x_{E,\rho,\sigma}$, a closed ordinary differential equation (ODE) system for the site concentration formalism is completed.

Section I: Parameters

All parameters are categorized into four groups and showed in four tables respectively. The first group in Table I1 includes $\bar{F}_A^{(0)}$ and $\bar{\Phi}_{M,Xyl}^{(0)}$, which describe the initial substrate morphology i.e. the enzymatic accessibilities of the whole substrate and xylan, respectively. Based on the values of these two parameters we can obtain the enzymatic accessibility of cellulose. We believe that the values of these two parameters could be measured by using reliable experimental techniques in the future. However, there are currently no values for these two parameters. So we adjust the values for $\bar{F}_A^{(0)}$ and $\bar{\Phi}_{M,Xyl}^{(0)}$ based on the values of enzymatic accessibility of cellulose, which is commonly measured in experiments. The values we used were from the literature (Zhu et al., 2009a; Zhu et al., 2009b). Based on the experiments by Zhu et al. (2009b), the enzymatic accessibility of cellulose was 0.243 for DA-pretreated corn stover and 0.0238 for non-pretreated corn stover. Thus we believe that the value of the enzymatic accessibility of cellulose for AFEX-pretreated corn stover, as

well as poplar, should range from 0.0238 to 0.243. The values of the enzymatic accessibility of cellulose we used in the model were 0.0832, 0.0998 and 0.0753.

The second group is adsorption and kinetic parameters and shown in Table I2. The values of $L_{1,N,Glu}$, $L_{1,X,Glu}$, $L_{1,Y,Glu}$, $L_{2,N,Glu}$, $L_{2,X,Glu}$, $L_{2,Y,Glu}$, $L_{3,N,Glu}$ and $L_{3,X,Glu}$, which describe the adsorption equilibrium between cellulose-sites and cellulases, were adopted from the work of Zhou et al. (2009b) with referenced experiments. $L_{1,N,Xyl}$, $L_{1,X,Xyl}$, $L_{1,Y,Xyl}$, $L_{2,N,Xyl}$, $L_{2,X,Xyl}$, $L_{2,Y,Xyl}$, $L_{3,N,Xyl}$ and $L_{3,X,Xyl}$ are parameters describing the adsorption equilibrium between xylan sites and cellulases. The values for these parameters were all set to be 0 as we assume that if there is no effective adsorption between enzyme molecule and bond site leading to bond cleavage, the parameter of adsorption equilibrium would be set to 0. For the same reason, $L_{4,N,Glu}$, $L_{4,X,Glu}$, $L_{4,Y,Glu}$, $L_{5,N,Glu}$, $L_{5,X,Glu}$, $L_{5,Y,Glu}$, $L_{5,N,Xyl}$, $L_{5,Y,Xyl}$, $L_{6,N,Xyl}$, $L_{6,X,Xyl}$, $L_{7,\mu,\rho}$ and $L_{8,\mu,\rho}$, which describe the adsorption equilibrium between sites and enzymes having no adsorption relationships, were also set to be 0. $L_{4,N,Xyl}$, $L_{4,X,Xyl}$ and $L_{4,Y,Xyl}$ describe the adsorption equilibrium between Endo-acting xylanases and xylan sites and the values of these parameters were from the experiments by Qing and Wyman (2011). The values of kinetic parameters $\gamma_{1,N,Glu}$, $\gamma_{1,X,Glu}$, $\gamma_{1,Y,Glu}$, $\gamma_{2,X,Glu}$, $\gamma_{3,Y,Glu}$, $\gamma_{4,N,Xyl}$, $\gamma_{4,X,Xyl}$ and $\gamma_{4,Y,Xyl}$ came from the literature (Banerjee et al., 2010a; Banerjee et al., 2010b) which used AFEX-pretreated corn stover as substrate. The relationship among these parameters was from the work by Zhang and Lynd (2006) in which the activity ratio of EG:CBH2:CBH1 was 5:2:1. For ineffective adsorptions that cannot lead to bond cleavage, the corresponding kinetic parameters would be 0. So the values of $\gamma_{1,N,Xyl}$, $\gamma_{1,X,Xyl}$, $\gamma_{1,Y,Xyl}$, $\gamma_{2,N,Glu}$, $\gamma_{2,Y,Glu}$, $\gamma_{2,N,Xyl}$, $\gamma_{2,X,Xyl}$, $\gamma_{2,Y,Xyl}$, $\gamma_{3,N,Glu}$,

$\gamma_{3,X,Glu}$, $\gamma_{3,N,Xyl}$, $\gamma_{3,X,Xyl}$, $\gamma_{3,Y,Xyl}$, $\gamma_{4,N,Glu}$, $\gamma_{4,X,Glu}$ and $\gamma_{4,Y,Glu}$ were all set to be 0. Currently, there are no reliable values of the adsorption and kinetic parameters of Exo-acting xylanases. So we assumed that values of $L_{5,N,Glu}$, $L_{5,X,Glu}$, $L_{5,Y,Glu}$, $L_{5,N,Xyl}$, $L_{5,X,Xyl}$, $L_{5,Y,Xyl}$, $L_{6,N,Glu}$, $L_{6,X,Glu}$, $L_{6,Y,Glu}$, $L_{6,N,Xyl}$, $L_{6,X,Xyl}$ and $L_{6,Y,Xyl}$ were equal to the values of corresponding parameters of Endo-acting xylanases. However, these parameters did not affect the simulation results since it is assumed that commercial enzyme mixtures do not contain significant amount of Exo-acting xylanases.

The third group is inhibition parameters and shown in Table I3. $I_{1,Glu}(1)$, $I_{2,Glu}(1)$ and $I_{3,Glu}(1)$ are D-glucose (G1) inhibition parameters for EG, CBH2 and CBH1 respectively, and their values were from the work by Levine et al. (2010). Similarly, $I_{1,Glu}(2)$, $I_{2,Glu}(2)$ and $I_{3,Glu}(2)$ are cellobiose (G2) inhibition parameters for EG, CBH2 and CBH1 respectively, and their values were from the work by Tolan and Foody (1999). There are limited reported values for cello-oligomers (G3-G6) inhibition parameters for cellulases. The values of $I_{1,Glu}(3)$, $I_{2,Glu}(3)$, $I_{3,Glu}(3)$, $I_{1,Glu}(4)$, $I_{2,Glu}(4)$, $I_{3,Glu}(4)$, $I_{1,Glu}(5)$, $I_{2,Glu}(5)$, $I_{3,Glu}(5)$, $I_{1,Glu}(6)$, $I_{2,Glu}(6)$ and $I_{3,Glu}(6)$ were based on the values of $I_{1,Glu}(2)$, $I_{2,Glu}(2)$ and $I_{3,Glu}(2)$ as well as the experiments by Lo Leggio and Pickersgill (1999) which describe the relationship among cello-oligomers (G2-G6) inhibition parameters for cellulases. Currently, there are no reliable values of the D-xylose (X1) inhibition parameters for EG, CBH2 and CBH1 respectively. So we assumed that values of $I_{1,Xyl}(1)$, $I_{2,Xyl}(1)$ and $I_{3,Xyl}(1)$ were equal to $I_{1,Glu}(1)$, $I_{2,Glu}(1)$ and $I_{3,Glu}(1)$ respectively due to the similarity between the structures of these two monomer units. $I_{1,Xyl}(2)$, $I_{2,Xyl}(2)$ and $I_{3,Xyl}(2)$ are xylobiose (X2) inhibition parameters for EG, CBH2 and CBH1 respectively,

and their values were from the work by Ntarima et al. (2000). The values of $I_{1,Xyl}(3)$, $I_{2,Xyl}(3)$, $I_{3,Xyl}(3)$, $I_{1,Xyl}(4)$, $I_{2,Xyl}(4)$, $I_{3,Xyl}(4)$, $I_{1,Xyl}(5)$, $I_{2,Xyl}(5)$, $I_{3,Xyl}(5)$, $I_{1,Xyl}(6)$, $I_{2,Xyl}(6)$ and $I_{3,Xyl}(6)$ were based on the values of $I_{1,Xyl}(2)$, $I_{2,Xyl}(2)$ and $I_{3,Xyl}(2)$ as well as the experiments by Lo Leggio and Pickersgill (1999) which also described the relationship among xylo-oligomers (X2-X6) inhibition parameters for cellulases. $I_{4,Glu}(1)$ is D-glucose (G1) inhibition parameter for Endo-acting xylanases which currently do not have too much reliable values. So we assumed that value of $I_{4,Glu}(1)$ was equal to $I_{1,Glu}(1)$ due to the same inhibitor. For the same reason, the values of cello-oligomers (G2-G6) inhibition parameters for Endo-acting xylanases, which are $I_{4,Glu}(2)$, $I_{4,Glu}(3)$, $I_{4,Glu}(4)$, $I_{4,Glu}(5)$ and $I_{4,Glu}(6)$, were all determined. The values of D-xylose (X1) and xylobiose (X2) inhibition parameters for Endo-acting xylanases $I_{4,Xyl}(1)$ and $I_{4,Xyl}(2)$ were based on the work by Ntarima et al. (2000). The values of $I_{4,Xyl}(3)$, $I_{4,Xyl}(4)$, $I_{4,Xyl}(5)$ and $I_{4,Xyl}(6)$ were based on the value of $I_{4,Xyl}(2)$ and the experiments by Lo Leggio and Pickersgill (1999) which described the relationship among xylo-oligomers (X2-X6) inhibition parameters for Endo-acting xylanases. Currently, there are no reliable values for the inhibition parameters of Exo-acting xylanases. So we assumed that the values of inhibition parameters of Exo-acting xylanases were equal to the values of corresponding inhibition parameters of Endo-acting xylanases. However, these parameters did not affect the simulation results since we did not consider Exo-acting xylanases as enzyme species in any commercial enzyme.

The fourth group is parameters about beta-enzymes and shown in Table I4. $I_{7,Glu}(1)$ and $I_{7,Glu}(2)$ are the D-glucose (G1) adsorption (or inhibition) parameter for beta-glucosidase

(BG) and the cellobiose (G2) adsorption parameter for BG respectively. The values of these parameters were from the experiment by Chauve et al. (2010). $I_{7,Xyl}(3)$, $I_{7,Xyl}(4)$, $I_{7,Xyl}(5)$ and $I_{7,Xyl}(6)$ are cello-oligomers (G3-G6) adsorption parameters for BG. Their values were based on the value of $I_{7,Glu}(2)$ and the experiments by Yazaki et al. (1997) which described the relationship among cello-oligomers (G2-G6) inhibition parameters for BG. $I_{8,Xyl}(1)$, $I_{8,Xyl}(2)$, $I_{8,Xyl}(3)$, $I_{8,Xyl}(4)$, $I_{8,Xyl}(5)$ and $I_{8,Xyl}(6)$ are D-xylose and xylo-oligomers (X2-X6) adsorption parameters for beta-xylosidase (BX). Their values were from the work by Rasmussen et al. (2006). Currently, there are no reliable values for the xylo-oligomers (X1-X6) adsorption parameters for BG and cello-oligomers (G1-G6) inhibition parameters for BX. We only considered the inhibitions of X1 for BG and G1 for BX and did not consider other "crossover" oligomers adsorption for beta-enzymes in the model. We assumed that the values of $I_{7,Xyl}(1)$ and $I_{8,Glu}(1)$ were equal to $I_{8,Xyl}(1)$ and $I_{7,Xyl}(1)$ respectively due to the same inhibitors. The value of BG kinetic parameter $\gamma_{7,Glu}(2)$ for cellobiose (G2) was from experiment by Chauve et al. (2010). $\gamma_{7,Xyl}(3)$, $\gamma_{7,Xyl}(4)$, $\gamma_{7,Xyl}(5)$ and $\gamma_{7,Xyl}(6)$ are BG kinetic parameters for cello-oligomers (G3-G6), their values were based on the value of $\gamma_{7,Glu}(2)$ and the experiments by Yazaki et al. (1997) which described the relationship among BG kinetic parameters for cello-oligomers (G2-G6). $\gamma_{8,Xyl}(2)$, $\gamma_{8,Xyl}(3)$, $\gamma_{8,Xyl}(4)$, $\gamma_{8,Xyl}(5)$ and $\gamma_{8,Xyl}(6)$ are BX kinetic parameters for xylo-oligomers (X2-X6) and their values from the work by Rasmussen et al. (2006). As we did not consider other "crossover" oligomers adsorption for beta-enzymes in the model, the corresponding kinetic parameters were all set to be 0

Table.I1 Key simulation parameters

Qing and Wyman (2011)		Banerjee et al. (2010a)		Kumar and Wyman (2009)	
Parameter	Value	Parameter	Value	Parameter	Value
$\bar{F}_A^{(0)}$	0.1051	$\bar{F}_A^{(0)}$	0.1431	$\bar{F}_A^{(0)}$	0.1046
$\bar{\Phi}_{M,Xyl}^{(0)}$	0.55	$\bar{\Phi}_{M,Xyl}^{(0)}$	0.50	$\bar{\Phi}_{M,Xyl}^{(0)}$	0.60

Table.I2 Adsorption and kinetic parameters

Parameter	Value (1/mM)	Ref.	Parameter	Value (1/min)	Ref.
$L_{1,N,Glu}$ $L_{1,X,Glu}$ $L_{1,Y,Glu}$	3	(Zhou et al., 2009a)	$\gamma_{1,N,Glu}$ $\gamma_{1,X,Glu}$ $\gamma_{1,Y,Glu}$	3317	(Banerjee et al., 2010a; Zhang and Lynd, 2006)
$L_{1,N,Xyl}$ $L_{1,X,Xyl}$ $L_{1,Y,Xyl}$	0		$\gamma_{1,N,Xyl}$ $\gamma_{1,X,Xyl}$ $\gamma_{1,Y,Xyl}$	0	(Zhou et al., 2009a)
$L_{2,N,Glu}$ $L_{2,Y,Glu}$	0		$\gamma_{2,N,Glu}$ $\gamma_{2,Y,Glu}$	0	
$L_{2,X,Glu}$	4		$\gamma_{2,X,Glu}$	1399	(Banerjee et al., 2010a; Zhang and Lynd, 2006)
$L_{2,N,Xyl}$ $L_{2,X,Xyl}$ $L_{2,Y,Xyl}$	0		$\gamma_{2,N,Xyl}$ $\gamma_{2,X,Xyl}$ $\gamma_{2,Y,Xyl}$	0	(Zhou et al., 2009a)
$L_{3,N,Glu}$ $L_{3,X,Glu}$	0		$\gamma_{3,N,Glu}$ $\gamma_{3,X,Glu}$	0	
$L_{3,Y,Glu}$	3		$\gamma_{3,Y,Glu}$	699.7	(Banerjee et al., 2010a; Zhang and Lynd, 2006)
$L_{3,N,Xyl}$ $L_{3,X,Xyl}$ $L_{3,Y,Xyl}$	0		$\gamma_{3,N,Xyl}$ $\gamma_{3,X,Xyl}$ $\gamma_{3,Y,Xyl}$	0	(Zhou et al., 2009a)
$L_{4,N,Glu}$ $L_{4,X,Glu}$ $L_{4,Y,Glu}$	0		$\gamma_{4,N,Glu}$ $\gamma_{4,X,Glu}$ $\gamma_{4,Y,Glu}$	0	
$L_{4,N,Xyl}$ $L_{4,X,Xyl}$ $L_{4,Y,Xyl}$	0.574	(Qing and Wyman, 2011; Zhang and Lynd, 2006)	$\gamma_{4,N,Xyl}$ $\gamma_{4,X,Xyl}$ $\gamma_{4,Y,Xyl}$	50.12	(Banerjee et al., 2010a; Zhang and Lynd, 2006)

$L_{5,N,Glu}$ $L_{5,X,Glu}$ $L_{5,Y,Glu}$	0		$\gamma_{5,N,Glu}$ $\gamma_{5,X,Glu}$ $\gamma_{5,Y,Glu}$	0	
$L_{5,N,Xyl}$ $L_{5,Y,Xyl}$	0		$\gamma_{5,N,Xyl}$ $\gamma_{5,Y,Xyl}$	0	
$L_{5,X,Xyl}$	0.574		$\gamma_{5,X,Xyl}$	50.12	
$L_{6,N,Glu}$ $L_{6,X,Glu}$ $L_{6,Y,Glu}$	0	Assumed	$\gamma_{6,N,Glu}$ $\gamma_{6,X,Glu}$ $\gamma_{6,Y,Glu}$	0	Assumed
$L_{6,N,Xyl}$ $L_{6,X,Xyl}$	0		$\gamma_{6,N,Glu}$ $\gamma_{6,X,Glu}$	0	
$L_{6,Y,Xyl}$	0.574		$\gamma_{6,Y,Xyl}$	50.12	
$L_{7,\mu,\rho}$ $L_{8,\mu,\rho}$	0		$\gamma_{7,\mu,\rho}$ $\gamma_{8,\mu,\rho}$	0	

Table.I3 Inhibition parameters

Parameter	Value (1/mM)	Reference	Parameter	Value (1/mM)	Reference
$I_{1,Glu}(1)$	0.06	(Levine et al., 2010)	$I_{2,Glu}(1)$ $I_{3,Glu}(1)$	0.032	(Levine et al., 2010)
$I_{1,Glu}(2)$	0.13	(Tolan and Foody, 1999)	$I_{2,Glu}(2)$ $I_{3,Glu}(2)$	0.13	(Tolan and Foody, 1999)
$I_{1,Glu}(3)$	0.3	(Lo Leggio and Pickersgill, 1999; Tolan and Foody, 1999)	$I_{2,Glu}(3)$ $I_{3,Glu}(3)$	0.3	(Lo Leggio and Pickersgill, 1999; Tolan and Foody, 1999)
$I_{1,Glu}(4)$	0.37		$I_{2,Glu}(4)$ $I_{3,Glu}(4)$	0.37	
$I_{1,Glu}(5)$	0.44		$I_{2,Glu}(5)$ $I_{3,Glu}(5)$	0.44	
$I_{1,Glu}(6)$	0.51		$I_{2,Glu}(6)$ $I_{3,Glu}(6)$	0.51	
$I_{1,Xyl}(1)$	0.06	Assumed	$I_{2,Xyl}(1)$ $I_{3,Xyl}(1)$	0.032	Assumed
$I_{1,Xyl}(2)$	2	(Lo Leggio and Pickersgill, 1999; Ntarima et al., 2000)	$I_{2,Xyl}(2)$ $I_{3,Xyl}(2)$	2	(Lo Leggio and Pickersgill, 1999; Ntarima et al., 2000)
$I_{1,Xyl}(3)$	2		$I_{2,Xyl}(3)$ $I_{3,Xyl}(3)$	2	
$I_{1,Xyl}(4)$	4		$I_{2,Xyl}(4)$ $I_{3,Xyl}(4)$	4	
$I_{1,Xyl}(5)$	10		$I_{2,Xyl}(5)$ $I_{3,Xyl}(5)$	10	
$I_{1,Xyl}(6)$	11		$I_{2,Xyl}(6)$ $I_{3,Xyl}(6)$	11	
$I_{4,Glu}(1)$	0.06	Assumed	$I_{5,Glu}(1)$ $I_{6,Glu}(1)$	0.032	Assumed
$I_{4,Glu}(2)$	0.13	(Lo Leggio and Pickersgill, 1999; Tolan and Foody, 1999)	$I_{5,Glu}(2)$ $I_{6,Glu}(2)$	0.13	
$I_{4,Glu}(3)$	0.3		$I_{5,Glu}(3)$ $I_{6,Glu}(3)$	0.3	
$I_{4,Glu}(4)$	0.37		$I_{5,Glu}(4)$ $I_{6,Glu}(4)$	0.37	
$I_{4,Glu}(5)$	0.44		$I_{5,Glu}(5)$ $I_{6,Glu}(5)$	0.44	
$I_{4,Glu}(6)$	0.51		$I_{5,Glu}(6)$ $I_{6,Glu}(6)$	0.51	
$I_{4,Xyl}(1)$	0.4	(Ntarima et al., 2000)	$I_{5,Xyl}(1)$ $I_{6,Xyl}(1)$	0.4	
$I_{4,Xyl}(2)$	0.85	(Lo Leggio and	$I_{5,Xyl}(2)$ $I_{6,Xyl}(2)$	0.85	

$I_{4,Xyl}(3)$	1.5	Pickersgill, 1999; Ntarima et al., 2000)	$I_{5,Xyl}(3)$ $I_{6,Xyl}(3)$	1.5	
$I_{4,Xyl}(4)$	2		$I_{5,Xyl}(4)$ $I_{6,Xyl}(4)$	2	
$I_{4,Xyl}(5)$	4		$I_{5,Xyl}(5)$ $I_{6,Xyl}(5)$	4	
$I_{4,Xyl}(6)$	4.5		$I_{5,Xyl}(6)$ $I_{6,Xyl}(6)$	4.5	

Table.I4 Beta-enzymes parameters

Parameter	Value (1/mM)	Reference	Parameter	Value (1/min)	Reference
$I_{7,Glu}(1)$	0.294	(Chauve et al., 2010)	$\gamma_{7,Glu}(1)$	0	Determined
$I_{7,Glu}(2)$	1.136	(Chauve et al., 2010; Yazaki et al., 1997)	$\gamma_{7,Glu}(2)$	1897	(Chauve et al., 2010)
$I_{7,Glu}(3)$	3.846		$\gamma_{7,Glu}(3)$	1738.9	(Chauve et al., 2010; Yazaki et al., 1997)
$I_{7,Glu}(4)$	4		$\gamma_{7,Glu}(4)$	1422.8	
$I_{7,Glu}(5)$	2.174		$\gamma_{7,Glu}(5)$	895.8	
$I_{7,Glu}(6)$	1.449		$\gamma_{7,Glu}(6)$	843.1	
$I_{7,Xyl}(1)$	0.417	Assumed	$\gamma_{7,Xyl}(1)$	0	Determined
$I_{7,Xyl}(2)$	0	Not considered	$\gamma_{7,Xyl}(2)$	0	
$I_{7,Xyl}(3)$	0		$\gamma_{7,Xyl}(3)$	0	
$I_{7,Xyl}(4)$	0		$\gamma_{7,Xyl}(4)$	0	
$I_{7,Xyl}(5)$	0		$\gamma_{7,Xyl}(5)$	0	
$I_{7,Xyl}(6)$	0		$\gamma_{7,Xyl}(6)$	0	
$I_{8,Glu}(1)$	0.294	Assumed	$\gamma_{8,Glu}(1)$	0	
$I_{8,Glu}(2)$	0	Not considered	$\gamma_{8,Glu}(2)$	0	
$I_{8,Glu}(3)$	0		$\gamma_{8,Glu}(3)$	0	
$I_{8,Glu}(4)$	0		$\gamma_{8,Glu}(4)$	0	
$I_{8,Glu}(5)$	0		$\gamma_{8,Glu}(5)$	0	
$I_{8,Glu}(6)$	0		$\gamma_{8,Glu}(6)$	0	
$I_{8,Xyl}(1)$	0.417	(Rasmussen et al., 2006)	$\gamma_{8,Xyl}(1)$	0	
$I_{8,Xyl}(2)$	2.5		$\gamma_{8,Xyl}(2)$	1897	(Rasmussen et al., 2006)

$I_{8,Xyl}(3)$	5		$\gamma_{8,Xyl}(3)$	1250.3	
$I_{8,Xyl}(4)$	6.25		$\gamma_{8,Xyl}(4)$	1164.1	
$I_{8,Xyl}(5)$	10		$\gamma_{8,Xyl}(5)$	1293.4	
$I_{8,Xyl}(6)$	12.5		$\gamma_{8,Xyl}(6)$	862.3	

Reference

Banerjee, G., Car, S., Scott-Craig, J. S., Borrusch, M. S., Aslam, N. and Walton, J. D. 2010a. "Synthetic enzyme mixtures for biomass deconstruction: production and optimization of a core set." Biotechnol Bioeng **106**(5): 707-720.

Banerjee, G., Car, S., Scott-Craig, J. S., Borrusch, M. S., Bongers, M. and Walton, J. D. 2010b. "Synthetic multi-component enzyme mixtures for deconstruction of lignocellulosic biomass." Bioresource technology **101**(23): 9097-9105.

Chauve, M., Mathis, H., Huc, D., Casanave, D., Monot, F. and Lopes Ferreira, N. 2010. "Comparative kinetic analysis of two fungal beta-glucosidases." Biotechnology for biofuels **3**(1): 3.

Kumar, R. and Wyman, C. E. 2009. "Does change in accessibility with conversion depend on both the substrate and pretreatment technology?" Bioresource Technology **100**(18): 4193-4202.

Levine, S. E., Fox, J. M., Blanch, H. W. and Clark, D. S. 2010. "A mechanistic model of the enzymatic hydrolysis of cellulose." Biotechnol Bioeng **107**(1): 37-51.

Lo Leggio, L. and Pickersgill, R. W. 1999. "Xylanase-oligosaccharide interactions studied by a competitive enzyme assay." Enzyme and Microbial Technology **25**(8-9): 701-709.

Ntarima, P., Nerinckx, W., Klarskov, K., Devreese, B., Bhat, M. K., Van Beeumen, J. and Claeyssens, M. 2000. "Epoxyalkyl glycosides of D-xylose and xylo-oligosaccharides are active-site markers of xylanases from glycoside hydrolase family 11, not from family 10." The Biochemical journal **347 Pt 3**: 865-873.

Qing, Q. and Wyman, C. E. 2011. "Supplementation with xylanase and beta-xylosidase to reduce xylo-oligomer and xylan inhibition of enzymatic hydrolysis of cellulose and pretreated corn stover." Biotechnology for biofuels **4**(1): 18.

Rasmussen, L. E., Sorensen, H. R., Vind, J. and Vikso-Nielsen, A. 2006. "Mode of action and properties of the beta-xylosidases from Talaromyces emersonii and Trichoderma reesei." Biotechnol Bioeng **94**(5): 869-876.

Tolan, J. S. and Foody, B. 1999. "Cellulase from submerged fermentation." Advances in Biochemical Engineering/Biotechnology **65**: 41-67.

Yazaki, T., Ohnishi, M., Rokushika, S. and Okada, G. 1997. "Subsite structure of the beta-glucosidase from Aspergillus niger, evaluated by steady-state kinetics with cello-oligosaccharides as substrates." Carbohydrate Research **298**(1-2): 51-57.

Zhang, Y. H. and Lynd, L. R. 2006. "A functionally based model for hydrolysis of cellulose by fungal cellulase." Biotechnol Bioeng **94**(5): 888-898.

Zhou, W., Hao, Z., Xu, Y. and Schuttler, H. B. 2009a. "Cellulose hydrolysis in evolving substrate morphologies II: Numerical results and analysis." Biotechnol Bioeng **104**(2): 275-289.

Zhou, W., Schuttler, H. B., Hao, Z. and Xu, Y. 2009b. "Cellulose hydrolysis in evolving substrate morphologies I: A general modeling formalism." Biotechnol Bioeng **104**(2): 261-274.

Zhu, Z., Sathitsuksanoh, N. and Percival Zhang, Y. H. 2009a. "Direct quantitative determination of adsorbed cellulase on lignocellulosic biomass with its application to study cellulase desorption for potential recycling." The Analyst **134**(11): 2267-2272.

Zhu, Z., Sathitsuksanoh, N., Vinzant, T., Schell, D. J., McMillan, J. D. and Zhang, Y. H. 2009b. "Comparative study of corn stover pretreated by dilute acid and cellulose solvent-based lignocellulose fractionation: Enzymatic hydrolysis, supramolecular structure, and substrate accessibility." Biotechnol Bioeng **103**(4): 715-724.

Appendix

Permission

RightsLink

Copyright Clearance Center

Thank You For Your Order!

Dear Mr. yang zhang,

Thank you for placing your order through Copyright Clearance Center's RightsLink service. John Wiley and Sons has partnered with RightsLink to license its content. This notice is a confirmation that your order was successful.

Your order details and publisher terms and conditions are available by clicking the link below:
http://s100.copyright.com/CustomerAdmin/PLF.jsp?ref=0976b7a8-ea2a-4e32-a096-496e9774c9bb

Order Details
Licensee: yang zhang
License Date: Sep 4, 2015
License Number: 3701960473892
Publication: Biotechnology & Bioengineering
Title: On a novel mechanistic model for simultaneous enzymatic hydrolysis of cellulose and hemicellulose considering morphology
Type Of Use: Dissertation/Thesis
Total: 0.00 USD

Chapter 4 A Mechanistic Design Framework for Optimal Enzyme Usage in Hydrolysis of Hemicellulose-cellulosic Substrates[3]

[3] Was submitted to the journal of *Bioresource Technology*

Abstract

A general approach is presented to optimize the composition of enzyme mixture for substrate conversion and monosaccharides yield during simultaneous enzymatic hydrolysis of cellulose and hemicellulose. This approach applies a novel mechanistic model which not only considers the morphology of the substrates, including the composition, degree of polymerization and enzyme accessibility, but also a wide range of enzyme kinetics during the hydrolysis process, including, but not limited to, endoglucanase I (EG1), cellobiohydrolase I (CBH1), cellobiohydrolase II (CBH2), endo-xylanase (EX), β-glucosidase (BG) and β-xylosidase (BX). This approach also considers adding enzymes at different time points during the hydrolysis process and investigates its effects on substrate conversion and monosaccharides yield. This approach is capable of predicting the optimal composition of enzyme mixtures during the simultaneous hydrolysis of cellulose and hemicelluloses in different types of lignocellulosic substrates. The effectiveness of the approach is demonstrated on the hydrolysis of Avicel and AFEX-pretreated corn stover.

4.1 Introduction

Biofuels have received enormous attention over decades due to the potential of decreasing the reliance on fossil fuels globally and reducing the greenhouse gas emissions. The US seeks to replace 20% of its current gasoline usage with alternative fuels by 2022, which would increase the US alternative fuel production to 36 billion gallons (Gu et al., 2013). Recently, more research efforts have been focusing on the second generation biofuels. Compared with the first generation biofuel, the second generation biofuel can reduce the greenhouse gas and have higher energy security level (Singhania et al., 2014). Moreover, the second generation biofuels are mainly generated from the lignocellulosic biomass so that the competition between food and biofuel production will become less (Cherubini et al., 2009).

Enzymatic hydrolysis, which biochemically converts biomass into mono- and oligo-saccharides, is a critical process of producing biofuels. However, the high cost caused by the enzyme loading is a major barrier of the industrial application (Klein-Marcuschamer et al., 2012). In order to reduce the total enzyme loading and make the biofuel production process more economical, many studies have been focused on developing enzyme mixtures that have optimal synergistic kinetics for the hydrolysis of lignocellulosic substrates (Berlin et al., 2007; Banerjee et al., 2010a; Banerjee et al., 2010b; Gao et al., 2010; Zhang et al., 2010; Levine et al., 2011; Billard et al., 2012; Singhania et al., 2014). For example, Berlin et al. (2007) developed optimal enzyme mixtures with commercial enzymes for the hydrolysis of dilute acid-pretreated corn stover, Gao et al. (2010) designed optimal enzyme mixtures with six core enzymes from *Trichoderma reesei*, *Aspergillus niger*, and

Aspergillus nidulans for the hydrolysis of AFEX-pretreated corn stover and Banerjee et al. (2010a) developed optimal enzyme mixtures with ten accessory and six purified core enzymes from *Trichoderma reesei* and *Trichoderma longibrachum* for the hydrolysis of AFEX-pretreated corn stover.

However, because of the variety of the lignocellulosic substrates, designing the optimal enzyme mixtures for each type of substrate will consume a large amount of enzymes and require tremendous experimental efforts. In this study, a general approach is presented to decide the optimal composition of enzyme mixtures for different lignocellulosic substrates during hydrolysis. The basis of this approach is a novel mechanistic model which not only considers the morphology and all the hydrolysable components (i.e. cellulose and hemicelluloses) of each lignocellulosic substrate, but also a wide range of enzyme kinetics during the hydrolysis process. Moreover, this approach for the first time considers the effect of adding enzymes at different time points during the hydrolysis process, and investigates such effect on substrate conversion and monosaccharides yield. Some experimental studies have shown that delaying the adding time of some enzymes could increase the total conversion level of the substrates (Qing and Wyman, 2011), probably because some parts of the substrate are not accessible for enzymes at the beginning of hydrolysis and the activity of free enzymes in solution keeps decreasing during the process of hydrolysis. This general approach can predict the composition of optimal enzyme mixtures either for the conversion level of total substrates or the yield of certain saccharide products during the simultaneous hydrolysis of cellulose and hemicelluloses in different types of lignocellulosic substrates. The predicted results can provide systematic information for the further experimental studies of developing optimal enzyme mixtures.

4.2 Methods

4.2.1 Morphology of lignocellulosic substrates

Lignocellulosic substrate morphology is described by the recently introduced concept "Smallest Accessible Compartment" (SAC) (Zhou et al., 2009b; Zhang et al., 2014). SAC is a minimal volume that is delimited by enzyme-accessible surfaces and contains several elementary layers. The geometries of SACs are mapped to a population of SAC classes, which are indexed by σ. These SAC classes represent different SAC sizes and differ by the initial number of SAC elementary layers λ_σ, which is a variable and will keep decreasing due to the substrate surface ablation by enzymes. In addition, some SACs may contain different types of polysaccharide chains (i.e. cellulose and hemicellulose chains), which are indexed by ρ. These SACs will have a fraction of type-ρ chains, which is set as a function of λ_σ, represented by $\Phi_{\sigma,\rho}(\lambda_\sigma)$. The fraction of type-ρ chains may also vary in different SAC classes and its initial value is represented by $\Phi^0_{\sigma,\rho}(\lambda_{\sigma,max})$. Gaussian distribution is applied for SAC concentrations and the initial fraction of type-ρ chains in all SAC classes. It also decides the initial fraction of accessible substrate in each SAC class, represented by $\bar{F}^0_{A,\sigma}$. This is the ratio of exposed substrate on the surfaces of class-σ SACs to the total substrate contained in class-σ SACs and can then be used to calculate the overall initial accessibility of the substrate $\bar{F}^0_A$, which can commonly be measured in experiments.

4.2.2 Reactions of enzyme mixture

During the process of enzymatic hydrolysis, different enzyme species will adsorb on different linkages between monosaccharide units in the solid substrates and cut the solid

polysaccharide chains. Based on the "Site Formalism" (Zhou et al., 2009a; Zhang et al., 2014), the linkages were classified into seven major groups of "sites", which are N-, O-, X-, Y-, L-, R- and J-sites. N-sites could only adsorb and be cut by endo-acting enzymes (e.g. endo-glucanase and endo-xylanase). X-sites could adsorb and be cut by either endo-acting or exo-L-acting enzymes (e.g. Cellobiohydrolase II), while Y-sites could adsorb and be cut by either endo-acting or exo-R-acting enzymes (e.g. Cellobiohydrolase I). J-sites could adsorb and be cut by debranching enzymes. O-sites were blocked sites and could not adsorb any enzyme. L- and R-sites represented the non-reducing and reducing ends of polysaccharide chains respectively. They were both broken and could not adsorb any enzyme. It is worth mentioning that these sites can be further divided into sub-groups based on different endo- or exo- enzymes. These site concentrations can be used to represent the amount of substrate materials and are tracked in the model (thus referred to as Site Formalism) considering their changing rates due to hydrolytic reactions. Compare to the "Chain Formalism" (i.e. tracking concentrations of chains of various length), the "Site Formalism" is more general and advanced, thus easier to be extended to include different types of hemicellulose chains.

After soluble oligosaccharides are released into solution from the solid substrate, beta-enzymes will hydrolyze them into monosaccharides. However, oligosaccharides and monosaccharides can also adsorb other enzymes that act on the solid substrates and thus cause the inhibition effects (Levine et al., 2010; Zhang and Zhou, 2014). Besides, the activity of enzymes will also decrease as hydrolysis proceeds, as described by Eq. (1) and Eq. (2).

$$u_\kappa(t) = 0 \ (t < t_\kappa) \tag{1}$$

$$u_\kappa(t) = u_{\kappa,0}\left(\frac{1}{2}\right)^{\frac{t-t_\kappa}{t_{\kappa,\frac{1}{2}}}} \ (t \geq t_\kappa) \tag{2}$$

Here, $u_\kappa(t)$ is the concentration of active enzyme κ in solution at time point t, $u_{\kappa,0}$ is the concentration of enzyme added into solution, t_κ is the adding time of enzyme κ and $t_{\kappa,1/2}$ is the half-life of enzyme κ. During the process of enzymatic hydrolysis, the surface layer of each SAC is ablated to release oligosaccharides into solution, which exposes the underneath SAC layers to enzymes. The enzymatic ablation of solid surface will naturally cause the shrinkage of SAC surface area and lead to a decrease of accessible sites for free enzymes. All these features are properly considered in our hydrolysis model.

4.2.3 Model parameters and optimization procedure

In this study, the model was applied to predict the optimal enzyme mixtures for Avicel and AFEX-pretreated corn stover hydrolysis. The cellulose (glucan) content of Avicel was set as 100%, the DP value of glucan chains was set as 300 and the initial enzymatic accessibility of Avicel $\bar{F}_A^0$ was set as 0.6% (Zhang and Lynd, 2004, 2006; Zhou et al., 2010). For corn stover, the ammonia fiber expansion (AFEX) pretreatment is a unique pretreatment because it mainly cuts the linkages between lignin and hemicelluloses and relocates extractable lignin to the substrate surface, which causes little destruction of cellulose and hemicelluloses of the lignocellulosic substrates (Chundawat et al., 2011). The cellulose (glucan) content was set as 39.6%, and the hemicellulose (xylan) content was set as 24.5% (Qing and Wyman, 2011). The DP values of glucan and xylan chains were set as

6800 and 300 respectively (Kumar et al., 2009). The lignin content and its effects were neglected during the enzymatic hydrolysis. The initial enzymatic accessibility of AFEX-corn stover $\bar{F}_A^0$ was set as 10.51%, which was from the work of Zhang et al. (2014).

The model has the capability of considering all the possible enzyme species involved in the hydrolysis process. In this study, six typical enzyme species were considered for both Avicel and AFEX-pretreated corn stover hydrolysis, including endoglucanase I (EG1), cellobiohydrolase I (CBH1), cellobiohydrolase II (CBH2), endo-xylanase (EX), β-glucosidase (BG) and β-xylosidase (BX).The values of kinetic and adsorption parameters for EG1, CBH1, CBH2 and EX were from the work of Banerjee et al. (2010b) and Zhang and Lynd (2006), and the values of inhibition parameters for these enzymes were from the work of Tolan and Foody (1999), Lo Leggio and Pickersgill (1999) and Ntarima et al. (2000). For BG and BX, the values of kinetic and adsorption parameters were from the work of Chauve et al. (2010), Rasmussen et al. (2006) and Yazaki et al. (1997).

The objective of enzymatic hydrolysis process being optimized (i.e. best process performance) could be either substrate conversion (e.g. glucan conversion for Avicel defined as yield of total soluble oligomers including from glucose to cellohexaose) or monosaccharides yield (e.g. glucose yield for Avicel) at 72 hours of hydrolysis. The total enzyme amount (i.e. mg enzyme per gram biomass) was fixed when the composition of the enzyme mixture was optimized to maximize the selected objective. The composition of the enzyme mixture, represented by w, was set as a 6-elementarray. Each element, denoted by w_κ (κ=1~6), represented the mass fraction of an enzyme species in the mixture and always satisfied the relationship $\sum_\kappa w_\kappa = 1$. The effect of total enzyme amount on the optimal

enzyme mixture composition was also investigated. The optimization procedure was based on iterative simulation over the feasible domain of the mass fraction array w. When w was changed as a model input, the simulation would obtain different results of final substrate conversion and monosaccharides yield. By comparing the results of these simulation, the composition of optimal enzyme mixture could be determined. To greatly reduce the solution time, w_κ (i.e. each dimension of w) was first set to change by an interval of 10% during the loop to obtain a sub-domain of w for the possible range of optimal enzyme mixture. Then the model was simulated iteratively again within the obtained sub-domain to refine the optimal enzyme mixture by setting the mass fraction $w_\kappa$changing interval as 1%. The total hydrolysis time was set as 100 hours and three situations of total enzyme loading were tested for both Avicel and AFEX-pretreated corn stover, which were 7.5, 15 and 30 mg enzyme/g glucan.

After the composition of the optimal enzyme mixtures for substrate conversion and monosaccharides yield were determined, each enzyme species was then tested as being added to solution at different time points (versus being added at time zero all together) to investigate the adding time effects on hydrolysis process. The solution procedure was also based on iterative simulation over the feasible domain of the adding time array for enzyme species. The adding time domain was set from time 0 to 48 hours. The interval of the time points was set as 6 hours at first to obtain a sub-domain where the effects were positive (i.e. higher substrate conversion or monosaccharides yield). Then the model was simulated iteratively again within the obtained sub-domain to refine the time points by setting the interval as 0.5 hour.

4.3 Results and Discussion

4.3.1 Enzyme optimization and adding time effects for Avicel hydrolysis

The optimal compositions of enzyme mixture for glucan conversion and glucose yield in all cases of Avicel hydrolysis were determined based on the simulation results. Figure 4.1 shows the ternary plots (i.e. can only show mass fractions of three main enzyme components) of glucan conversion and glucose yield at 72 hours with enzyme loadings of 7.5, 15 and 30 mg enzyme/g glucan and Table 4.1 shows the predicted optimal enzyme mixture compositions for glucan conversion at 72 hours with enzyme loadings of 7.5, 15 and 30 mg enzyme/g glucan. The supplementary section provides the optimal enzyme mixture compositions for glucan conversion at 24 and 48 hours with enzyme loadings of 7.5, 15 and 30 mg enzyme/g glucan.

It can be found that EG1 is the dominant enzyme in cellulose hydrolysis, followed by CBH2 and CBH1. This phenomenon agrees with the experimental evidence from many studies on Avicel hydrolysis (Tomme et al., 1988; Nidetzky et al., 1994; Zhang and Lynd, 2004) and the predicted results agree with those from the work of Levine et al. (2011), although in the work the enzyme parameters came from *Trichoderma longibrachiatum*, *Taleromyces emersonii*, and *Trichoderma reesei*. As enzyme loading increases from 7.5 to 15 mg enzyme/g glucan, the optimal enzyme composition for glucan conversion of Avicel will have an increased mass fraction of EG1 and decreased mass fraction of CBH2. This is likely because as the enzyme loading increases, the amount of accessible sites for exo-acting enzymes is not changed too much at the beginning of hydrolysis, but EG1 can create more additional accessible sites that exo-acting enzymes can adsorb on as hydrolysis

proceeds. However, as the enzyme loading increases from 15 to 30 mg enzyme/g glucan, the mass fraction of EG1 will decrease and the mass fraction of CBH2 will increase in the optimal enzyme mixture for glucan conversion. This observation shows that although EG1 is critical of acting synergistically with CBH2 and CBH1 to increase the hydrolysis rate, it is not true that the more endo-acting enzymes the better synergy with the presence of exo-acting enzymes. Also, the BG mass fraction in the optimal mixture increases from 0 to 2%. In fact, when the enzyme loading reaches 30 mg enzyme/g glucan and the hydrolysis time is long enough (≥48 hours), it is necessary to involve BG in the optimal enzyme mixtures for glucan conversion (shown in the supplementary section). The reason may be that as the glucan conversion level increases, more gluco-oligomers (i.e. from glucose to cellohexaose) will be released into solution and cause severe inhibition effects so that it is more important to lower the inhibition effects by adding BG to hydrolyze gluco-oligomers with high inhibitory ability into glucose that has lower inhibitory ability (Lo Leggio and Pickersgill, 1999; Tolan and Foody, 1999). Many studies have shown that the hydrolysis rate will be significantly limited without BG (Banerjee et al., 2010a; Zhang et al., 2010; Qing and Wyman, 2011), which agree with the simulation results.

For the purpose of maximizing the glucose yield from cellulose hydrolysis, BG becomes more critical than some other cellulases like CBHI. From the ternary plots shown as Figure 4.1D-F, the mass fraction of BG in the optimal enzyme mixtures for glucose yield always ranges between 0.1 and 0.3. This agrees with the study of Zhang et al. (2010) which showed 9.1 mg enzyme/g glucan Spezyme CP (cellulase) with 1.45 mg enzyme/g glucan Novozyme 188 (BG). In addition, because the BG takes large fraction of the enzyme mixture, the mass fraction of EG1 in the optimal enzyme mixtures for glucose yield

increases as the total enzyme loading increases to enhance the synergy activities between EG1 and CBH2.

The enzyme adding time effects during hydrolysis was investigated after analyzing the optimization of enzymes for Avicel hydrolysis. For endo- and exo- acting enzymes, no positive effects can be found on either glucan conversion or glucose yield if adding these enzymes later. However, adding BG later will be beneficial for increasing the glucose yield after long time period of hydrolysis, as shown in Figure 4.2. Compared with adding BG at the beginning of hydrolysis, if BG is added at 24 hours the glucose yield after 100 hours will increases from 52% to 63%. Besides, before the hydrolysis time reaches 48 hours, the later the adding time point of BG, the higher the glucose yield will be. These observations are reasonable because it is assumed in the model that no soluble gluco-oligomers exists before hydrolysis, meaning that there is no need for too much BG at the beginning of hydrolysis. In addition, BG has a shorter half-life, so adding BG too early will waste its activity a lot. Therefore, it is reasonable to delay the time of adding BG into solution in order to increase the glucose yield.

4.3.2 Enzyme optimization and adding time effects for AFEX-pretreated corn stover hydrolysis

The optimal enzyme mixture compositions for substrate (i.e. "glucan+xylan") conversions and monosaccharides (i.e. "glucose+xylose") yields in all cases of AFEX-pretreated corn stover hydrolysis were determined based on the simulation results. Figure 4.3 shows ternary plots of substrate conversion and monosaccharides yield, and Table 4.2 shows the predicted optimal enzyme mixture compositions for substrate conversion at 72

hours with enzyme loadings of 7.5, 15 and 30 mg enzyme/g glucan. The supplementary section provides optimized enzyme mixture compositions for substrate conversion at 24 and 48 hours with enzyme loadings of 7.5, 15, and 30 mg enzyme/g glucan.

It can be found that for maximum substrate conversion, CBH2 is the dominant enzyme at enzyme loading of 7.5 mg enzyme/g glucan and EX becomes the dominant one at enzyme loadings of 15 and 30 mg enzyme/g glucan. Then for maximizing the monosaccharides yield, CBH2 is the dominant enzyme at enzyme loadings of 7.5 and 15 mg enzyme/g glucan and EX becomes the dominant one at enzyme loading of 30 mg enzyme/g glucan. Not like CBH2, CBH1 is not necessary in the optimal enzyme mixture for substrate conversion, probably because CBH2 was set to have higher catalytic rate than CBH1 in the model based on the studies of Nidetzky et al. (1994) and Zhang and Lynd (2004). However, when the enzyme loading reaches 30 mg enzyme/g glucan, the mass fraction of CBH2 becomes less and CBH1 becomes a necessary species in the optimal enzyme mixture. The reason may be that as the concentration of CBH2 becomes too high, the accessible X-sites at the non-reducing ends of glucan chains for CBH2 will become insufficient so that substituting CBH1 for certain amount of CBH2 may become beneficial to higher substrate conversion level. It is worth noticing that some studies of the enzyme optimization for lignocellulose hydrolysis also showed that CBH1 had higher catalytic rate than CBH2 (Banerjee et al., 2010a; Banerjee et al., 2010b; Gao et al., 2010), and the simulation results might be totally different if the kinetic parameter settings of CBH1 and CBH2 are changed. So the catalytic abilities of CBH1 and CBH2 still need to be further investigated by experiments.

It can be also found that EG1 has a much lower mass fraction than EX in all cases of AFEX-pretreated corn stover hydrolysis. The main reason may be that the rate of EX1 hydrolyzing xylan is faster than that of EG1 hydrolyzing cellulose. So less EG1 is needed in the enzyme mixture to hydrolyze AFEX-pretreated corn stover. Then the influence of the enzyme accessibility $\bar{F}_A^0$ on the results of enzyme optimization was investigated (shown in the supplementary section). The results show that as $\bar{F}_A^0$ becomes larger the mass fractions of EG1 and CBH2 will also become larger but the mass fraction of EX will become smaller. The study of Gao et al. (2010) showed that the optimal enzyme composition of hydrolyzing AFEX-pretreated corn stover for substrate conversions was 27–30% CBH1, 17–20% CBH2, 29–35% EG1, 14–15% EX, 2–6% BX and 1–5% BG. The comparison between the simulation results and the experimental data indicates that the enzyme accessibility of AFEX-pretreated corn stover is critical to determine its optimal enzyme composition and needs more experimental studies to determine.

The enzyme adding time effects during AFEX-pretreated corn stover hydrolysis was investigated. Again, no positive effects can be found on either substrate conversion or monosaccharides yield if adding endo- or exo- acting enzymes later. Figure 4.4 shows the glucose yields of AFEX-pretreated corn stover when BG is added at different time points, and the xylose yields of AFEX-pretreated corn stover when BX is added at different time points. Like the adding time effect of BG in the Avicel hydrolysis process, adding BG later in the hydrolysis process of AFEX-pretreated corn stover can increase the glucose yield. However, it can be also found that adding BX later will not be beneficial for increasing the xylose yield. Compared with adding BX at the beginning of hydrolysis, there will be a

decrease in xylose yield if BX is added at 24 and 48 hours. The reason may be that the production rates of soluble xylo-oligomers are very fast at the beginning of hydrolysis since most xylan locates on the outer part of the substrate and is easy to hydrolyze. Without the presence of BX, these soluble xylo-oligomers will remain in solution and act as stronger inhibitors of EG1, CBH1 and CBH2 which not only slows down the hydrolysis rate of cellulose but also xylan (Qing et al., 2010). Therefore, it is necessary to add BX in solution at the beginning of hydrolysis to hydrolyze the soluble xylo-oligomers early enough and reduce the inhibition effects. In addition, Figure 4.5 shows the simulation results of adding BG, EX and BG+EX at 8 hours. It can be found that to maximize the glucose yield, it is more beneficial to add BG+EX later than adding only BG or EX later. But there is no such effect that can be found for the xylose yield, which indicates that adding EX and BX at the beginning of AFEX-pretreated corn stover hydrolysis may be the best way to only maximize the xylose yield.

4.4 Conclusions

We have applied our newly developed mechanistic modeling of lignocellulose hydrolysis as a tool to optimize enzymes for the yield of saccharide products and conversion of substrates. The model predicted the optimal enzyme mixture compositions and enzyme adding time during the hydrolysis of Avicel and AFEX-pretreated corn stover.

For Avicel hydrolysis, EG1 was found to be the dominant enzyme in the optimal enzyme mixture for glucan conversion. But as the total enzyme loading increased from 7.5 to 30 mg enzyme/g glucan, the mass fraction of EG1 would first increase then decrease in the optimal enzyme mixture. In the case of high enzyme loading (30 mg enzyme/g glucan)

and long hydrolysis time (≥48 hours), BG should be included in the optimal enzyme mixture for glucan conversion to reduce the inhibition effects by gluco-oligomers. And for maximizing the glucose yield from cellulose hydrolysis, the mass fraction of BG would be between 10% and 30%.

For AFEX-pretreated corn stover hydrolysis, CBH2 was predicted to be the dominant enzyme for maximum substrate conversion. But in the case of high enzyme loading (30 mg enzyme/g glucan), CBH1 was shown to replace certain amount of CBH2 in the optimal enzyme mixture for substrate conversion although its catalytic rate was lower than CBH2. And in almost all the cases of AFEX-pretreated corn stover hydrolysis, the mass fraction of EG1 was much lower than that of EX in the optimal enzyme mixture for substrate conversion or monosaccharides yield.

From the analysis of the enzyme adding time effects, no positive effects were found in both Avicel and AFEX-pretreated corn stover hydrolysis if adding endo- or exo- acting enzymes later, but adding BG later would increase the glucose yields in the hydrolysis of both substrates. However, adding BX later would not increase the xylose yield in AFEX-pretreated corn stover hydrolysis. It was also found that adding BG and EX together and later in AFEX-pretreated corn stover hydrolysis would increase the glucose yield more than adding only one of them later, but no such result was found for the xylose yield.

Acknowledgments

We acknowledge the National Science Foundation (CBET 1138734, CHE 1230803) for financial support.

Tables

Table 4.1 Optimal enzyme mass fractions for 72 hours hydrolysis of Avicel

Optimal Enzyme Mass Fractions for Glucan Conversion							
Enzyme Loading (mg/g)	EG1	CBH1	CBH2	EX	BG	BX	Glucan Conversion (%)
7.5	0.64	0.00	0.36	0	0.00	0	48.5
15	0.74	0.00	0.26	0	0.00	0	77.8
30	0.66	0.00	0.32	0	0.02	0	94.2
Optimal Enzyme Mass Fractions for Glucose Yield							
Enzyme Loading (mg/g)	EG1	CBH1	CBH2	EX	BG	BX	Glucose Yield (%)
7.5	0.38	0.00	0.38	0	0.24	0	27.5
15	0.46	0.00	0.32	0	0.22	0	52.6
30	0.52	0.00	0.24	0	0.24	0	81.0

Table 4.2 Optimal enzyme mass fractions for 72 hours hydrolysis of AFEX pretreated corn stover

Optimal Enzyme Mass Fractions for "Glucan+Xylan" Conversion							
Enzyme Loading (mg/g)	EG1	CBH1	CBH2	EX	BG	BX	"Glucan+Xylan" Yield (%)
7.5	0.075	0.00	0.50	0.40	0.00	0.025	43.7
15	0.07	0.00	0.40	0.50	0.00	0.03	67.1
30	0.03	0.03	0.36	0.53	0.01	0.04	96.1
Optimal Enzyme Mass Fractions for "Glucose+Xylose" Yield							
Enzyme Loading (mg/g)	EG1	CBH1	CBH2	EX	BG	BX	"Glucose+Xylose" Yield (%)
7.5	0.05	0.00	0.50	0.29	0.12	0.04	33.4
15	0.05	0.00	0.41	0.39	0.12	0.03	56.3
30	0.06	0.00	0.35	0.46	0.10	0.03	87.1

Figures

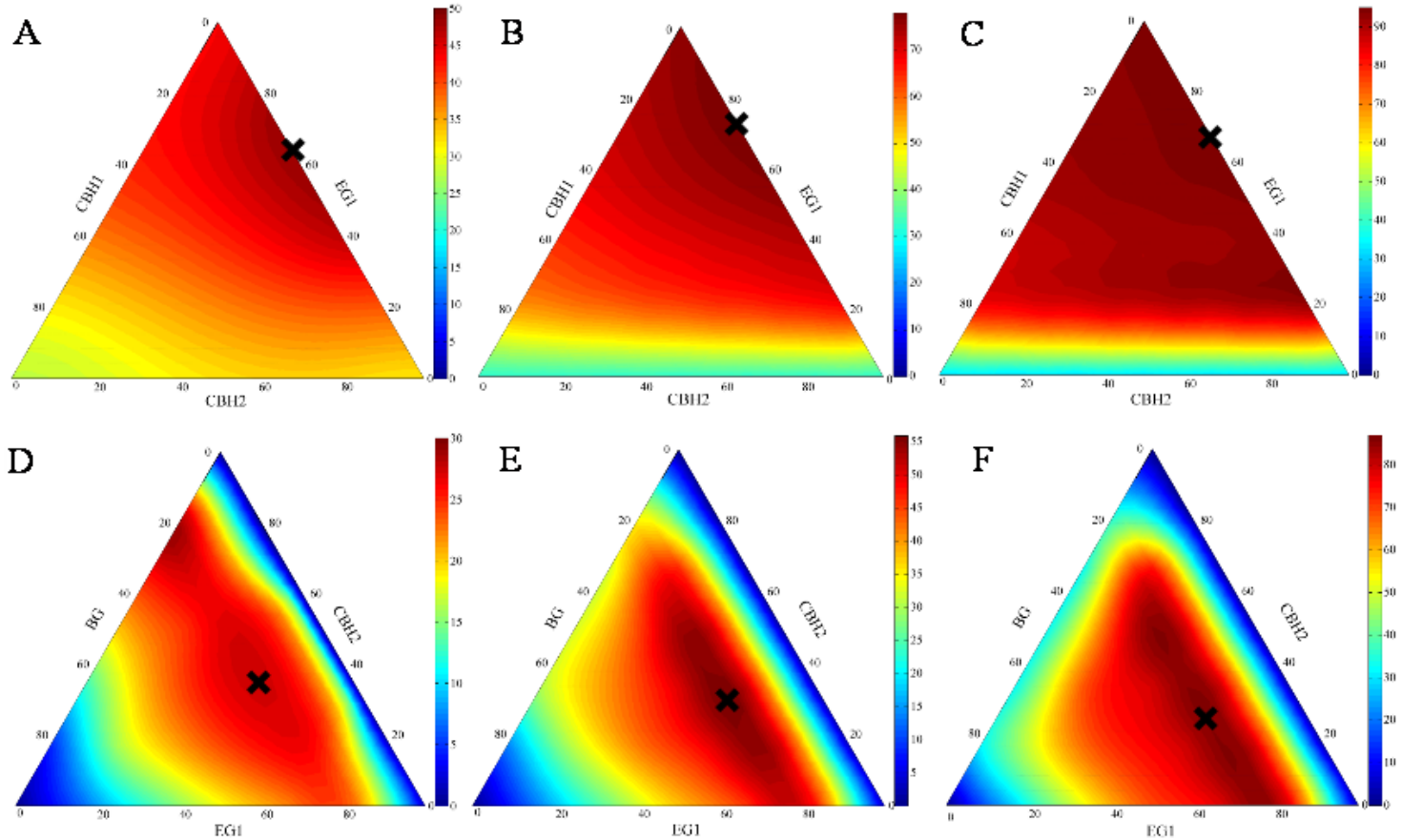

Figure 4.1 Ternary plot predictions of glucan conversion (A, B, C) and glucose yield (D, E, F) at 72 hours with 7.5 (A, D), 15 (B, E) and 30 (C, F) mg enzyme/g glucan. Mass fractions of EG1, CBH1 and CBH2 are given for glucan conversions. Mass fractions of EG1, CBH2 and BG are given for glucose yields. Cross mark shows the optimization point

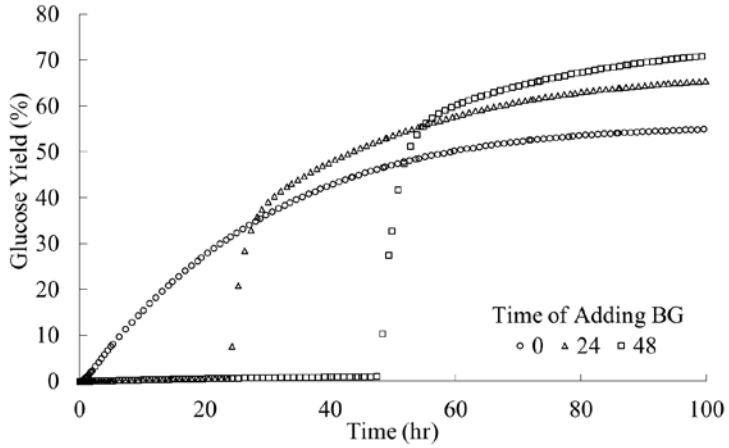

Figure 4.2 Simulation results of adding BG at 0, 24 and 48 hours during the hydrolysis of Avicel. Total enzyme loading is 15 mg enzyme/g glucan and enzyme fractions are optimal for glucose yield at 72 hours hydrolysis

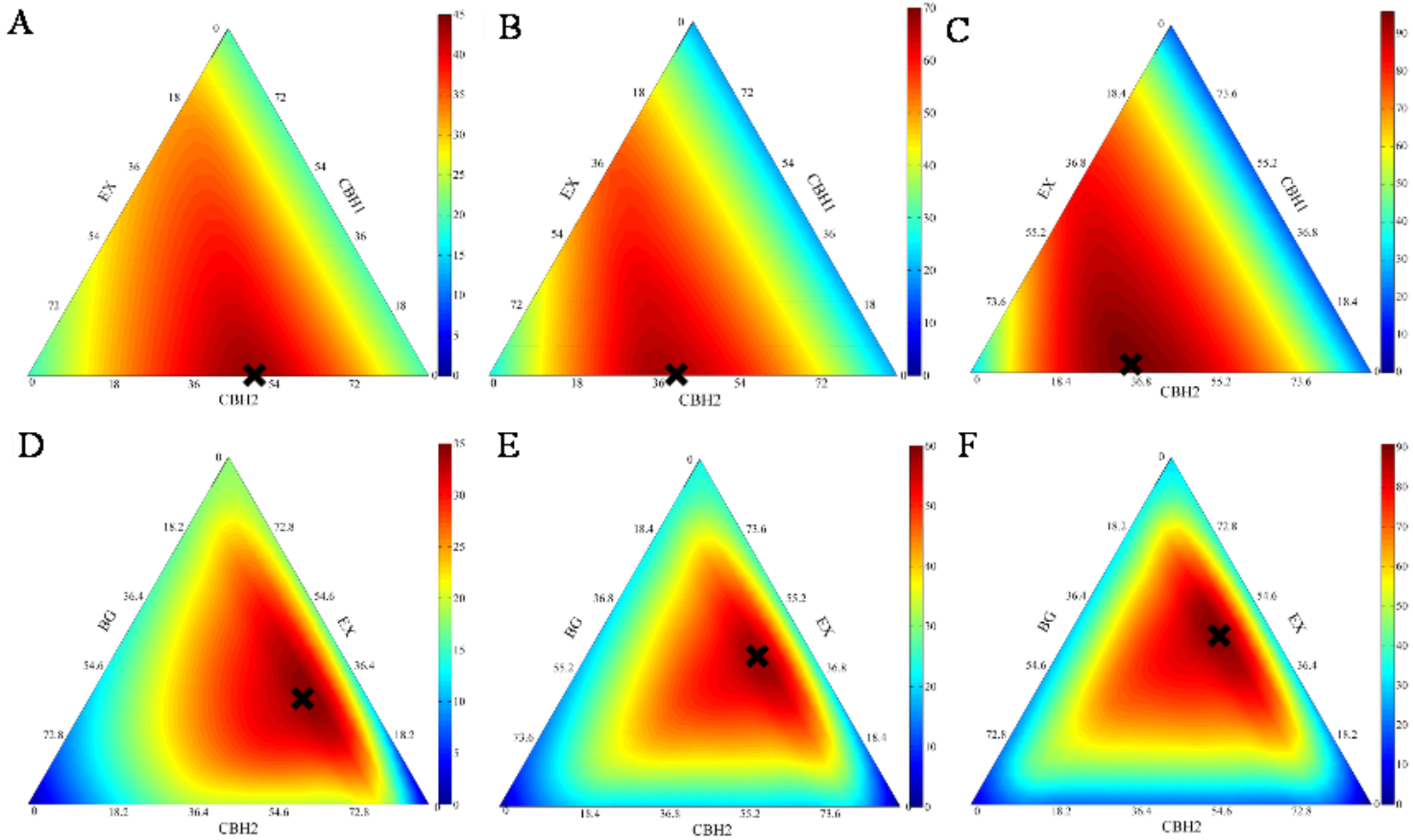

Figure 4.3 Ternary plot predictions of "glucan+xylan" conversion (A, B, C) and "glucose+xylose" yield (D, E, F) at 72 hours with 7.5 (A, D), 15 (B, E), and 30 (C, F) mg enzyme/g glucan. Mass fractions of CBH1, CBH2, and EX are given for "glucan+xylan" conversion. Mass fractions of CBH2, EX, and BG are given for "glucose+xylose" yield. Cross mark shows the optimization point

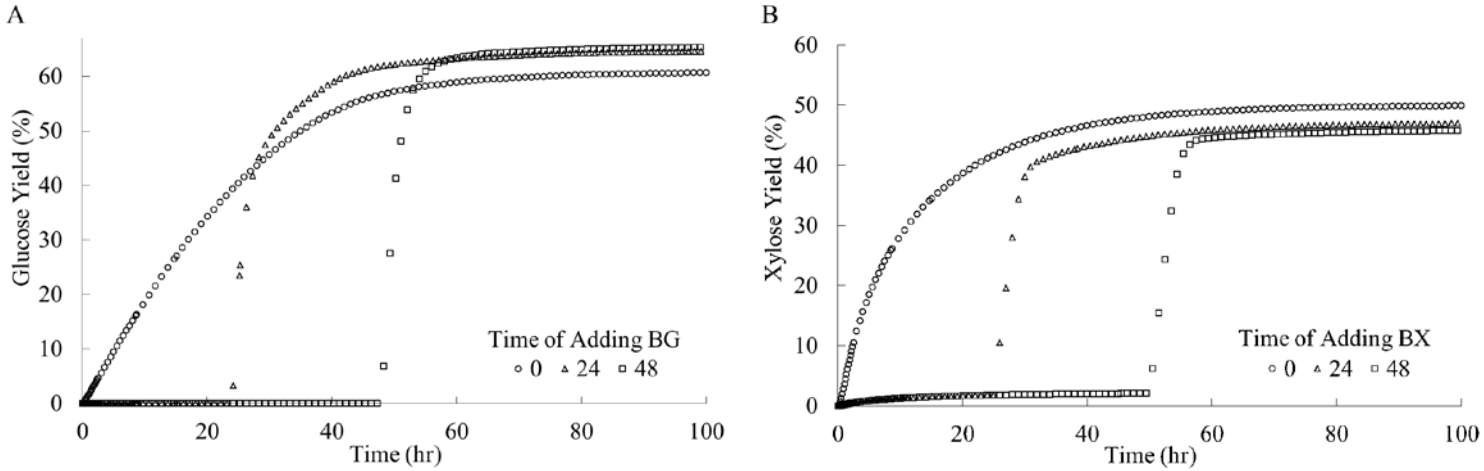

Figure 4.4 Simulation results of adding BG (A) and BX (B) at 0, 24 and 48 hours for the hydrolysis of AFEX pretreated corn stover. Total enzyme loading is 15 mg enzyme/g glucan and enzyme fractions are optimal for "glucose+xylose" yield at 72 hours hydrolysis

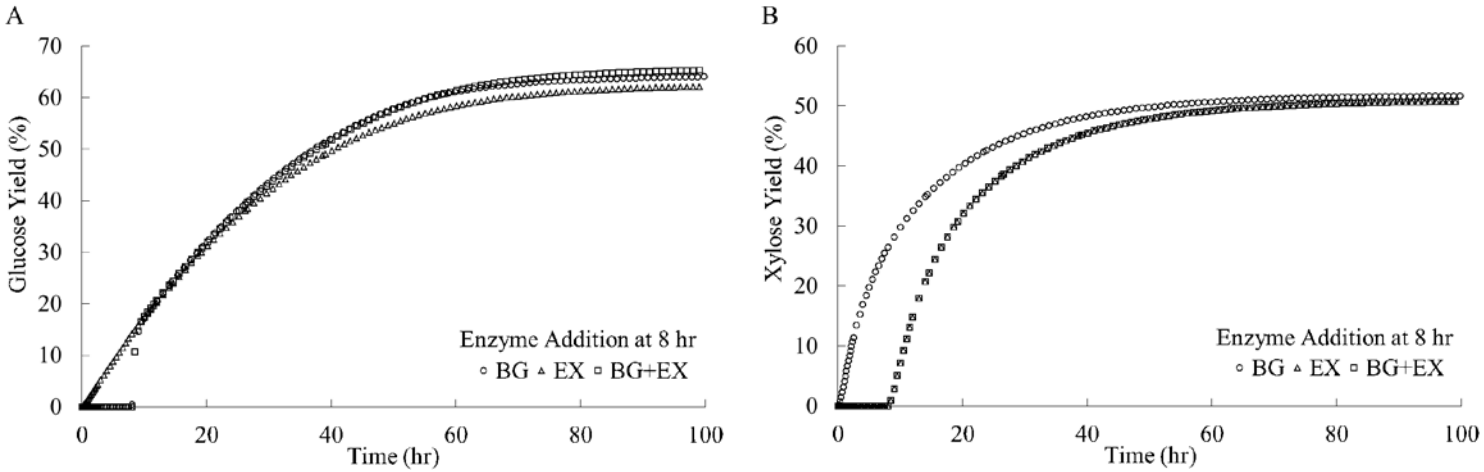

Figure 4.5 Simulation results of adding BG, EX and BG+EX after 8 hours hydrolysis of AFEX pretreated corn stover to investigate the yields of glucose (A) and xylose (B). Total enzyme loading and fractions are the same as in Figure 4.4

References

Banerjee, G., Car, S., Scott-Craig, J. S., Borrusch, M. S., Aslam, N. and Walton, J. D. 2010a. "Synthetic enzyme mixtures for biomass deconstruction: production and optimization of a core set." Biotechnol Bioeng 106(5): 707-720.

Banerjee, G., Car, S., Scott-Craig, J. S., Borrusch, M. S., Bongers, M. and Walton, J. D. 2010b. "Synthetic multi-component enzyme mixtures for deconstruction of lignocellulosic biomass." Bioresour Technol 101(23): 9097-9105.

Berlin, A., Maximenko, V., Gilkes, N. and Saddler, J. 2007. "Optimization of enzyme complexes for lignocellulose hydrolysis." Biotechnol Bioeng 97(2): 287-296.

Billard, H., Faraj, A., Lopes Ferreira, N., Menir, S. and Heiss-Blanquet, S. 2012. "Optimization of a synthetic mixture composed of major Trichoderma reesei enzymes for the hydrolysis of steam-exploded wheat straw." Biotechnol Biofuels 5(1): 9.

Chauve, M., Mathis, H., Huc, D., Casanave, D., Monot, F. and Lopes Ferreira, N. 2010. "Comparative kinetic analysis of two fungal beta-glucosidases." Biotechnol Biofuels 3(1): 3.

Cherubini, F., Bird, N. D., Cowie, A., Jungmeier, G., Schlamadinger, B. and Woess-Gallasch, S. 2009. "Energy- and greenhouse gas-based LCA of biofuel and bioenergy systems: Key issues, ranges and recommendations." Resources, Conservation and Recycling 53(8): 434-447.

Chundawat, S. P. S., Donohoe, B. S., da Costa Sousa, L., Elder, T., Agarwal, U. P., Lu, F., Ralph, J., Himmel, M. E., Balan, V. and Dale, B. E. 2011. "Multi-scale visualization and characterization of lignocellulosic plant cell wall deconstruction during thermochemical pretreatment." Energy & Environmental Science 4(3): 973.

Gao, D., Chundawat, S. P., Krishnan, C., Balan, V. and Dale, B. E. 2010. "Mixture optimization of six core glycosyl hydrolases for maximizing saccharification of ammonia fiber expansion (AFEX) pretreated corn stover." Bioresour Technol 101(8): 2770-2781.

Gu, T., Held, M. A. and Faik, A. 2013. "Supercritical CO2 and ionic liquids for the pretreatment of lignocellulosic biomass in bioethanol production." Environ Technol 34(13-16): 1735-1749.

Klein-Marcuschamer, D., Oleskowicz-Popiel, P., Simmons, B. A. and Blanch, H. W. 2012. "The challenge of enzyme cost in the production of lignocellulosic biofuels." Biotechnol Bioeng 109(4): 1083-1087.

Kumar, R., Mago, G., Balan, V. and Wyman, C. E. 2009. "Physical and chemical characterizations of corn stover and poplar solids resulting from leading pretreatment technologies." Bioresour Technol 100(17): 3948-3962.

Levine, S. E., Fox, J. M., Blanch, H. W. and Clark, D. S. 2010. "A mechanistic model of the enzymatic hydrolysis of cellulose." Biotechnol Bioeng 107(1): 37-51.

Levine, S. E., Fox, J. M., Clark, D. S. and Blanch, H. W. 2011. "A mechanistic model for rational design of optimal cellulase mixtures." Biotechnol Bioeng 108(11): 2561-2570.

Lo Leggio, L. and Pickersgill, R. W. 1999. "Xylanase-oligosaccharide interactions studied by a competitive enzyme assay." Enzyme and Microbial Technology 25(8-9): 701-709.

Nidetzky, B., Steiner, W. and Claeyssens, M. 1994. "Cellulose hydrolysis by the cellulases from Trichoderma reesei: adsorptions of two cellobiohydrolases, two endocellulases and their core proteins on filter paper and their relation to hydrolysis." Biochem J 303 (Pt 3): 817-823.

Ntarima, P., Nerinckx, W., Klarskov, K., Devreese, B., Bhat, M. K., Van Beeumen, J. and Claeyssens, M. 2000. "Epoxyalkyl glycosides of D-xylose and xylo-oligosaccharides are active-site markers of xylanases from glycoside hydrolase family 11, not from family 10." Biochem J 347 (Pt 3): 865-873.

Qing, Q. and Wyman, C. E. 2011. "Supplementation with xylanase and beta-xylosidase to reduce xylo-oligomer and xylan inhibition of enzymatic hydrolysis of cellulose and pretreated corn stover." Biotechnol Biofuels 4(1): 18.

Qing, Q., Yang, B. and Wyman, C. E. 2010. "Xylooligomers are strong inhibitors of cellulose hydrolysis by enzymes." Bioresour Technol 101(24): 9624-9630.

Rasmussen, L. E., Sorensen, H. R., Vind, J. and Vikso-Nielsen, A. 2006. "Mode of action and properties of the beta-xylosidases from Talaromyces emersonii and Trichoderma reesei." Biotechnol Bioeng 94(5): 869-876.

Singhania, R. R., Saini, J. K., Saini, R., Adsul, M., Mathur, A., Gupta, R. and Tuli, D. K. 2014. "Bioethanol production from wheat straw via enzymatic route employing Penicillium janthinellum cellulases." Bioresour Technol 169: 490-495.

Tolan, J. S. and Foody, B. 1999. "Cellulase from submerged fermentation." Advances in Biochemical Engineering/Biotechnology 65: 41-67.

Tomme, P., Van Tilbeurgh, H., Pettersson, G., Van Damme, J., Vandekerckhove, J., Knowles, J., Teeri, T. and Claeyssens, M. 1988. "Studies of the cellulolytic system of Trichoderma reesei QM 9414. Analysis of domain function in two cellobiohydrolases by limited proteolysis." Eur J Biochem 170(3): 575-581.

Yazaki, T., Ohnishi, M., Rokushika, S. and Okada, G. 1997. "Subsite structure of the beta-glucosidase from Aspergillus niger, evaluated by steady-state kinetics with cello-oligosaccharides as substrates." Carbohydrate Research 298(1-2): 51-57.

Zhang, M., Su, R., Qi, W. and He, Z. 2010. "Enhanced enzymatic hydrolysis of lignocellulose by optimizing enzyme complexes." Appl Biochem Biotechnol 160(5): 1407-1414.

Zhang, Y., Xu, B. and Zhou, W. 2014. "On a novel mechanistic model for simultaneous enzymatic hydrolysis of cellulose and hemicellulose considering morphology." Biotechnol Bioeng 111(9): 1767-1781.

Zhang, Y. and Zhou, W. 2014. "On Improved Mechanistic Modeling for Enzymatic Hydrolysis of Cellulose." J Chem Eng Process Technol 5: 190.

Zhang, Y. H. and Lynd, L. R. 2004. "Toward an aggregated understanding of enzymatic hydrolysis of cellulose: noncomplexed cellulase systems." Biotechnol Bioeng 88(7): 797-824.

Zhang, Y. H. and Lynd, L. R. 2006. "A functionally based model for hydrolysis of cellulose by fungal cellulase." Biotechnol Bioeng 94(5): 888-898.

Zhou, W., Hao, Z., Xu, Y. and Schuttler, H. B. 2009a. "Cellulose hydrolysis in evolving substrate morphologies II: Numerical results and analysis." Biotechnol Bioeng 104(2): 275-289.

Zhou, W., Schuttler, H. B., Hao, Z. and Xu, Y. 2009b. "Cellulose hydrolysis in evolving substrate morphologies I: A general modeling formalism." Biotechnol Bioeng 104(2): 261-274.

Zhou, W., Xu, Y. and Schuttler, H. B. 2010. "Cellulose hydrolysis in evolving substrate morphologies III: time-scale analysis." Biotechnol Bioeng 107(2): 224-234.

Supporting Information (SI)

Table S.I. Optimized enzyme mass fraction predictions for Avicel hydrolysis

A					
Time	EG1	CBH1	CBH2	BG	Glucan Conversion (%)
24	0.58	0.00	0.42	0.00	24.7
48	0.62	0.00	0.38	0.00	39.3
B					
Time	EG1	CBH1	CBH2	BG	Glucan Conversion (%)
24	0.64	0.00	0.36	0.00	43.2
48	0.70	0.00	0.30	0.00	52.3
C					
Time	EG1	CBH1	CBH2	BG	Glucan Conversion (%)
24	0.62	0.00	0.38	0.00	62.8
48	0.64	0.00	0.32	0.02	85.2
D					
Time	EG1	CBH1	CBH2	BG	Glucose Yield (%)
24	0.40	0.00	0.40	0.20	15.9
48	0.40	0.00	0.38	0.22	24.1
E					
Time	EG1	CBH1	CBH2	BG	Glucose Yield (%)
24	0.46	0.00	0.36	0.18	31.7
48	0.48	0.00	0.32	0.2	46.6
F					
Time	EG1	CBH1	CBH2	BG	Glucose Yield (%)
24	0.5	0.00	0.32	0.18	53.4
48	0.52	0.00	0.26	0.22	73.5

Predicted optimized enzyme mass fractions are presented for the hydrolysis of Avicel substrate with predicted optimized glucan conversion (%), and predicted optimized glucose conversion (%) for a given time of hydrolysis (24, 48, 72 hours). A&D - 7.5 mg enzyme/g glucan, B&E - 15 mg enzyme/g glucan, C& F - 30 mg enzyme/g glucan.

Table S.II. Optimized enzyme mass fraction predictions for AFEX pretreated corn stover hydrolysis

A							
Time	EG1	CBH1	CBH2	EX	BG	BX	Glucan + Xylan Conversion (%)
24	0.10	0.00	0.60	0.28	0.00	0.02	27.5
48	0.10	0.00	0.55	0.33	0.00	0.02	39.0
B							
Time	EG1	CBH1	CBH2	EX	BG	BX	Glucan + Xylan Conversion (%)
24	0.08	0.00	0.55	0.35	0.00	0.02	48.7
48	0.08	0.00	0.45	0.45	0.00	0.02	62.6
C							
Time	EG1	CBH1	CBH2	EX	BG	BX	Glucan + Xylan Conversion (%)
24	0.08	0.00	0.45	0.45	0.00	0.02	76.9
48	0.07	0.00	0.40	0.50	0.00	0.03	92.9
D							
Time	EG1	CBH1	CBH2	EX	BG	BX	Glucose + Xylose Conversion (%)
24	0.05	0.00	0.50	0.33	0.08	0.04	22.7
48	0.06	0.00	0.52	0.27	0.12	0.03	30.5
E							
Time	EG1	CBH1	CBH2	EX	BG	BX	Glucose + Xylose Conversion (%)
24	0.06	0.00	0.53	0.30	0.08	0.03	41.4
48	0.06	0.00	0.45	0.36	0.10	0.03	53.1
F							
Time	EG1	CBH1	CBH2	EX	BG	BX	Glucose + Xylose Conversion (%)
24	0.07	0.00	0.44	0.35	0.10	0.04	68.7
48	0.06	0.00	0.37	0.44	0.10	0.03	83.4

Predicted optimized enzyme mass fractions are presented for the hydrolysis of AFEX pretreated corn stover with predicted optimized glucan + xylan conversion (%), and predicted optimized glucose + xylose conversion (%) for a given time of hydrolysis (24, 48hours). A &D - 7.5 mg enzyme/g glucan, B&E - 15 mg enzyme/g glucan, C& F - 30 mg enzyme/g glucan.

Table S.III. Optimized enzyme mass fraction predictions for AFEX pretreated corn stover hydrolysis using reduced cellulase adsorption parameters

Cellulase Adsorption Divisor	EG1	CBH1	CBH2	EX	BG	BX	Glucan + Xylan Conversion (%)
1.5	0.09	0.00	0.37	0.51	0.00	0.03	66.7
2.0	0.10	0.00	0.37	0.50	0.00	0.03	66.2
10	0.20	0.00	0.33	0.44	0.00	0.03	62.0
50	0.32	0.00	0.26	0.38	0.00	0.04	54.8
Cellulase Adsorption Divisor	EG1	CBH1	CBH2	EX	BG	BX	Glucose + Xylose Conversion (%)
1.5	0.06	0.00	0.41	0.38	0.11	0.04	55.7
2.0	0.06	0.00	0.43	0.36	0.11	0.04	55.2
10	0.11	0.00	0.40	0.34	0.11	0.04	50.0
50	0.21	0.00	0.34	0.32	0.08	0.05	45.4

Predicted optimized enzyme mass fractions are presented for the hydrolysis of AFEX pretreated corn stover using reduced cellulase adsorption parameters. Predicted optimized glucan + xylan conversion (%), and predicted optimized glucose + xylose conversion (%) are presented at 72 hours of hydrolysis for a 15 mg enzyme/g glucan enzyme loading. A &E–cellulase adsorption parameters divided by 1.5, B &F–cellulase adsorption parameters divided by 2, C &G–cellulase adsorption parameters divided by 20, D & H–cellulase adsorption parameters divided by 50.

Table S.IV. Optimized enzyme mass fraction predictions for AFEX pretreated corn stover hydrolysis using increased $\bar{F}_A^0$

EG1	CBH1	CBH2	EX	BG	BX	Glucan + Xylan Conversion (%)
0.09	0.00	0.44	0.45	0.00	0.02	77.0
0.08	0.00	0.43	0.34	0.12	0.03	61.4

Predicted optimized enzyme mass fractions are presented for the hydrolysis of AFEX pretreated corn stover using decreased $\bar{F}_A^0 = 0.1599$. Predicted optimized glucan + xylan conversion (%), and predicted optimized glucose + xylose conversion (%) are presented at 72 hours of hydrolysis for a 15 mg enzyme/g glucan enzyme loading.

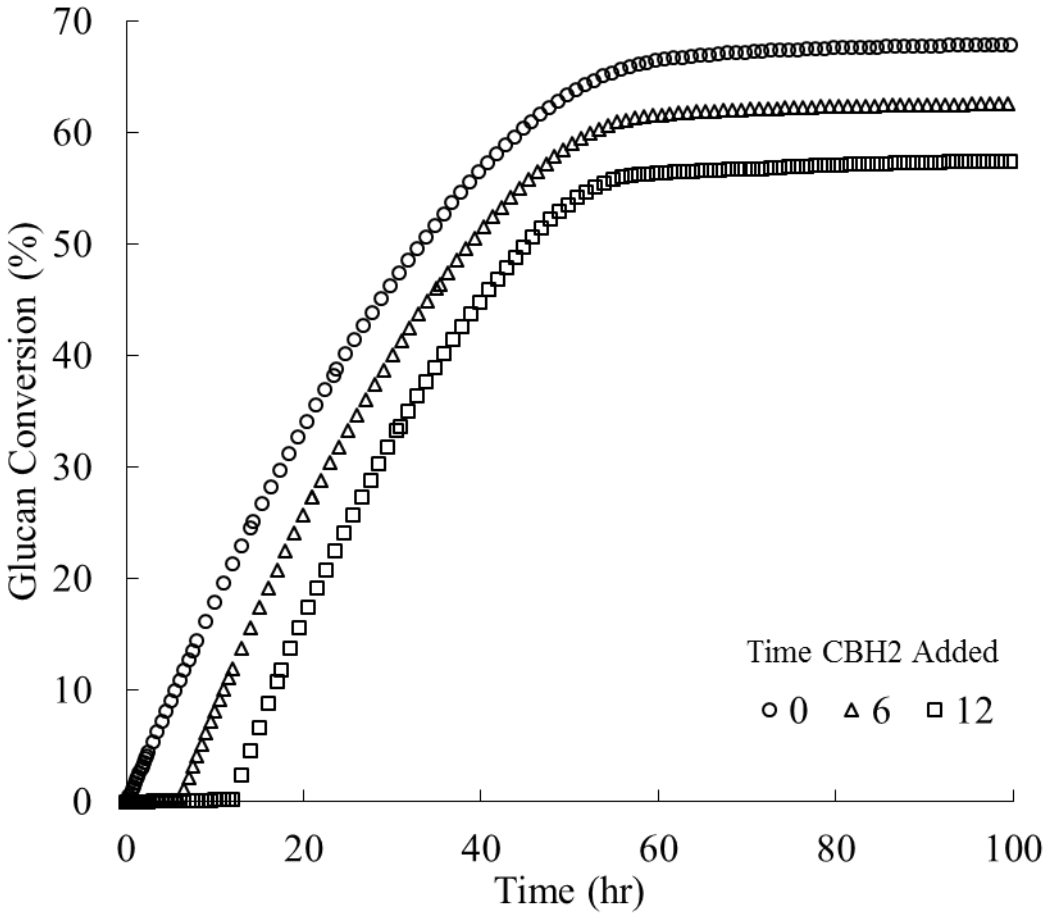

Figure S.1 Time addition of CBH2. CBH2 was modeled as being added to solution at 0, 6, and 12 hours for the hydrolysis of AFEX pretreated corn stover. Enzyme fractions were at the optimized glucose + xylose conversion (AFEX pretreated corn stover) titer at 15 mg enzyme/g glucan and 72 hours.

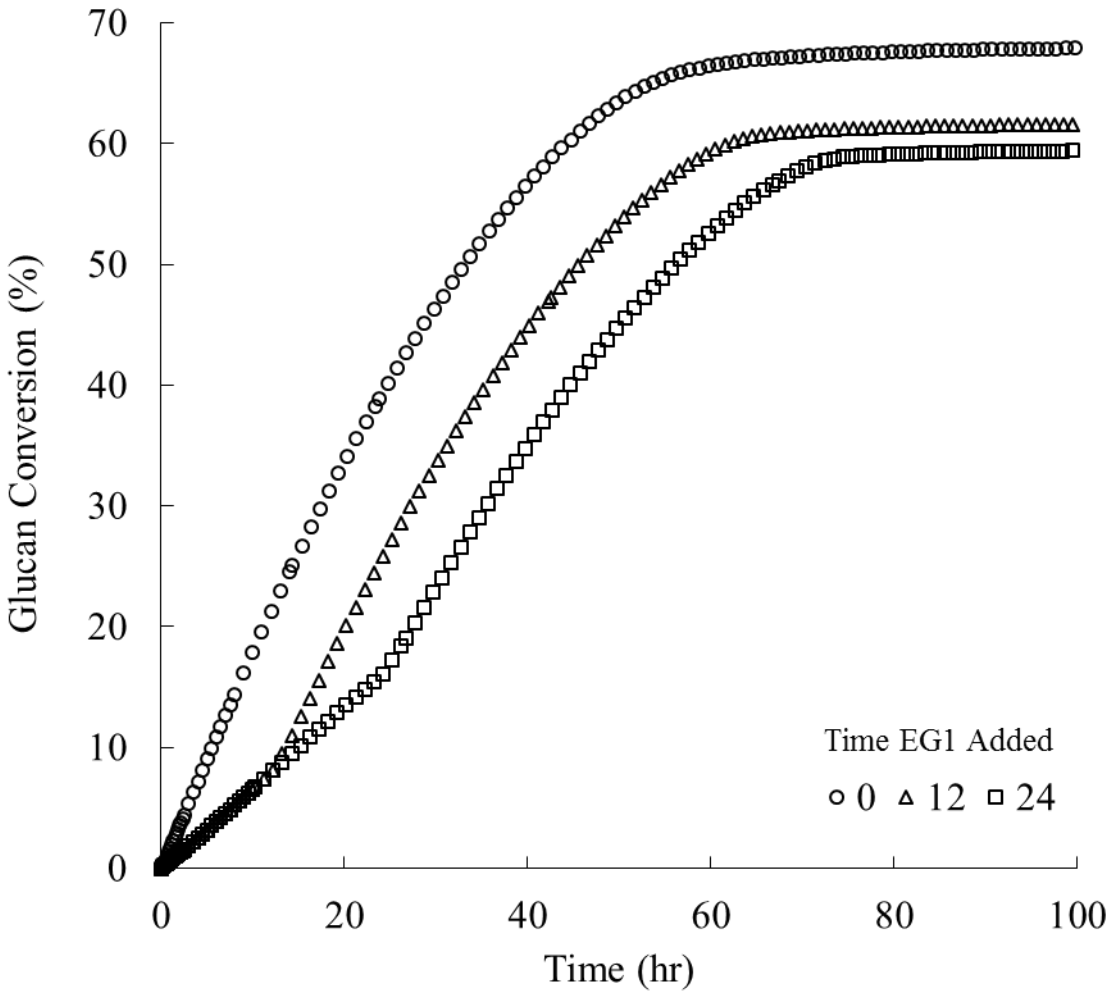

Figure S.2 Time addition of EG1. EG1 was modeled as being added to solution at 0, 12, and 24 hours for the hydrolysis of AFEX pretreated corn stover. Enzyme fractions were at the optimized glucose + xylose conversion (AFEX pretreated corn stover) titer at 15 mg enzyme/g glucan and 72 hours.

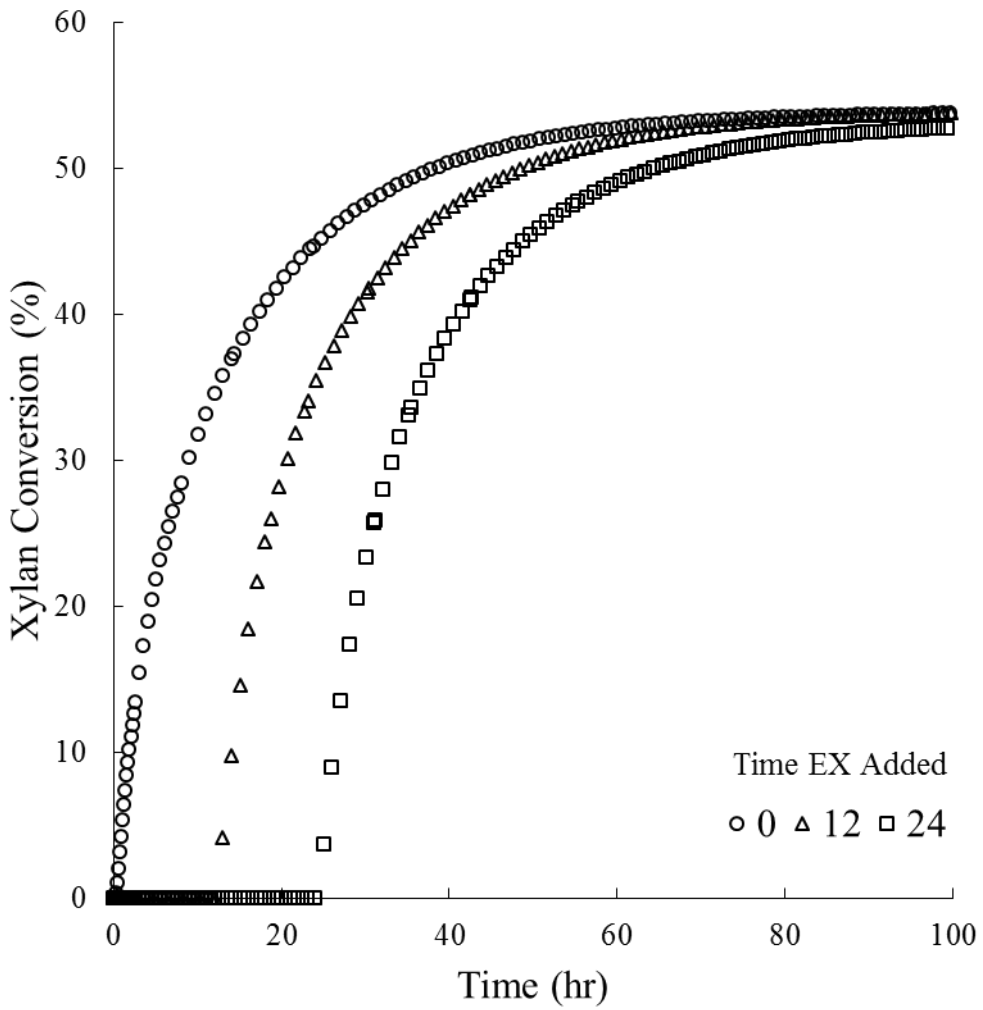

Figure S.3 Time addition of EX. EX was modeled as being added to solution at 0, 24, and 48 hours for the hydrolysis of AFEX pretreated corn stover. Enzyme fractions were at the optimized glucose + xylose conversion (AFEX pretreated corn stover) titer at 15 mg enzyme/g glucan and 72 hours.

Table S.V. Substrate Parameters

Avicel			AFEX pretreated Corn Stover		
Parameter	Value	Ref.	Parameter	Value	Ref.
$\bar{F}_A^{(0)}$	0.006	(Zhou et al. 2009b; Zhang and Lynd 2006)	$\bar{F}_A^{(0)}$	0.1051	(Zhang et al, 2014)
$\bar{\Phi}_{M,Xyl}^{0}$	0	Assumed	$\bar{\Phi}_{M,Xyl}^{0}$	0.55	(Zhang et al., 2014)
DP Cellulose	300	(Zhou 2009b; Zhang and Lynd 2006)	DP Cellulose	6800	(Kumar et al., 2009)
DP Hemicellulose	N/A	Assumed	DP Hemicellulose	200	Assumed

Table S.VI. Adsorption parameters

Parameter	Value (L/mmol)	Ref.
$L_{EG,N,Glu}$, $L_{EG1,X,Glu}$, $L_{EG1,Y,Glu}$	560	(Nidetzky et al., 1994)
$L_{EG1,N,Xyl}$, $L_{EG,X,Xyl}$, $L_{EG,Y,Xyl}$	0	
$L_{CBH2,N,Glu}$, $L_{CBH2,Y,Glu}$	0	
$L_{CBH2,X,Glu}$	950	
$L_{CBH2,N,Xyl}$, $L_{CBH2,X,Xyl}$, $L_{CBH2,Y,Xyl}$	0	
$L_{CBH1,N,Glu}$, $L_{CBH1,X,Glu}$	0	
$L_{CBH1,Y,Glu}$	1410	
$L_{CBH1,N,Xyl}$, $L_{CBH1,X,Xyl}$, $L_{CBH1,Y,Xyl}$	0	
$L_{EX,N,Glu}$, $L_{EX,X,Glu}$, $L_{EX,Y,Glu}$	0	(Zhang et al., 2014)
$L_{EX,N,Xyl}$, $L_{EX,X,Xyl}$, $L_{EX,Y,Xyl}$	0.574	

This represents the equilibrium adsorption constant of enzymes EG1, CBH1, CBH2, EX to sites N, X, Y for glucan and xylan chains.

Table S.VII. Activity parameters

Parameter	Value (mmol bond cleaved mmol enzyme^{-1} min^{-1})	Ref.
$\gamma_{EG1,N,Glu}$, $\gamma_{EG1,X,Glu}$, $\gamma_{EG1,Y,Glu}$	2.475	(Zhang and Lynd, 2004)
$\gamma_{EG1,N,Xyl}$, $\gamma_{EG1,X,Xyl}$, $\gamma_{EG1,Y,Xyl}$	0	
$\gamma_{CBH2,N,Glu}$, $\gamma_{CBH2,Y,Glu}$	0	(Zhang and Lynd, 2006)
$\gamma_{CBH2,X,Glu}$	9.28	
$\gamma_{CBH2,N,Xyl}$, $\gamma_{CBH2,X,Xyl}$, $\gamma_{CBH2,Y,Xyl}$	0	
$\gamma_{CBH1,N,Glu}$, $\gamma_{CBH1,X,Glu}$	0	
$\gamma_{CBH1,Y,Glu}$	5.44	
$\gamma_{CBH1,N,Xyl}$, $\gamma_{CBH1,X,Xyl}$, $\gamma_{CBH1,Y,Xyl}$	0	
$\gamma_{EX,N,Glu}$, $\gamma_{EX,X,Glu}$, $\gamma_{EX,Y,Glu}$	0	(Zhang et al., 2014)
$\gamma_{EX,N,Xyl}$, $\gamma_{EX,X,Xyl}$, $\gamma_{EX,Y,Xyl}$	8.771	

This represents the specific activity of the enzyme-substrate complex of EG1, CBH2, CBH1, EX on sites N, X, Y with glucan or xylan chains.

Table S.VIII. Beta-Enzyme Parameters

Parameter	Value (1/mM)	Reference	Parameter	Value (mmol bond cleaved mmol enzyme^{-1} min^{-1})	Reference
$I_{BG,Glu}(1)$	0.294	(Zhang et al., 2014)	$\gamma_{BG,Glu}(1)$	0	(Zhang et al., 2014)
$I_{BG,Glu}(2)$	1.136		$\gamma_{BG,Glu}(2)$	1897	
$I_{BG,Glu}(3)$	3.846		$\gamma_{BG,Glu}(3)$	1738.9	
$I_{BG,Glu}(4)$	4.000		$\gamma_{BG,Glu}(4)$	1422.8	
$I_{BG,Glu}(5)$	2.174		$\gamma_{BG,Glu}(5)$	895.8	
$I_{BG,Glu}(6)$	1.449		$\gamma_{BG,Glu}(6)$	843.1	
$I_{BG,Xyl}(1)$	0.417		$\gamma_{BG,Xyl}(1)$	0	
$I_{BG,Xyl}(2)$	0		$\gamma_{BG,Xyl}(2)$	0	
$I_{BG,Xyl}(3)$	0		$\gamma_{BG,Xyl}(3)$	0	
$I_{BG,Xyl}(4)$	0		$\gamma_{BG,Xyl}(4)$	0	
$I_{BG,Xyl}(5)$	0		$\gamma_{BG,Xyl}(5)$	0	
$I_{BG,Xyl}(6)$	0		$\gamma_{BG,Xyl}(6)$	0	
$I_{BX,Glu}(1)$	0.294		$\gamma_{BX,Glu}(1)$	0	
$I_{BX,Glu}(2)$	0		$\gamma_{BX,Glu}(2)$	0	
$I_{BX,Glu}(3)$	0		$\gamma_{BX,Glu}(3)$	0	
$I_{BX,Glu}(4)$	0		$\gamma_{BX,Glu}(4)$	0	
$I_{BX,Glu}(5)$	0		$\gamma_{BX,Glu}(5)$	0	
$I_{BX,Glu}(6)$	0		$\gamma_{BX,Glu}(6)$	0	
$I_{BX,Glu}(1)$	0.417		$\gamma_{BX,Xyl}(1)$	0	
$I_{BX,Xyl}(2)$	2.500		$\gamma_{BX,Xyl}(2)$	1897	
$I_{BX,Xyl}(3)$	5.00		$\gamma_{BX,Xyl}(3)$	1250.3	
$I_{BX,Xyl}(4)$	6.250		$\gamma_{BX,Xyl}(4)$	1164.1	
$I_{BX,Xyl}(5)$	10.000		$\gamma_{BX,Xyl}(5)$	1293.4	
$I_{BX,Xyl}(6)$	12.500		$\gamma_{BX,Xyl}(6)$	862.3	

Table S.IX. Half-life of enzymes.

Parameter	Value (hour)	Ref.
$t_{EG1,1/2}$	42.5	(Levine et al., 2010)
$t_{CBH2,1/2}$	42.5	
$t_{CBH1,1/2}$	42.5	
$t_{EX,1/2}$	12.5	(Hakulinen et al., 2003)
$t_{BG,1/2}$	12.5	Assumed
$t_{BX,1/2}$	12.5	Assumed

Table S.X. Inhibition Parameters

Parameter	Value (1/mM)	Ref.	Parameter	Value (1/mM)	Ref.
$I_{EG1,Glu}(1)$	0.06	(Zhang et al., 2014)	$I_{CBH1,Glu}(1)I_{CBH2,Glu}(1)$	0.032	(Zhang et al., 2014)
$I_{EG1,Glu}(2)$	0.13		$I_{CBH1,Glu}(2)I_{CBH2,Glu}(2)$	0.13	
$I_{EG1,Glu}(3)$	0.3		$I_{CBH1,Glu}(3)I_{CBH2,Glu}(3)$	0.3	
$I_{EG1,Glu}(4)$	0.37		$I_{CBH1,Glu}(4)I_{CBH2,Glu}(4)$	0.37	
$I_{EG1,Glu}(5)$	0.44		$I_{CBH1,Glu}(5)I_{CBH2,Glu}(5)$	0.44	
$I_{EG1,Glu}(6)$	0.51		$I_{CBH1,Glu}(6)I_{CBH2,Glu}(6)$	0.51	
$I_{EG1,Xyl}(1)$	0.06		$I_{CBH1,Xyl}(1)I_{CBH2,Xyl}(1)$	0.06	
$I_{EG1,Xyl}(2)$	2		$I_{CBH1,Xyl}(2)I_{CBH2,Xyl}(2)$	2	
$I_{EG1,Xyl}(3)$	2		$I_{CBH1,Xyl}(3)I_{CBH2,Xyl}(3)$	2	
$I_{EG1,Xyl}(4)$	4		$I_{CBH1,Xyl}(4)I_{CBH2,Xyl}(4)$	4	
$I_{EG1,Xyl}(5)$	10		$I_{CBH1,Xyl}(5)I_{CBH2,Xyl}(5)$	10	
$I_{EG1,Xyl}(6)$	11		$I_{CBH1,Xyl}(6)I_{CBH2,Xyl}(6)$	11	
$I_{EX,Glu}(1)$	0.06				
$I_{EX,Glu}(2)$	0.13				
$I_{EX,Glu}(3)$	0.3				
$I_{EX,Glu}(4)$	0.37				
$I_{EX,Glu}(5)$	0.44				
$I_{EX,Glu}(6)$	0.51				
$I_{EX,Xyl}(1)$	0.4				
$I_{EX,Xyl}(2)$	0.85				
$I_{EX,Xyl}(3)$	1.5				
$I_{EX,Xyl}(4)$	2				
$I_{EX,Xyl}(5)$	4				
$I_{EX,Xyl}(6)$	4.5				

Reference

Drissen, R. E. T., Maas, R. H. W., Van Der Maarel, M. J. E. C., Kabel, M. A., Schols, H. A., Tramper, J. and Beeftink, H. H. 2007. "A generic model for glucose production from various cellulose sources by a commercial cellulase complex." Biocatalysis and Biotransformation 25(6): 419-429.

Hakulinen, N., Turunen, O., Janis, J., Leisola, M. and Rouvinen, J. 2003. "Three-dimensional structures of thermophilic beta-1,4-xylanases from Chaetomium thermophilum and Nonomuraea flexuosa. Comparison of twelve xylanases in relation to their thermal stability." Eur J Biochem 270(7): 1399-1412.

Kumar, R., Mago, G., Balan, V. and Wyman, C. E. 2009. "Physical and chemical characterizations of corn stover and poplar solids resulting from leading pretreatment technologies." Bioresour Technol 100(17): 3948-3962.

Nidetzky, B., Steiner, W. and Claeyssens, M. 1994. "Cellulose hydrolysis by the cellulases from Trichoderma reesei: adsorptions of two cellobiohydrolases, two endocellulases and their core proteins on filter paper and their relation to hydrolysis." Biochem J 303 (Pt 3): 817-823.

Zhang, Y., Xu, B. and Zhou, W. 2014. "On a novel mechanistic model for simultaneous enzymatic hydrolysis of cellulose and hemicellulose considering morphology." Biotechnol Bioeng 111(9): 1767-1781.

Zhang, Y. H. and Lynd, L. R. 2006. "A functionally based model for hydrolysis of cellulose by fungal cellulase." Biotechnol Bioeng 94(5): 888-898.

Zhou, W., Hao, Z., Xu, Y. and Schuttler, H. B. 2009. "Cellulose hydrolysis in evolving substrate morphologies II: Numerical results and analysis." Biotechnol Bioeng 104(2): 275-289.

Chapter 5 Improved ADM1 Model for Anaerobic Digestion Process Considering Physico-chemical Reactions[4]

[4] Published in *Bioresource Technology*

Reprinted with permission from (Zhang Y, Piccard S, Zhou W. 2015 "Improved ADM1 model for anaerobic digestion process considering physico-chemical reactions." Bioresource Technology, 196, 279-289). © 2015 Elsevier Ltd.

See Appendix for documentation of permission to republish this material

Abstract

The "Anaerobic Digestion Model No.1" (ADM1) was modified in the study by improving the bio-chemical framework and integrating a more detailed physico-chemical framework. Inorganic carbon and nitrogen balance terms were introduced to resolve the discrepancies in the original bio-chemical framework between the carbon and nitrogen contents in the degraders and substrates. More inorganic components and solids precipitation processes were included in the physico-chemical framework of ADM1. The modified ADM1 was validated with the experimental data and used to investigate the effects of calcium ions, magnesium ions, inorganic phosphorus and inorganic nitrogen on anaerobic digestion in batch reactor. It was found that the entire anaerobic digestion process might exist an optimal initial concentration of inorganic nitrogen for methane gas production in the presence of calcium ions, magnesium ions and inorganic phosphorus.

5.1 Introduction

The "Anaerobic Digestion Model No.1" (ADM1) developed by the International Water Association (IWA) task group is a mathematical model mainly describing the biochemical processes involved in anaerobic digestion (Batstone et al., 2002; Batstone et al., 2006). The whole process of anaerobic digestion can be divided into five steps, which are disintegration, hydrolysis, acidogenesis, acetogenesis and methanogenesis. First, composite particulate substrate is disintegrated into carbohydrates, proteins, lipids, soluble and particulate inerts in the disintegration step. Then carbohydrates, proteins, and lipids are hydrolyzed into monosaccharides (MSs), amino acids (AAs), and long chain fatty acids (LCFAs) in the hydrolysis step (Vavilin et al., 2001). Next in the acidogenesis step, MSs and AAs are degraded by acidogenic bacteria into dissolved hydrogen, carbon dioxide and volatile fatty acids (VFAs), such as propionic acid, acetic acid, butyric acid and valeric acid. Then in the acetogenesis step, these VFAs, as well as some LCFAs from the hydrolysis step, are converted into acetates, dissolved hydrogen and carbon dioxide by acetogenic bacteria. Finally in the methanogenesis step, acetates from the acetogenesis step are converted by aceticlastic methanogenic bacteria into dissolved methane, while dissolved hydrogen and carbon dioxide are converted by hydrogen-utilizing methanogenic bacteria into dissolved methane. During the whole process of anaerobic digestion, all the bacteria (or component degraders) gradually decay and become inactive. These inactive degraders maintain in the reactor as a part of substrate and involve in anaerobic digestion with the original composite particulates. ADM1 employs a set of 24 differential rate equations to describe the bio-chemical processes involved in anaerobic digestion. The disintegration, hydrolysis and bacterial decay steps are represented by first order kinetics,

while all the other steps are represented by Monod-type kinetics. Besides, ADM1 includes several inhibition factors such as LCFAs, dissolved hydrogen and ammonia (Angelidaki et al., 1993; Chen et al., 2008; Schievano et al., 2010; Zonta et al., 2013). In conjunction with the rate equations, 24 dynamic state concentration variables are set for the components involved in anaerobic digestion. These rate equations can be solved simultaneously and have complete mass balances over all components in the solid, gas and liquid phases if appropriate initial values are determined for the concentration variables.

The ADM1 modeling framework is a powerful tool that has been applied in the industrial process design and optimization for wastewater treatment (Batstone and Keller, 2003; Biernacki et al., 2013; Girault et al., 2012; Mairet et al., 2011; Parker, 2005; Shang et al., 2005). Many researches of anaerobic-digestion-involved processes are also based on the application of ADM1 modeling framework, especially the process of methane production (Antonopoulou et al., 2012; Hafez et al., 2010; Parawira et al., 2008; Takiguchi et al., 2004).

However, many deficiencies of the original ADM1 have been noted since its publication. First, the ADM1 does not accommodate complete component mass balances over the nitrogen and carbon components, which can result in the discrepancies between the carbon and nitrogen contents in the biomass and those in the composite particulate material (Blumensaat and Keller, 2005). Second, the ADM1 does not consider too much physico-chemical processes which are not directly mediated by microbes but can affect the bio-chemical processes of anaerobic digestion (Horiuchi et al., 2001; Loewenthal et al., 1989; Loewenthal et al., 1991; Mikkelsen and Keiding, 2002). The most critical physico-

chemical processes omitted in the ADM1 are the solids precipitation processes caused by metal ions. The main reason of excluding the solids precipitation processes from the ADM is that the range of precipitating ions is wide, which leads to a large number of precipitate types (Ekama et al., 2006). Also, the presence of some types of metal ions may have inhibition effects on the precipitation processes involving other metal ion types. In addition, precipitates formed by same ions may exist two different forms: amorphous precipitates and crystalline precipitates, which have different formation mechanisms, precipitation kinetics and the rate-limited factors (Koutsoukos et al., 1980). Third, the ADM1 does not consider phosphoric acid and phosphate as components involved in the physico-chemical processes of anaerobic digestion. It has been shown in many studies that metal ions and phosphate may cause solids precipitation, such as struvite ($MgNH_4PO_4$), affect the pH of the anaerobic digestion circumstances and have strong effects on bio-chemical processes as well as physico-chemical processes (Britton et al., 2005).

The deficiencies of the original ADM1 will unavoidably limit the ability of the model to precisely represent the changing rates of some of the components and to correctly predict the final concentrations of these components. Recently, many studies have focused on developing a more complicated anaerobic digestion model (Fedorovich et al., 2003; Musvoto et al., 2000a; Musvoto et al., 2000b; Sotemann et al., 2005a; Sotemann et al., 2005b). However, most of them do not consider critical inorganic components and physico-chemical processes in all three phases. In this study, the original ADM1 is extended to incorporate more inorganic components, such as metal ions and phosphates, and more physico-chemical processes, such as the association/dissociation processes of carbonate and phosphate ions and the solids precipitation processes of metal ions. Integrating a more

detailed physico-chemical framework into ADM1 can enhance its abilities of keeping track of the change of circumstances pH value and each component involved in anaerobic digestion. The modifications to the original ADM1 may contribute useful information for its further development. After the model validation, the improved ADM1 is used to investigate the effects of some dissolved metal ions and inorganic components on the whole process of anaerobic digestion. Findings of the investigation may be useful for the design and scale-up of anaerobic digestion units for waste water treatment and biogas production processes.

5.2 Methodology

The structures of the modified AMD1 are shown in Tables 5.1-5.5. The entire model can be categorized into two bio-chemical framework and physico-chemical framework and contains totally 47 dynamic state variables representing the concentrations of 47 components in three phases during anaerobic digestion. In addition, the model describes 38 possible bio-chemical and physico-chemical processes involved in anaerobic digestion. The kinetic rate of each process is represented by ρ_j and the detailed expressions are given in the *supplementary material* and the parameter values can be found in the work of Batstone et al. (2002).

5.2.1 Bio-chemical framework

Anaerobic digestion mainly includes two extracellular steps (i.e. disintegration and hydrolysis) and three intracellular steps (i.e. acidogenesis, acetogenesis and methanogenesis). In the intracellular steps, inorganic carbon is the carbon source for, or a

product of, the uptake of sugars, amino acids, propionate, acetate and hydrogen, while inorganic nitrogen is the nitrogen source for the uptake of sugars, amino acids, LCFA, valerate, butyrate, propionate, acetate and hydrogen. However, the original ADM1 did not consider the inorganic carbon and nitrogen changes for some possible processes, especially the decay processes of component degraders. Since the decaying component degraders remain in the reactor and involve in the anaerobic digestion processes together with the original composite particulates, the carbon balance and nitrogen balance must be closed by adding balance terms of inorganic carbon and nitrogen for the bacteria decay processes. In the work of Blumensaat and Keller (2005), two balance terms were introduced to resolve the discrepancies between the carbon and nitrogen contents in the degraders and substrates, which were Eq. (1) (used to close the carbon cycle) and Eq. (2) (used to close the nitrogen cycle). These two terms describe inorganic carbon and nitrogen releases caused by the decay of degraders and the effects on the total dissolved inorganic carbon and nitrogen contents.

$$v_{10,j} = -\sum_{i=13,17\sim23} C_i \, v_{i,j} \tag{1}$$

$$v_{33,j} = -\sum_{i=13,17\sim23} N_i \, v_{i,j} \tag{2}$$

5.2.2 Physico-chemical framework

5.2.2.1 Liquid-gas processes

Liquid-gas transfer processes were originally incorporated in ADM1 as major physico-chemical processes. Hydrogen (H_2), methane (CH_4) and carbon dioxide (CO_2) were considered in the reactor not only in liquid phase, but also in gas phase and represented as

dynamic state concentration variables in the ADM1.At steady-state the relationship between the partial pressure of each biogas component in gas phase and its concentration in liquid phase was described by the Henry's law as Eq. (3). However during the dynamic anaerobic digestion process each biogas component in the reactor would become supersaturated in liquid phase and transfer into gas phase, which was described by the gas transfer rate equation shown as Eq. (4).

$$0 = S_{liq,i,ss} - K_{H,i}P_{gas,i,ss} \tag{3}$$

$$\rho_{T,i} = k_L a_i (S_{liq,i} - K_{H,i}P_{gas,i}) \tag{4}$$

The concentrations of biogas components were obtained by solving the gas transfer rate equations together with the differential rate equations in liquid phase describing the bio-chemical processes. Due to the fact that liquid-gas transfer of ammonia (NH_3) may occur in high pH solution, NH_3 is introduced in the ADM1 as a new component of biogas in this study as shown in Table 5.3.

5.2.2.2 Liquid-liquid processes

The original ADM1 incorporated 6 acid-base reactions which described the acid/base equilibria of acetic acid/acetate, propionic acid/propionate, butyric acid/butyrate, valeric acid/valerate, dissolved carbon dioxide/bicarbonate and ammonium/ammonia. When considering the acid-base reactions in ADM1, 6 original dynamic state concentration variables (i.e. valerate, butyrate, propionate, acetate, inorganic carbon and inorganic nitrogen) were separated into 6 pairs of acid/base variables, generating 6 additional

variables in the model. The acid-base reaction rates were applied to the differential equations of the 6 pairs of acid/base variables as shown in Eq. (5).

$$\rho_{A,i} = k_{A|B,i}(S_{liq,H}S_{liq,i} - K_{a,i}S_{liq,Hi}) \tag{5}$$

To better describe the acid-base reactions and their effects on other processes, more inorganic components and acid/base equilibria are incorporated into the original ADM1 model as shown in Table 5.5. First, the inorganic carbon components in liquid phase include dissolved carbon dioxide (CO_2), bicarbonate (HCO_3^-) and carbonate (CO_3^{2-}) for considering the carbonate precipitation process together with the equilibrium among the three inorganic carbon components ($CO_2/HCO_3^-/CO_3^{2-}$). Second, phosphate (PO_4^{3-}), hydrogen phosphate (HPO_4^2), dihydrogen phosphate ($H_2PO_4^-$) and phosphoric acid (H_3PO_4) are introduced in the model as inorganic phosphorus components for considering the phosphate precipitation together with the equilibrium among the four inorganic phosphorus components ($PO_4^{3-}/HPO_4^{2-}/H_2PO_4^-/H_3PO_4$). Furthermore, the charge balance equation is used to calculate the concentration of H^+ (S_H) so as to keep track of the pH value. As shown in Eq. (6), the total concentration of cationic ions is always equal to the total concentration of anionic ions. S_{CAT} and S_{AN} represent the inert cationic and anionic ions respectively with no changing rate terms in the model. The concentration of OH^- (S_{OH}) is always equal to 10^{-14} divided by S_H based on the acid/base equilibrium of water.

$$S_{CAT} + S_{NH4} + 2S_{Mg} + 2S_{Ca} + S_H - S_{AN} - S_{va}/208 - S_{bu}/160 - S_{pro}/112 - S_{ac}/64 - S_{HCO3} - 2S_{CO3} - 3S_{PO4} - 2S_{HPO4} - S_{H2PO4} - S_{OH} = 0 \tag{6}$$

5.2.2.3 Liquid-solid processes

Solids precipitation processes are major liquid-solid processes that were not included in the original ADM1. The presence of the precipitates could affect other physico-chemical processes and even the bio-chemical processes. To improve the model's ability to describe the non-biologically mediated processes during anaerobic digestion, Eq. (7) is introduced in the original ADM1 to describe the formation rate of precipitates.

$$\frac{d}{dt} M_{v+}A_{v-} = k'_{r,M_{v+}A_{v-}} \left[([M^{m+}]^{v+}[A^{a-}]^{v-})^{1/v} - K'_{sp,M_{v+}A_{v-}}{}^{1/v} \right]^{v} \quad (7)$$

In Eq. (7) $[M^{m+}]$ and $[A^{a-}]$ are the concentrations of M^{m+} and A^{a-} ions respectively; $k'_{r,M_{v+}A_{v-}}$ and $K'_{sp,M_{v+}A_{v-}}$ are the precipitation rate constant and solubility product respectively. v^{+} and v^{-} are the total number of cationic and anionic species respectively with $mv^{+} = av^{-}$ and $v = v^{+} + v^{-}$. The precipitation processes are irreversible in the model so Eq. (7) will have valid value only if the value of $[M^{m+}]^{v+}[A^{a-}]^{v-}$ is larger than $K'_{sp,M_{v+}A_{v-}}$. In this study, calcium ions (Ca^{2+}) and magnesium ions (Mg^{2+}) are considered as two types of M^{m+} ions that will cause 5 major types of precipitates based on the reactions shown in Table 5.6. Not like the common methods of modeling precipitation which usually use simple rate equations based on the pseudo-equilibrium with first order rate coefficients, the form of Eq. (7) is based on the fundamental relationship used for crystallization process (Koutsoukos et al., 1980), which can better describe the mechanisms of solids precipitation

5.3 Results and Discussion

5.3.1 Model validation

In order to testify the accuracy and the predictive ability of the physico-chemical framework of the modified model, the model outputs were compared with experimental data measured at 25°C in the work of Musvoto et al. (2000a). As can be seen in Figure 5.1 and Figure 5.2, the model results accurately predict the changing trends of inorganic components and pH value in the batch reactor, and exhibit good agreement with the experimental results. The comparison demonstrates that the model is able to accurate predict the changes of physico-chemical processes involved inorganic components. Such ability enables the further application of the model for investigating the effects of the inorganic components on the entire anaerobic digestion process.

5.3.2 Effects of inorganic components on anaerobic digestion

In this section, the validated model was used to investigate the effects of dissolved Ca^{2+}, Mg^{2+}, inorganic phosphorus (P_i) and inorganic nitrogen (N_i) on anaerobic digestion in batch reactor. Compared with the original ADM1, dissolved Ca^{2+}, Mg^{2+} and P_i were new components and N_i had different rate equations. The temperature was still set at 25°C so that it would not influence the precipitation rates of metal ions.

First the impacts of dissolved Ca^{2+} and Mg^{2+} on anaerobic digestion were examined by removing one or both of their initial concentrations. As shown in Figure 5.3a-b, the presence of Ca^{2+} and Mg^{2+} in liquid phase not only affects the formation rate of precipitates, but also the release rate of gases, especially ammonia (NH_3) gas, indicating that the liquid-

gas processes could be affected by the liquid-solid processes during anaerobic digestion. To better understand how Ca^{2+} and Mg^{2+} impact biogas release and precipitates generation during anaerobic digestion, different initial ratios of Ca^{2+} to Mg^{2+} were tested with a fixed total concentration in the model. As can be seen in Figure 5.3c, higher initial ratio of Ca^{2+} to Mg^{2+} result in slower production rate of ammonia gas. In addition, the generation process of each type of precipitate also changes significantly as the initial ratio of Ca^{2+} to Mg^{2+} decreases. As shown in Figure 5.3d, at the 2:1 initial ratio of Ca^{2+} to Mg^{2+}, only two types of precipitate, struvite ($MgNH_4PO_4$) and $Ca_3(PO_4)_2$, are generated, but when the initial ratio decreases to 1:2, $CaCO_3$ will be generated as another type of Ca^{2+} precipitate with $Ca_3(PO_4)_2$ and $MgNH_4PO_4$ together. The simulation results in Figure 5.3d reveals that substituting Mg^{2+} for Ca^{2+} may increase the formation rate of $CaCO_3$ in the presence of PO_4^{3-} although the precipitation rate of $Ca_3(PO_4)_2$ is much faster than $CaCO_3$.

Then the effect of dissolved P_i was examined by changing its initial concentration. Dissolved P_i was composed of 4 components in the new model, which were phosphate (PO_4^{3-}), hydrogen phosphate (HPO_4^{2-}), dihydrogen phosphate ($H_2PO_4^-$) and phosphoric acid (H_3PO_4). Among these 4 components, PO_4^{3-} and HPO_4^{2-} were involved in both liquid-liquid and liquid-solid processes of anaerobic digestion while others were only involved in the liquid-liquid processes. However, as shown in Figure 5.3a-c, the finial yields of methane (CH_4), carbon dioxide (CO_2) and ammonia (NH_3) in gas phase can also be influenced by the initial concentration of dissolved P_i, indicating that the presence of P_i in liquid phase has a noticeable effect on liquid-gas processes of anaerobic digestion. Furthermore, as shown in Figure 5.4d, the total concentration of acetate and acetic acid (S_{ac}+S_{Hac}) will have different changing trends as the initial concentration of P_i changes in

liquid phase, indicating that the presence of P_i in liquid phase may affect bio-chemical processes of anaerobic digestion such as the uptake of acetate, the decay of acetate degraders (X_{ac}) and the generation of CH_4 in liquid phase. In addition, as demonstrated in Figure 5.3a, increasing the initial concentration of P_i will decrease the final yield of CH_4 gas. As the initial concentration of P_i becomes higher, less $CaCO_3$ and $MgCO_3$ will form in solid phase, as shown in Figure 5.4f, and more CO_3^{2-} will remain in solution, which will increase the concentration of CO_2 in liquid phase as well as gas phase and thus affect the concentration of CH_4 in gas phase.

Next the effect of dissolved N_i was examined also by changing its initial concentration. Dissolved N_i was originally considered in the ADM1 model as NH_4^+ and NH_3 which were only involved in bio-chemical and liquid-liquid processes. In this study, NH_4^+ was considered to be able to form precipitate with Mg^{2+} (Britton et al., 2005) and NH_3 was considered as a components in both liquid and gas phase. Since dissolved N_i is involved in all kinds of anaerobic digestion processes in the model, changing the initial concentration of dissolved N_i will inevitably affect the yields of many components in liquid, gas or solid phase. As shown in Figure 5.5a, neither increasing nor decreasing the initial concentration of N_i in liquid phase can increase the yield of CH_4 in gas phase, indicating that for CH_4 gas production during anaerobic digestion there may be an optimal initial concentration of dissolved N_i in the presence of Mg^{2+}, Ca^{2+} and dissolved P_i. If the initial concentration of N_i is too high, large amount of NH_3 may remain in solution after Mg^{2+} being precipitated and result in strong inhibition effect on the production of CH_4 in liquid phase. Besides, high concentration of NH_3 in liquid phase may also cause high percentage of NH_3 in gas phase and thus affect the content of CH_4 gas. However, as shown in Figure 5.5f, if the

initial concentration of N_i is too low, no $CaCO_3$ will form in solution. The reason may be that low initial concentration of N_i leads to low initial pH in solution, which will inhibit the formation of $CaCO_3$ in solution. So large amount of CO_3^{2-} will remain in solution after Ca^{2+} being precipitated, which will increase the concentration of CO_2 in liquid phase as well as gas phase and affect the content of CH_4 gas.

To understand how dissolved N_i and P_i together can impact the yield of CH_4 gas during anaerobic digestion, different initial dissolved N_i to P_i ratios (N_i:P_i) were tested with different fixed initial concentrations of dissolved N_i and P_i (N_i+P_i) in the model. Several specific measurement results about the initial N_i:P_i ratio were found in the literature. For example, in the work of Musvoto et al. (2000b) the initial N_i:P_i ratios in real situations were from 2.21 to 9.21. So it is believe that the initial N_i:P_i ratio differs case by case and varies in a very large range in real situations. As shown in Figure 5.6a, increasing the initial N_i:P_i ratio will have a positive effect on the final yield of CH_4 gas. Then the initial concentration of "N_i+P_i" was set as 10% of the original value. As shown in Figure 5.6b, higher initial N_i:P_i ratio will also result in higher yield of CH_4 gas in the 1st day and after the 3rd day. However during the 1st and 3rd day, the CH_4 gas production rate with lower initial N_i:P_i ratio becomes a little faster, which results in more CH_4 gas during this time period. After that the initial concentration of "N_i+P_i" was set as 1000% of the original value. As shown in Figure 5.6c, the effect of initial N_i:P_i ratio will become significantly different compared to those with lower initial "N_i+P_i" concentrations. As the initial N_i:P_i ratio increases, the yield of CH_4 gas will drop a lot, meaning that in the case of high initial "N_i+P_i" concentration, high initial N_i:P_i ratio may have negative effect on the yield of CH_4 gas.

These simulations reflect the complex combination effects of dissolved P_i and N_i on the yield of CH_4 gas in the presence of Mg^{2+} and Ca^{2+}.

5.4 Conclusions

The original ADM1 has been modified by improving its bio-chemical framework and integrating a more detailed physico-chemical framework. The modified ADM1 was validated by a set of experimental data and used to investigate the effects of dissolved calcium and magnesium ions, inorganic phosphorus and nitrogen on anaerobic digestion in batch reactor. The modifications improved the ADM1's ability to keep track of the biogas production in gas phase, the pH value in liquid phase and the precipitates in solid phase, and provided a way of developing a complete anaerobic digestion mathematical model in future.

Nomenclature

A_i: acid-base reaction index involving *i* component

C_i: carbon content of component *i* (kmole/kgCOD)

$f_{product,substrate}$: yield of product on substrate

i: component index

j: process index

N_i: nitrogen content of component *i* (kmole/kgCOD)

P_i: precipitation process index involving *i* component

S_{su}: suger (monosaccharides) (kgCOD/m^3)

S_{aa}: amino acids (kgCOD/m^3)

S_{fa}: fatty acids (long chain) (kgCOD/m^3)

S_{va}: valerate (kgCOD/m^3)

S_{bu}: butyrate (kgCOD/m^3)

S_{pro}: propionate (kgCOD/m^3)

S_{ac}: acetate (kgCOD/m^3)

S_{H2}: hydrogen gas (dissolved) (kgCOD/m^3)

S_{CH4}: methane gas (dissolved) (kgCOD/m^3)

S_{HCO3}: bicarbonate (M)

S_{NH3}: ammonia gas (dissolved) (M)

S_I: inerts (dissolved) (kgCOD/m^3)

S_{Hva}: valeric acid (kgCOD/m^3)

S_{Hbu}: butyric acid (kgCOD/m^3)

S_{Hpro}: propionic acid (kgCOD/m^3)

S_{Hac}: acetic acid (kgCOD/m^3)

S_{CO2}: carbon dioxide gas (dissolved) (M)

S_{NH4}: ammonium (M)

S_{Ca}: calcium ions (M)

S_{Mg}: magnesiumions (M)

S_{H3PO4}: phosphoric acid (M)

S_{H2PO4}: dihydrogen phosphate (M)

S_{HPO4}: hydrogen phosphate (M)

S_{PO4}: phosphate (M)

S_{CO3}: carbonate (M)

T_i: liquid-gas transfer process index involving *i* component

$v_{i,j}$: rate coefficients for component i on process j

X_c: composites (kgCOD/m^3)

X_{ch}: carbohydrates (kgCOD/m^3)

X_{pr}: proteins (kgCOD/m^3)

X_{li}: lipids (kgCOD/m^3)

X_{su}: suger degraders (monosaccharides) (kgCOD/m^3)

X_{aa}: amino acids degraders (kgCOD/m^3)

X_{fa}: LCFA degraders (kgCOD/m^3)

X_{c4}: valerate and butyrate degraders (kgCOD/m^3)

X_{pro}: propionate degraders (kgCOD/m^3)

X_{ac}: acetate degraders (kgCOD/m^3)

X_{H2}: hydrogen degraders (kgCOD/m^3)

X_I: inerts (particulate) (kgCOD/m^3)

$Y_{substrate}$: yield of biomass on substrate

ρ_j: kinetic rate of process j

Acknowledgments

We acknowledge the National Science Foundation (CBET 1138734, CHE 1230803) for financial support.

Tables

Table 5.1 Matrix representation of the rate coefficients and equations for ADM1 bio-chemical framework part 1: soluble components

j	Process	Component i												Rate
		1	2	3	4	5	6	7	8	9	10	12	33	
		S_{su}	S_{aa}	S_{fa}	S_{va}	S_{bu}	S_{pro}	S_{ac}	S_{H2}	S_{CH4}	S_{HCO3}	S_I	S_{NH4}	ρ_j
1	Disintegration											$f_{sl,xc}$		ρ_1
2	Hydrolysis Carbohydrates	1												ρ_2
3	Hydrolysis of Proteins		1											ρ_3
4	Hydrolysis of Lipids	$1-f_{fa,li}$		$f_{fa,li}$										ρ_4
5	Uptake of Sugars	-1				$(1-Y_{su})f_{bu,su}$	$(1-Y_{su})f_{pro,su}$	$(1-Y_{su})f_{ac,su}$	$(1-Y_{su})f_{H2,su}$		$v_{10,5}$		$(-Y_{su})N_{bac}$	ρ_5
6	Uptake of Amino Acids		-1		$(1-Y_{aa})f_{va,aa}$	$(1-Y_{aa})f_{bu,aa}$	$(1-Y_{aa})f_{pro,aa}$	$(1-Y_{aa})f_{ac,aa}$	$(1-Y_{aa})f_{H2,aa}$		$v_{10,6}$		$N_{aa}-Y_{aa}N_{bac}$	ρ_6
7	Uptake of LCFA			-1				$(1-Y_{fa})0.7$	$(1-Y_{fa})0.3$				$(-Y_{fa})N_{bac}$	ρ_7
8	Uptake of Valerate				-1		$(1-Y_{c4})0.54$	$(1-Y_{c4})0.31$	$(1-Y_{c4})0.15$				$(-Y_{c4})N_{bac}$	ρ_8
9	Uptake of Butyrate					-1		$(1-Y_{c4})0.8$	$(1-Y_{c4})0.2$				$(-Y_{c4})N_{bac}$	ρ_9
10	Uptake of Propionate						-1	$(1-Y_{pro})0.57$	$(1-Y_{pro})0.43$		$v_{10,10}$		$(-Y_{pro})N_{bac}$	ρ_{10}
11	Uptake of Acetate							-1		$(1-Y_{ac})$	$v_{10,11}$		$(-Y_{ac})N_{bac}$	ρ_{11}
12	Uptake of Hydrogen								-1	$(1-Y_{H2})$	$v_{10,12}$		$(-Y_{H2})N_{bac}$	ρ_{12}
13	Decay of X_{su}										$v_{10,13}$		$v_{33,13}$	ρ_{13}
14	Decay of X_{aa}										$v_{10,14}$		$v_{33,14}$	ρ_{14}
15	Decay of X_{fa}										$v_{10,15}$		$v_{33,15}$	ρ_{15}
16	Decay of X_{c4}										$v_{10,16}$		$v_{33,16}$	ρ_{16}
17	Decay of X_{pro}										$v_{10,17}$		$v_{33,17}$	ρ_{17}
18	Decay of X_{ac}										$v_{10,18}$		$v_{33,18}$	ρ_{18}
19	Decay of X_{H2}										$v_{10,19}$		$v_{33,19}$	ρ_{19}

Table 5.2 Matrix representation of the rate coefficients and equations for ADM1 bio-chemical framework part 2: particulate components

j	Process	Component i												Rate
		13	14	15	16	17	18	19	20	21	22	23	24	
		X_c	X_{ch}	X_{pr}	X_{li}	X_{su}	X_{aa}	X_{fa}	X_{c4}	X_{pro}	X_{ac}	X_{H2}	X_I	ρ_j
1	Disintegration	-1	$f_{oh,xc}$	$f_{pr,xc}$	$f_{li,xc}$								$f_{xl,xc}$	ρ_1
2	Hydrolysis Carbohydrates		-1											ρ_2
3	Hydrolysis of Proteins			-1										ρ_3
4	Hydrolysis of Lipids				-1									ρ_4
5	Uptake of Sugars					Y_{su}								ρ_5
6	Uptake of Amino Acids						Y_{aa}							ρ_6
7	Uptake of LCFA							Y_{fa}						ρ_7
8	Uptake of Valerate								Y_{c4}					ρ_8
9	Uptake of Butyrate								Y_{c4}					ρ_9
10	Uptake of Propionate									Y_{pro}				ρ_{10}
11	Uptake of Acetate										Y_{ac}			ρ_{11}
12	Uptake of Hydrogen											Y_{H2}		ρ_{12}
13	Decay of X_{su}	1				-1								ρ_{13}
14	Decay of X_{aa}	1					-1							ρ_{14}
15	Decay of X_{fa}	1						-1						ρ_{15}
16	Decay of X_{c4}	1							-1					ρ_{16}
17	Decay of X_{pro}	1								-1				ρ_{17}
18	Decay of X_{ac}	1									-1			ρ_{18}
19	Decay of X_{H2}	1										-1		ρ_{19}

Table 5.3 Matrix representation of the rate coefficients and equations for ADM1 physico-chemical framework part 1: liquid-gas processes

j	Process	Component i				Rate
		8	9	11	32	
		S_{H2}	S_{CH4}	S_{NH3}	S_{CO2}	ρ_j
T8	H_2 Transfer	-1				ρ_{T8}
T9	CH_4 Transfer		-1			ρ_{T9}
T11	NH_3 Transfer			-1		ρ_{T11}
T32	CO_2 Transfer				-1	ρ_{T32}

Table 5.4 Matrix representation of the rate coefficients and equations for ADM1 physico-chemical framework part 2: liquid-liquid processes

j	Process	Component i																	Rate
		4	5	6	7	10	11	28	29	30	31	32	33	37	38	39	40	41	
		S_{va}	S_{bu}	S_{pro}	S_{ac}	S_{HCO3}	S_{NH3}	S_{Hva}	S_{Hbu}	S_{Hpro}	S_{Hac}	S_{CO2}	S_{NH4}	S_{H3PO4}	S_{H2PO4}	S_{HPO4}	S_{PO4}	S_{CO3}	ρ_j
A4	Valerate Acid-Base	-1						1											ρ_{A4}
A5	Butyrate Acid-Base		-1						1										ρ_{A5}
A6	Propionate Acid-Base			-1						1									ρ_{A6}
A7	Acetate Acid-Base				-1						1								ρ_{A7}
A10	HCO_3^- Acid-Base					-1						1							ρ_{A10}
A11	NH_4^+ Acid-Base						-1						1						ρ_{A11}
A38	$H_2PO_4^-$ Acid-Base													1	-1				ρ_{A38}
A39	HPO_4^{2-} Acid-Base														1	-1			ρ_{A39}
A40	PO_4^{3-} Acid-Base															1	-1		ρ_{A40}
A41	CO_3^{2-} Acid-Base					1												-1	ρ_{A41}

Table 5.5 Matrix representation of the rate coefficients and equations for ADM1 physico-chemical framework part 3: liquid-solid processes

j	Process	Component i						Rate
		33	35	36	39	40	41	
		S_{NH4}	S_{Ca}	S_{Mg}	S_{HPO4}	S_{PO4}	S_{CO3}	ρ_j
P42	$CaCO_3$ Precipitation		-1				-1	ρ_{P42}
P43	$MgCO_3$ Precipitation			-1			-1	ρ_{P43}
P44	$MgNH_4PO_3$ Precipitation	-1		-1		-1		ρ_{P44}
P45	$MgHPO_4$ Precipitation			-1	-1			ρ_{P45}
P46	$Ca_3(PO_4)_2$ Precipitation		-1			- 2/3		ρ_{P46}

Table 5.6 Acid-base and precipitation reactions considered in anaerobic digestion

Acid-base reactions	Precipitation reactions
$H_3PO_4 \rightleftharpoons H^+ + H_2PO_4^-$	$Ca^{2+} + CO_3^{2-} \rightleftharpoons CaCO_3\ (s)$
$H_2PO_4^- \rightleftharpoons H^+ + HPO_4^{2-}$	$Mg^{2+} + CO_3^{2-} \rightleftharpoons MgCO_3\ (s)$
$HPO_4^{2-} \rightleftharpoons H^+ + PO_4^{3-}$	$Mg^{2+} + NH_4^+ + PO_4^{3-} \rightleftharpoons MgNH_4PO_4\ (s)$
$H_2CO_3 \rightleftharpoons +H^+ + HCO_3^-$	$Mg^{2+} + HPO_4^{2-} \rightleftharpoons MgHPO_4\ (s)$
$HCO_3^- \rightleftharpoons H^+ + CO_3^{2-}$	$3Ca^{2+} + 2PO_4^{3-} \rightleftharpoons Ca_3(PO_4)_2\ (s)$
$NH_4^+ + \rightleftharpoons H^+ + NH_3$	
$Hva \rightleftharpoons H^+ + va^-$	
$Hbu \rightleftharpoons H^+ + bu^-$	
$Hpro \rightleftharpoons H^+ + pro^-$	
$Hac \rightleftharpoons H^+ + ac^-$	

Figures

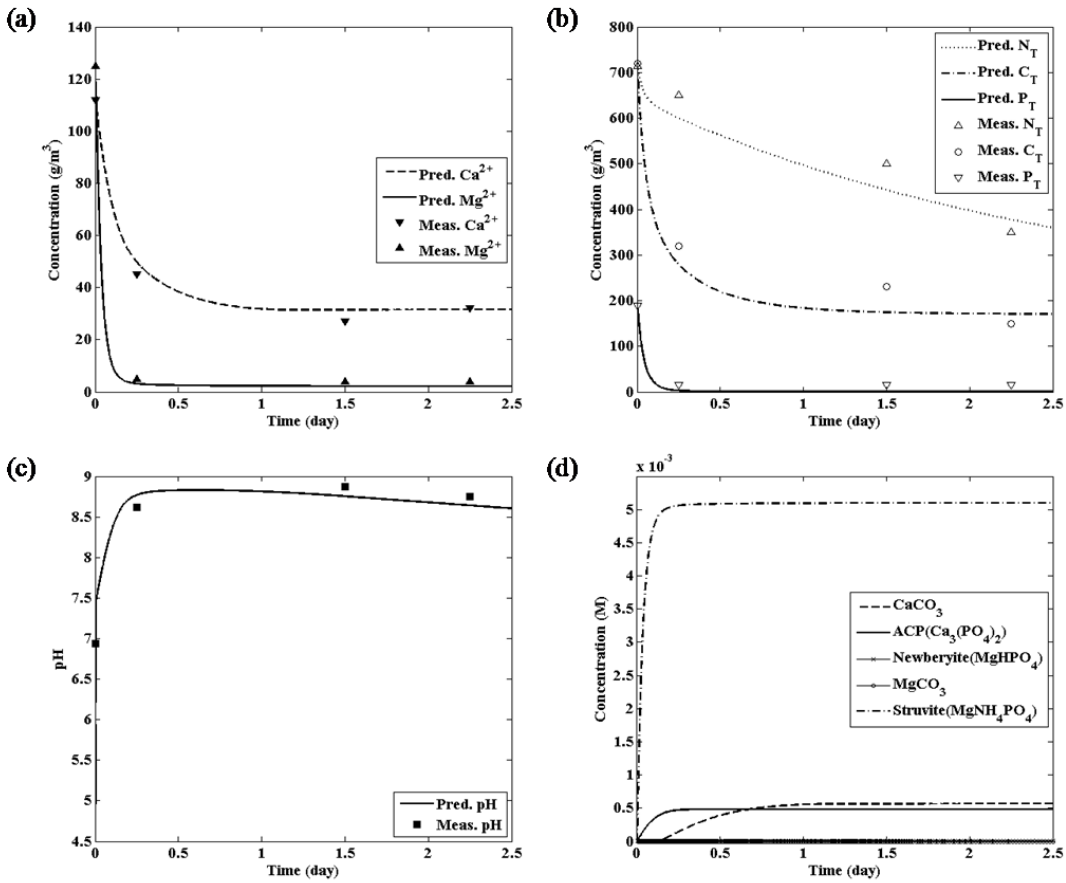

Figure 5.1 Comparison between the predicted (pred.) and measured (meas.) data for calcium and magnesium ions, total carbonate, phosphate, ammonia/ammonium, pH in liquid phase and model prediction of precipitate generation rates in solid phase

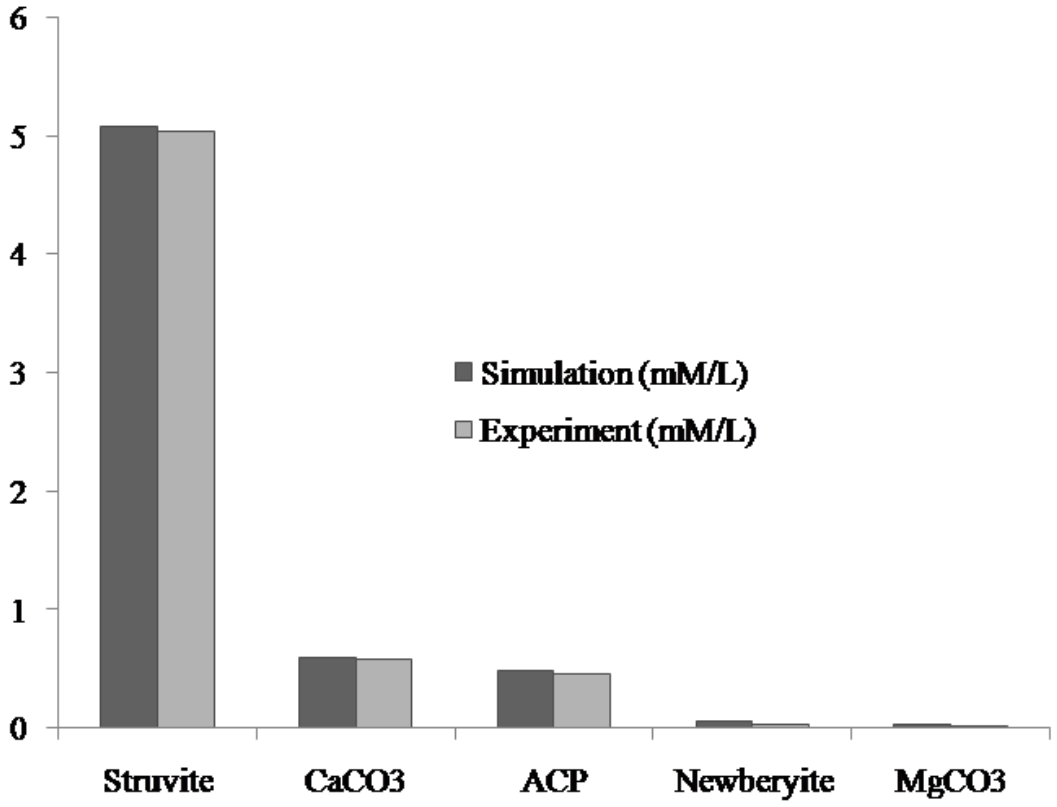

Figure 5.2 Comparison between the simulation results and experimental data of finial concentrations of precipitates

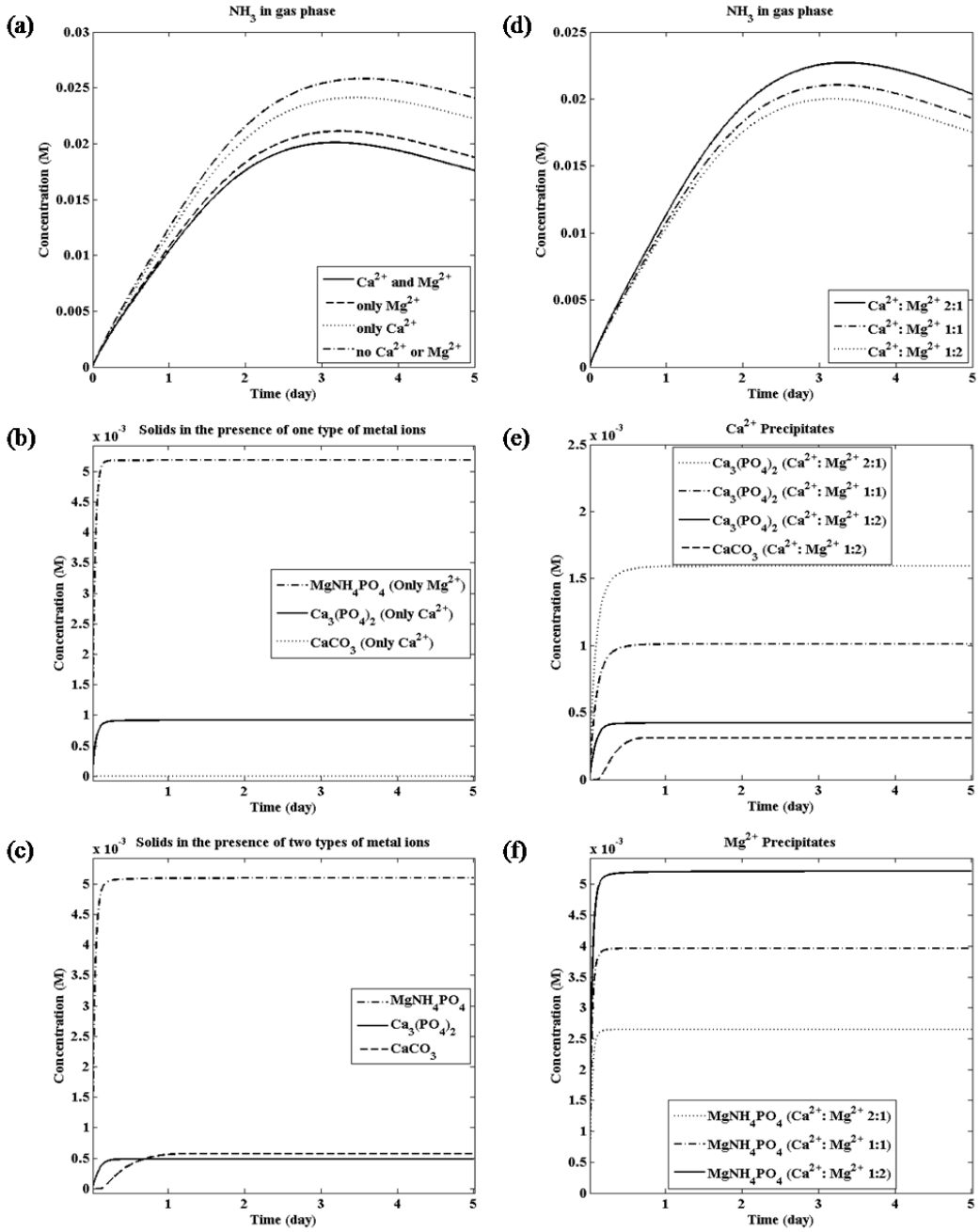

Figure 5.3 Effects of metal ions on biogas production and precipitates generation

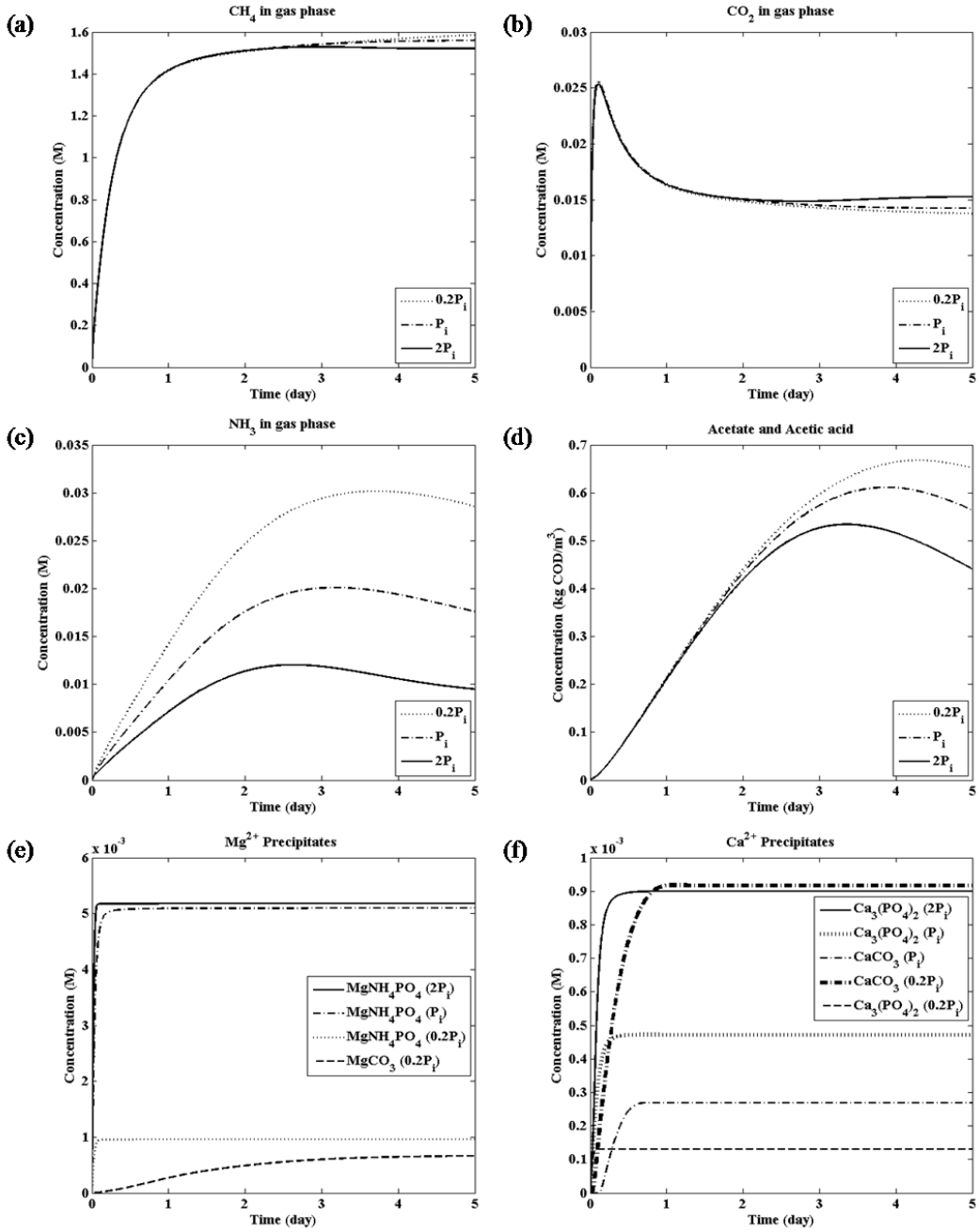

Figure 5.4 Effects of inorganic phosphorus on biogas in gas phase, substrate in liquid phase and precipitates in solid phase

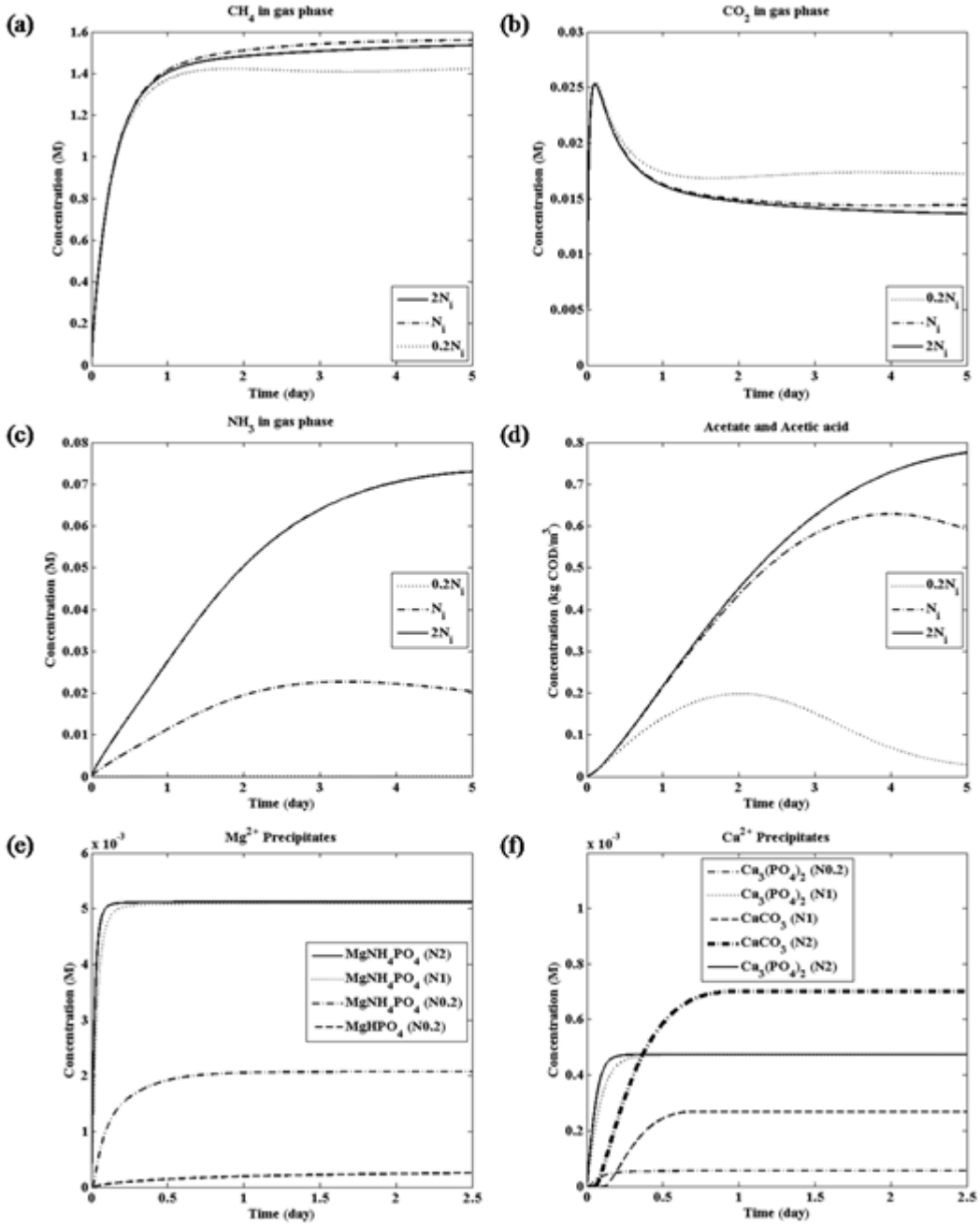

Figure 5.5 Effects of inorganic nitrogen on biogas in gas phase, substrate in liquid phase and precipitates in solid phase

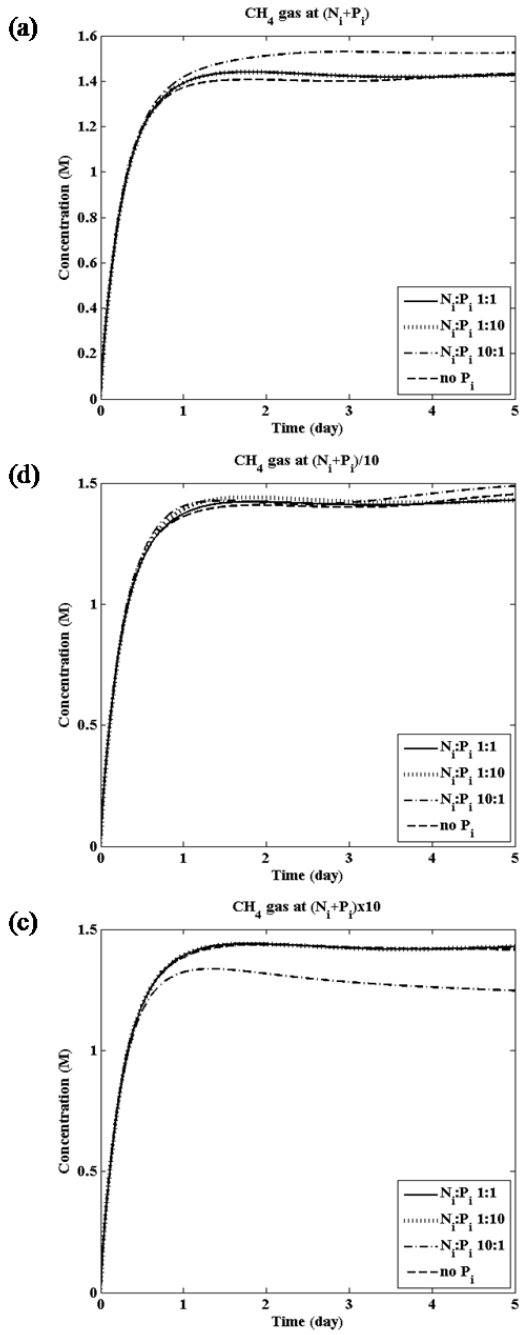

Figure 5.6 Effects of different initial inorganic phosphorus to nitrogen ratios on the production of CH4 in gas phase

References

Angelidaki, I., Ellegaard, L., Ahring, B.K., 1993. A mathematical model for dynamic simulation of anaerobic digestion of complex substrates: focusing on ammonia inhibition. Biotechnol Bioeng 42(2), 159-166.

Antonopoulou, G., Gavala, H.N., Skiadas, I.V., Lyberatos, G., 2012. ADM1-based modeling of methane production from acidified sweet sorghum extract in a two stage process. Bioresour Technol 106, 10-19.

Batstone, D.J., Keller, J., 2003. Industrial applications of the IWA anaerobic digestion model No. 1 (ADM1). Water Science and Technology 47(12), 199-206.

Batstone, D.J., Keller, J., Angelidaki, I., Kalyuzhnyi, S.V., Pavlostathis, S.G., Rozzi, A., Sanders, W.T.M., Siegrist, H., Vavilin, V.A., 2002. The IWA Anaerobic Digestion Model No 1 (ADM1). Water Science and Technology 45(10), 65-73.

Batstone, D.J., Keller, J., Steyer, J.P., 2006. A review of ADM1 extensions, applications, and analysis: 2002-2005. Water Sci Technol 54(4), 1-10.

Biernacki, P., Steinigeweg, S., Borchert, A., Uhlenhut, F., 2013. Application of Anaerobic Digestion Model No. 1 for describing anaerobic digestion of grass, maize, green weed silage, and industrial glycerine. Bioresour Technol 127, 188-194.

Blumensaat, F., Keller, J., 2005. Modelling of two-stage anaerobic digestion using the IWA Anaerobic Digestion Model No. 1 (ADM1). Water Res 39(1), 171-183.

Britton, A., Koch, F.A., Adnan, A., Oldham, W.K., Mavinic, D.S., 2005. Pilot-scale struvite recovery from anaerobic digester supernatant at an enhanced biological phosphorus removal wastewater treatment plant. Journal of Environmental Engineering and Science 4(4), 265-277.

Chen, Y., Cheng, J.J., Creamer, K.S., 2008. Inhibition of anaerobic digestion process: A review. Bioresource Technology 99(10), 4044-4064.

Ekama, G.A., Wentzel, M.C., Loewenthal, R.E., 2006. Integrated chemical--physical processes kinetic modelling of multiple mineral precipitation problems. Water Sci Technol 53(12), 65-73.

Fedorovich, V., Lens, P., Kalyuzhnyi, S., 2003. Extension of Anaerobic Digestion Model No. 1 with processes of sulfate reduction. Appl Biochem Biotechnol 109(1-3), 33-45.

Girault, R., Bridoux, G., Nauleau, F., Poullain, C., Buffet, J., Steyer, J.P., Sadowski, A.G., Beline, F., 2012. A waste characterisation procedure for ADM1 implementation based on degradation kinetics. Water Res 46(13), 4099-4110.

Hafez, H., Naggar, M.H.E., Nakhla, G., 2010. Steady-state and dynamic modeling of biohydrogen production in an integrated biohydrogen reactor clarifier system. International Journal of Hydrogen Energy 35(13), 6634-6645.

Horiuchi, J., Kikuchi, S., Kobayashi, M., Kanno, T., Shimizu, T., 2001. Modeling of pH response in continuous anaerobic acidogenesis by an artificial neural network. Biochemical Engineering Journal 9(3), 199-204.

Koutsoukos, P., Amjad, Z., Tomson, M.B., Nancollas, G.H., 1980. Crystallization of Calcium Phosphates - Constant Composition Study. Journal of the American Chemical Society 102(5), 1553-1557.

Loewenthal, R.E., Ekama, G.A., Marais, G., 1989. Mixed Weak Acid-Base Systems .1. Mixture Characterization. Water Sa 15(1), 3-24.

Loewenthal, R.E., Wentzel, M.C., Ekama, G.A., Marais, G.R., 1991. Mixed Weak Acid-Base Systems .2. Dosing Estimation, Aqueous Phase. Water Sa 17(2), 107-122.

Mairet, F., Bernard, O., Ras, M., Lardon, L., Steyer, J.P., 2011. Modeling anaerobic digestion of microalgae using ADM1. Bioresour Technol 102(13), 6823-6829.

Mikkelsen, L.H., Keiding, K., 2002. Physico-chemical characteristics of full scale sewage sludges with implications to dewatering. Water Res 36(10), 2451-2462.

Musvoto, E.V., Wentzel, M.C., Ekama, G.A., 2000a. Integrated chemical-physical processes modelling - II. Simulating aeration treatment of anaerobic digester supernatants. Water Research 34(6), 1868-1880.

Musvoto, E.V., Wentzel, M.C., Loewenthal, R.E., Ekama, G.A., 2000b. Integrated chemical-physical processes modelling - I. Development of a kinetic-based model for mixed weak acid/base systems. Water Research 34(6), 1857-1867.

Parawira, W., Read, J.S., Mattiasson, B., Bjornsson, L., 2008. Energy production from agricultural residues: High methane yields in pilot-scale two-stage anaerobic digestion. Biomass & Bioenergy 32(1), 44-50.

Parker, W.J., 2005. Application of the ADM1 model to advanced anaerobic digestion. Bioresour Technol 96(16), 1832-1842.

Schievano, A., D'Imporzano, G., Malagutti, L., Fragali, E., Ruboni, G., Adani, F., 2010. Evaluating inhibition conditions in high-solids anaerobic digestion of organic fraction of municipal solid waste. Bioresour Technol 101(14), 5728-5732.

Shang, Y., Johnson, B.R., Sieger, R., 2005. Application of the IWA anaerobic digestion model (ADM1) for simulating full-scale anaerobic sewage sludge digestion. Water Sci Technol 52(1-2), 487-492.

Sotemann, S.W., Musvoto, E.V., Wentzel, M.C., Ekama, G.A., 2005a. Integrated biological, chemical and physical processes kinetic modelling Part 1 - Anoxic-aerobic C and N removal in the activated sludge system. Water Sa 31(4), 529-544.

Sotemann, S.W., van Rensburg, P., Ristow, N.E., Wentzel, M.C., Loewenthal, R.E., Ekama, G.A., 2005b. Integrated chemical/physical and biological processes modelling Part 2 - Anaerobic digestion of sewage sludges. Water Sa 31(4), 545-568.

Takiguchi, N., Kishino, M., Kuroda, A., Kato, J., Ohtake, H., 2004. A laboratory-scale test of anaerobic digestion and methane production after phosphorus recovery from waste activated sludge. Journal of Bioscience and Bioengineering 97(6), 365-368.

Vavilin, V.A., Rytov, S.V., Lokshina, L.Y., Rintala, J.A., Lyberatos, G., 2001. Simplified hydrolysis models for the optimal design of two-stage anaerobic digestion. Water Research 35(17), 4247-4251.

Zonta, Z., Alves, M.M., Flotats, X., Palatsi, J., 2013. Modelling inhibitory effects of long chain fatty acids in the anaerobic digestion process. Water Res 47(3), 1369-1380.

Supporting Information (SI)

S.1. Expressions of kinetic rate terms

$$\rho_1 = k_{dis} * X_c$$

$$\rho_2 = k_{hyd,ch} * X_{ch}$$

$$\rho_3 = k_{hyd,pr} * X_{pr}$$

$$\rho_4 = k_{hyd,li} * X_{li}$$

$$\rho_5 = k_{m,su} * \frac{S_{su}}{K_S + S_{su}} * X_{su} * I_1$$

$$\rho_6 = k_{m,aa} * \frac{S_{aa}}{K_S + S_{aa}} * X_{aa} * I_1$$

$$\rho_7 = k_{m,fa} * \frac{S_{fa}}{K_S + S_{fa}} * X_{fa} * I_{2,fa}$$

$$\rho_8 = k_{m,c4} * \frac{(S_{va} + S_{Hva})}{K_S + (S_{va} + S_{Hva})} * X_{c4} * \frac{1}{1 + (S_{bu} + S_{Hbu})/(S_{va} + S_{Hva})} * I_{2,c4}$$

$$\rho_9 = k_{m,c4} * \frac{(S_{bu} + S_{Hbu})}{K_S + (S_{bu} + S_{Hbu})} * X_{c4} * \frac{1}{1 + (S_{va} + S_{Hva})/(S_{bu} + S_{Hbu})} * I_{2,c4}$$

$$\rho_{10} = k_{m,pro} * \frac{(S_{pro} + S_{Hpro})}{K_S + (S_{pro} + S_{Hpro})} * X_{pro} * I_{2,pro}$$

$$\rho_{11} = k_{m,ac} * \frac{(S_{ac} + S_{Hac})}{K_S + (S_{ac} + S_{Hac})} * X_{ac} * I_3$$

$$\rho_{12} = k_{m,H2} * \frac{S_{H2}}{K_S + S_{H2}} * X_{H2} * I_1$$

$$\rho_{13} = k_{dec,Xsu} * X_{su}$$

$$\rho_{14} = k_{dec,Xaa} * X_{aa}$$

$$\rho_{15} = k_{dec,Xfa} * X_{fa}$$

$$\rho_{16} = k_{dec,Xc4} * X_{c4}$$

$$\rho_{17} = k_{dec,Xpro} * X_{pro}$$

$$\rho_{18} = k_{dec,Xac} * X_{ac}$$

$$\rho_{19} = k_{dec,XH2} * X_{H2}$$

$$\rho_{A4} = k_{A|B,va}(S_H S_{va} - K_{a,va} S_{Hva})$$

$$\rho_{A5} = k_{A|B,bu}(S_H S_{bu} - K_{a,bu} S_{Hbu})$$

$$\rho_{A6} = k_{A|B,pro}(S_H S_{pro} - K_{a,pro} S_{Hpro})$$

$$\rho_{A7} = k_{A|B,ac}(S_H S_{ac} - K_{a,ac} S_{Hac})$$

$$\rho_{A10} = k_{A|B,HCO3}(S_H S_{HCO3} - K_{a,HCO3} S_{CO2})$$

$$\rho_{A11} = k_{A|B,NH3}(S_H S_{NH3} - K_{a,NH3} S_{NH4})$$

$$\rho_{A38} = k_{A|B,H2PO4}(S_H S_{H2PO4} - K_{a,H2PO4} S_{H3PO4})$$

$$\rho_{A39} = k_{A|B,HPO4}(S_H S_{HPO4} - K_{a,HPO4} S_{H2PO4})$$

$$\rho_{A40} = k_{A|B,PO4}(S_H S_{PO4} - K_{a,PO4} S_{HPO4})$$

$$\rho_{A41} = k_{A|B,CO3}(S_H S_{CO3} - K_{a,CO3} S_{HCO3})$$

$$\rho_{T8} = k_L a(S_{H2} - 16 K_{H,H2} P_{gas,H2})$$

$$\rho_{T9} = k_L a(S_{CH4} - 64 K_{H,CH4} P_{gas,CH4})$$

$$\rho_{T11} = k_L a(S_{NH3} - K_{H,NH3} P_{gas,NH3})$$

$$\rho_{T32} = k_L a(S_{CO2} - K_{H,CO2} P_{gas,CO2})$$

$$\rho_{P42} = k'_{r,CaCO_3}\left[(S_{Ca} S_{CO3})^{1/2} - K'_{sp,CaCO_3}{}^{1/2}\right]^2$$

$$\rho_{P43} = k'_{r,MgCO_3}\left[(S_{Mg} S_{CO3})^{1/2} - K'_{sp,MgCO_3}{}^{1/2}\right]^2$$

$$\rho_{P44} = k'_{r,MgNH_4PO_4}\left[(S_{Mg} S_{NH4} S_{PO4})^{1/3} - K'_{sp,MgNH_4PO_4}{}^{1/3}\right]^3$$

$$\rho_{P45} = k'_{r,MgHPO_4}\left[(S_{Mg} S_{HPO4})^{1/2} - K'_{sp,MgHPO_4}{}^{1/2}\right]^2$$

$$\rho_{P46} = k'_{r,Ca_3(PO_4)_2}\left[S_{Ca}{}^{3/5} S_{PO4}{}^{2/5} - K'_{sp,Ca_3(PO_4)_2}{}^{1/5}\right]^2$$

S.2. Expressions of rate coefficient terms

$$v_{10,5} = -\sum_{i=1\sim9,13\sim24} C_i\, v_{i,5}$$

$$v_{10,6} = -\sum_{i=1\sim9,13\sim24} C_i\, v_{i,6}$$

$$v_{10,10} = -\sum_{i=1\sim9,13\sim24} C_i\, v_{i,10}$$

$$v_{10,11} = -\sum_{i=1\sim9,13\sim24} C_i\, v_{i,11}$$

$$v_{10,12} = -\sum_{i=1\sim9,13\sim24} C_i\, v_{i,12}$$

$$v_{10,13} = -\sum_{i=13,17\sim23} C_i\, v_{i,13}$$

$$v_{10,14} = -\sum_{i=13,17\sim23} C_i\, v_{i,14}$$

$$v_{10,15} = -\sum_{i=13,17\sim23} C_i\, v_{i,15}$$

$$v_{10,16} = -\sum_{i=13,17\sim23} C_i\, v_{i,16}$$

$$v_{10,17} = -\sum_{i=13,17\sim23} C_i\, v_{i,17}$$

$$v_{10,18} = -\sum_{i=13,17\sim23} C_i\, v_{i,18}$$

$$v_{10,19} = -\sum_{i=13,17\sim23} C_i\, v_{i,19}$$

$$v_{33,13} = -\sum_{i=13,17\sim23} N_i\, v_{i,13}$$

$$v_{33,14} = -\sum_{i=13,17\sim23} N_i\, v_{i,14}$$

$$v_{33,15} = -\sum_{i=13,17\sim23} N_i\, v_{i,15}$$

$$v_{33,16} = -\sum_{i=13,17\sim23} N_i\, v_{i,16}$$

$$v_{33,17} = -\sum_{i=13,17\sim23} N_i\, v_{i,17}$$

$$v_{33,18} = -\sum_{i=13,17\sim23} N_i\, v_{i,18}$$

$$v_{33,19} = -\sum_{i=13,17\sim23} N_i\, v_{i,19}$$

Appendix

Permission

RightsLink

Copyright Clearance Center

Thank You For Your Order!

Dear Mr. yang zhang,

Thank you for placing your order through Copyright Clearance Center's RightsLink service. Elsevier has partnered with RightsLink to license its content. This notice is a confirmation that your order was successful.

Your order details and publisher terms and conditions are available by clicking the link below:
http://s100.copyright.com/CustomerAdmin/PLF.jsp?ref=a7279ced-ea4c-453a-ba19-0b1cbfa68da5

Order Details
Licensee: yang zhang
License Date: Oct 16, 2015
License Number: 3730830712025
Publication: Bioresource Technology
Title: Improved ADM1 model for anaerobic digestion process considering physico-chemical reactions
Type Of Use: reuse in a thesis/dissertation
Total: 0.00 USD